

Design, Construction and Testing of an Ocean Renewable Energy
Storage Scaled Prototype

By

James D. C. Meredith

B. Eng. Mechanical Engineering, McGill University (2009)

Submitted to the Department of Mechanical Engineering
in partial fulfillment of the requirement for the degree of

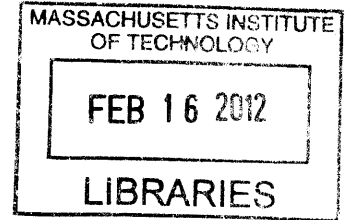
Master of Science in Mechanical Engineering

at the

Massachusetts Institute of Technology

February 2012

© 2012 Massachusetts Institute of Technology. All rights reserved.



ARCHIVES

Signature of Author: _____

A handwritten signature in black ink, appearing to read "James D. C. Meredith".

Department of Mechanical Engineering
January 6th, 2012

Certified by: _____

Alexander H. Slocum
Pappalardo Professor of Mechanical Engineering
Thesis Supervisor

A handwritten signature in black ink, appearing to read "Alexander H. Slocum".

Accepted by: _____

David E. Hardt
Professor of Mechanical Engineering
Chairman, Committee for Graduate Students

A handwritten signature in black ink, appearing to read "David E. Hardt".

Design, Construction and Testing of an Ocean Renewable Energy Storage Scaled Prototype

By

James D. C. Meredith

Submitted to the Department of Mechanical Engineering on January 20th, 2012
in Partial Fulfillment of the Requirements for the Degree of

Master of Science in Mechanical Engineering

Abstract

The concept for a new form of pumped storage hydro is being developed within the Precision Engineering Research Group at MIT: the Ocean Renewable Energy Storage (ORES) project. Large, hollow concrete spheres are created, fitted with a reversible pump-turbine and deployed to the sea floor. Water is then allowed to flow through the turbine, into the sphere, to produce power and power is stored back in the device by running the turbine backwards as a pump and evacuating the sphere. The first prototype of that concept is presented here. A land-based system was designed, built and tested to demonstrate its ability to store energy and test the viability of the manufacturing methods planned.

The device was successfully built and cycled, storing 2Wh of energy. The round-trip efficiency of the device was severely affected by the low efficiency of the scaled down rotating equipment. It was also found that casting a monolithic sphere is preferable to assembling multiple pieces and that the interior of the sphere should be maintained at atmospheric pressure via a vent line.

Thesis Supervisor: Alexander H. Slocum

Title: Pappalardo Professor of Mechanical Engineering

Acknowledgements

I would like to acknowledge the following people for their help and support during the preparation of this document:

- Alex H. Slocum: His mentorship and continuous support made this work possible. Alex's insight into mechanical design and his dedication to the projects he is involved in are unparalleled and I am grateful for his help, guidance and hospitality. His relentless energy and passion for technology are an inspiration and with him and others like him at MIT, the institute has a bright future ahead of it.
- Bill Miskoe and Nishan Nahikian: Their services were instrumental in the creation of the prototype documented here. Bill Miskoe's shop was the battleground where the most of the fabrication was done and where the machine finally came together. Bill's experience, patience and creativity got the project over many of the hurdles it encountered. To Bill, I wish many more seasons of Miata racing and many more projects in the back yard.
- The team: Bruna Moscol, Greg Fennell, Gokhan Dunder and Brian Hodder. It was a privilege to work with such dedicated and capable people. I hope our paths cross again soon.
- I would also like to thank my family and friends for their continued support and encouragement.

Table of Contents

Abstract	3
Acknowledgements	5
Table of Contents.....	6
List of figures	8
List of Tables	12
Abbreviations and Acronyms	13
1 Introduction.....	14
1.1 Motivation.....	14
1.2 Previous Studies.....	15
2 Energy storage.....	16
2.1 Grid scale Energy storage.....	16
2.2 Ocean energy storage.....	18
2.2.1 Ocean CAES	18
2.2.2 PSH Ocean Storage.....	19
3 ORES Concept Overview	21
3.1 Prototype Concept Overview.....	22
4 Design.....	23
4.1 Overall system design.....	23
4.2 Concrete Sphere.....	24
4.3 Hemisphere Joint	31
4.4 Mold	38
4.5 Turbine	44
4.6 Pump	54
4.7 Electrical	56
4.7.1 Turbine Circuit.....	57
4.7.2 Pump circuit	58
4.8 Data Acquisition and sensors.....	59
4.9 Piping	63
5 Build (Procedure).....	68
5.1 Concrete Hemispheres	68
5.2 Handling	70

5.3	Core drill	72
5.4	Turbine Installation	73
5.5	Piping installation and manifold support.....	75
5.6	High Reservoir.....	77
5.7	Vacuum Sealing.....	78
5.8	Vents/ports and gas handling	79
6	Test.....	80
6.1	Overview	80
6.2	Test procedure.....	80
6.2.1	Start-up	80
6.2.2	Vent line.....	81
6.2.3	No Vent Line.....	82
6.2.4	Shut down	83
6.3	Leak test	83
6.4	Turbine Tuning.....	85
6.5	Results.....	87
6.5.1	Calculations	87
6.5.2	Result	88
7	Conclusion	92
7.1	Lessons Learned:.....	92
7.1.1	Joint.....	92
7.1.2	Mold.....	92
7.1.3	Pump/Turbine	92
7.2	Future Work.....	93
7.3	Closing Remarks.....	94
8	Bibliography.....	95
9	Appendices	97
9.1	Turbine Efficiency Chart.....	97
9.2	Additional Design Calculations.....	97
9.2.1	Pressure Drop Calculator	97
9.2.2	Piping Losses in the turbine piping system.....	100
9.3	Piping Diagram.....	101
9.4	Wiring Diagram	103

List of figures

Figure 1: Comparison of Energy Storage Technologies. Source: Roberts, 2009	16
Figure 2: Compressed air energy storage conceptual layout. Source: www.sandia.gov/media/NewsRel/NR2001/images/jpg/minebw.jpg.....	17
Figure 3: Pumped Storage Hydro conceptual layout. Source: www.tva.gov/power/pumpstorart.htm	18
Figure 4: Thin Red Line Inc.'s energy bags. Left: First wet test of the energy bag concept. Right: A larger untested bag. Source: http://www.thin-red-line.com/	19
Figure 5: Artist's impression of Gottlieb Paludan Architects and Risø-DTU's Energy Island. Source: http://www.gottliebpaludan.dk/dk/menu_projekter/projekt_gpi/billeder/www/greenpowerisland.pdf.....	20
Figure 6: The German professors' depiction of undersea PSH. Source:faz.net.....	20
Figure 7: Simple ORES concept image.	21
Figure 8 : 120 degree concrete sphere section. The red arrow on the scale at right indicates the yield strength of the concrete. This structure will fail in several locations.....	25
Figure 9: 180 degree concrete sphere sections. While stress concentrations still exist with this geometry, there are no stresses above the yield strength of the concrete.....	25
Figure 10: Radial and Hoop stress in the thick-walled spherical shell.	29
Figure 11: Maximum deployable depth for 25m spheres with varying wall thickness using both the thick- walled spherical shell model and the thin wall approximatoin	29
Figure 12 A concrete hemisphere fresh out of the mold. The pipe coupling can be seen embedded in the pole.....	30
Figure 13: Annular channel with injection ports for epoxy injection.	31
Figure 14: Left: Annular channel with stud ports. Right: Cross section of the same.	32
Figure 15: Steel ring with welded studs used to create the epoxy channels.	33
Figure 16: The lower hemisphere with sealant applied and stud ports filled with epoxy.....	35
Figure 17: The upper hemisphere prior to being joined with the lower hemisphere. The four studs are visible, protruding downward from the upper stud ports.....	35
Figure 18: Assembled concrete sphere.	36
Figure 19: The open channel used to join the two hemispheres. Left: Cross section of the channel. Right: The channel filled with epoxy.....	37
Figure 20: The failed stud ports. Left: Separation between the concrete and the epoxy within the stud port. A gap around the edge is visible. Center: Weather stripping retains the epoxy. Right: The sealed stud port.	38

Figure 21: Early models of the mold.	39
Figure 22: Model of the final mold.	39
Figure 23: Draft angle on the inner hemispherical mold.	41
Figure 24: Lifting on the inner steel hemisphere and the direction of loading.	42
Figure 25: FEA of the outer mold. Loading case based on lifting the sphere.	43
Figure 26: Model of the pole assembly.	44
Figure 27: A reversible pump/turbine. source: www.voithhydro.com	45
Figure 28 Available turbines capable of meeting the project requirements.	47
Figure 29: The LV750 fresh out of the box. The nozzle port is seen protruding from the left of the turbine casing. The generator is shown connected to the rectifier that was included with the turbine.	48
Figure 30: Turbine efficiency as stated by the manufacturer.	49
Figure 31: Left: The turgo turbine runner and nozzle. Right: Several of the different nozzles used.	50
Figure 32: First iteration of the turbine draft tube.	51
Figure 33: 6 inch turbine draft tube. Model and completed installation.	52
Figure 34: Model section view of the generator cap, showing the turbine casing, generator and cap. Coloured to distinguish the separate components.	53
Figure 35: Right: Model section view of the bulkhead fitting. Note that the fitting has three wires; one is not visible due to the sectioned view. Left: The completed bulkhead fitting (grey fitting at top) is shown fastened to the generator cap via a pipe coupling.	53
Figure 36: Pump performance curve as given by the manufacturer.	55
Figure 37: Left: A schematic drawing of the pump(1), motor coupling(3) and flange adapter(5). Right: The pump coupled to its motor.	56
Figure 38: Electrical system box.	57
Figure 39: Left: The generator with its top cover and bearing removed. Right: The connection between the bulkhead fitting and the rectifier.	57
Figure 40: Left: The TDK-Lambda Zup36V-24A. Source: datatec.de . Center: The external control connector on the rear panel of the power supply; the horizontal lines indicate jumpers between connecting ports. Source: User manual. Right: Connections on the rear panel of the power supply. Source: User manual.	59
Figure 41: USB-6009 Source: ni.com	59
Figure 42: Internal layout of the USB-6009. Source: ni.com	60

Figure 43: Pressure transducers.	61
Figure 44: Left: The FP-5603 shown without its pipe housing. The paddle wheel paddles can be seen at the bottom of the unit. Right: Wiring for the FP-5600 series of which the FP-5603 is a part.	62
Figure 45: Locations of the sensors. PX indicates a pressure transducer.	62
Figure 46: Manufacturer’s recommended length of straight pipe prior into and following the FP-5603 flow meter.	64
Figure 47: The first version of the single line drawing.	64
Figure 48: Left: Close-up of the turbine piping. Center and right: Close-up of the pump piping.	65
Figure 49: 3D model of the piping system close to the sphere.	66
Figure 50: The mold being filled with concrete. Mold release (engine oil) can be seen to darken the surfaces of the mold where contact with the concrete will occur. Bolts holding the mold to the vibration table can be seen bottom right.	69
Figure 51: The studded steel ring being pressed into the concrete. The plastic wrap used in attempts to seal the backer rod can be seen on the stud in the foreground. This plastic wrap caused several problems during assembly.	70
Figure 52: Lifting a concrete hemisphere.	70
Figure 53: The assembled concrete sphere being manipulated through the use of nylon slings. Left: A tractor lifts the sphere. Right: The sphere is rotated through successive lifts with a chain fall.	71
Figure 54: The core drill in action.	72
Figure 55: Core drill results. Left: The enlarged hole in the sphere. Right: The core resulting from the drilling process. The pipe coupling used previously can be seen embedded in the centre.	73
Figure 56: The completed turbine assembly.	74
Figure 57: A wooden structure provides support for the valve assembly.	75
Figure 58: The completed piping assembly. Left: “No Vent line” case testing. Right: “Vent line” testing. Notice that the vacuum pump is not connected to the system for this test.	76
Figure 59: The high reservoir shown behind the completed system.	77
Figure 60: The vacuum pump.	78
Figure 61: Results of a leak rate test. The pressure in the draft tube was measured for over 10 minutes after the system had been brought to 9 kPa internal pressure. Linear regression yielded the equation shown. The leak rate was 4.21 Pa/s or 0.253kPa/min.	85
Figure 62: Energy recovered by the turbine using various nozzle sizes.	86
Figure 63: Turbine power output using a 12.7mm nozzle with various load resistances applied.	87

Figure 64: Energy stored and discharged for all tests.	89
Figure 65: Typical charge and discharge power curves during a “vent line” test cycle.	90
Figure 66: Typical charge and discharge power curves during a “no vent line” test cycle.	90
Figure 67: Storage Vessel. Left: Size comparison. Right: Cut-away showing wall cross section.....	94
Figure 68: The pressure drop calculator spreadsheet.....	98
Figure 69: Turbine Circuit	103
Figure 70: Pump Circuit.....	103

List of Tables

Table 1: Eyer and Corey’s “Five Categories of Energy Storage Applications”	15
Table 2: Buoyancy Calculations	26
Table 3 Calculation of maximum deployable depth	28
Table 4: Pressure drop of epoxy during injection.	34
Table 5: Lifting eye calculations.....	42
Table 6: Minimum specifications for the turbine unit (shown in red). Values used to estimate the specifications are shown in black.....	46
Table 7: Flow rates for various nozzle sizes in the LV750 micro-hydro turbine. Source: Hydro Induction Power	49
Table 8: Pump performance requirements.	55
Table 9: Connections to the data acquisition module.	60
Table 10: Example calculations of the piping losses in the pump system near the sphere using $\frac{3}{4}$ inch size threaded pipe fittings. Black numbers are inputs and red numbers are calculated.	67
Table 11: The total pressure loss estimated for the pump piping system near the sphere. The price, in the right-most column, is the price of a typical brass ball valve in that size from McMaster Carr Supply Company.	67
Table 12: Turbine piping system pressure loss for various pipe sizes.	68
Table 13: Summary of piping losses for the hose connecting the near-sphere piping system to the high reservoir.	68
Table 14: Equations used to determine energy flows for a given test.....	88
Table 15: Detailed results comparing the “vent line” and “no vent line” cases.....	91
Table 16: Overall specifications of the 3m concrete sphere.	93
Table 17: Estimated turbine piping system losses. This is an example calculation. For each pipe size, the internal diameter is entered as the hydraulic diameter, D_h , and the calculations are completed.	100
Table 18: The summary of turbine piping loss estimates.	100

Abbreviations and Acronyms

A	Amperes
AC	Alternating current
AWG	American wire gauge
CAES	Compressed air energy storage
DC	Direct current
d	Depth
K	Minor loss coefficient
LRA	Locked rotor amperage
ρ	Density
ρ_f	Density of fresh water: 1000kg/m ³
ρ_s	Density of seawater: 1025kg/m ³
g	Gravity: 9.81 m/s ²
H	Head height
n	Rotational speed in revolutions per minute (rpm)
NPT	National pipe thread
Q	Flow rate
P	Power
PSH	Pumped Storage Hydro
p	Pressure
p_i	Internal pressure
p_o	External pressure
V	Voltage
I	Electrical current
σ	Stress
S	Material strength
FOS	Factor of safety
R	Ratio of maximum to minimum stress in cyclic loading
r	Radius
r_i	Inner radius of the sphere
r_o	Outer radius of the sphere
V	Volts
VI	Virtual Instrument
W	Watts

1 Introduction

1.1 Motivation

Renewable energy sources have increased grid integration costs and cause increase loading on fast-response generation capacity because of their intermittent nature. Energy storage has the potential to reduce that intermittency. As renewable power increases its contribution to the grid, energy storage will become increasingly important. In the limit where all power is supplied by renewable sources, a significant amount of energy storage would be needed to bridge the inherent gaps, or curtailments, in power output (Corbus et al, 2009).

While fast-response energy storage technology has its uses, storage methods with longer discharge times and greater amounts of energy stored are needed for widespread grid integration. A majority of the potential applications for storage require several hours of discharge time (Eyer & Corey, 2010).

In addition to the enabling effects of storage on renewable energy sources, a number of benefits have been identified that individually allow economics gains to be made. Eyer & Corey of Sandia National Laboratory have compiled a list of applications for storage and have elaborated on the benefits provided in serving these applications. The list is shown below in Table 1.

It should also be noted that this work is in the wake of a detailed economic analysis by Gregory Fennell (2011) in which the economics of offshore energy storage were evaluated as they relate to the concept described here and deemed favourable.

Category 1 — Electric Supply
1. Electric Energy Time-shift
2. Electric Supply Capacity
Category 2 — Ancillary Services
3. Load Following
4. Area Regulation
5. Electric Supply Reserve Capacity
6. Voltage Support
Category 3 — Grid System
7. Transmission Support
8. Transmission Congestion Relief
9. Transmission & Distribution (T&D) Upgrade Deferral
10. Substation On-site Power
Category 4 — End User/Utility Customer
11. Time-of-use (TOU) Energy Cost Management
12. Demand Charge Management
13. Electric Service Reliability
14. Electric Service Power Quality
Category 5 — Renewables Integration
15. Renewables Energy Time-shift
16. Renewables Capacity Firming
17. Wind Generation Grid Integration

Table 1: Eyer and Corey’s “Five Categories of Energy Storage Applications”

1.2 Previous Studies

The ORES project was started by Alexander H. Slocum in the Precision Engineering Research Group (PREG) at MIT in 2007. An initial concept development was conducted by Alison Greenlee (Greenlee, 2009) within PERG, who found that spherical shells offered the best performance and required the least material to construct. Subsequently, the concept was further developed and expanded upon by Gregory Fennell, also in PERG. Gregory also conducted a detailed economic analysis to estimate the overall cost of creating ORES devices at scale (Fennell, 2011).

These works have indicated that further development of the concept is warranted and form part of the motivation of this paper.

2 Energy storage

2.1 Grid scale Energy storage

There are a variety of technologies used to store energy with various power and energy capacities; some providing high power for a few seconds and others capable of running for hours. Figure 1 shows the spread of available energy storage technologies. There are several applications where short duration storage is acceptable (e.g. managing power quality) however a large proportion of the benefits of storage require longer discharge time, on the order of hours. While several of the technologies shown in Figure 1 can store power for multiple hours, the chemical storage methods are still much more expensive than the more conventional energy storage methods that use rotating equipment, such as PSH and compressed air energy storage (CAES).

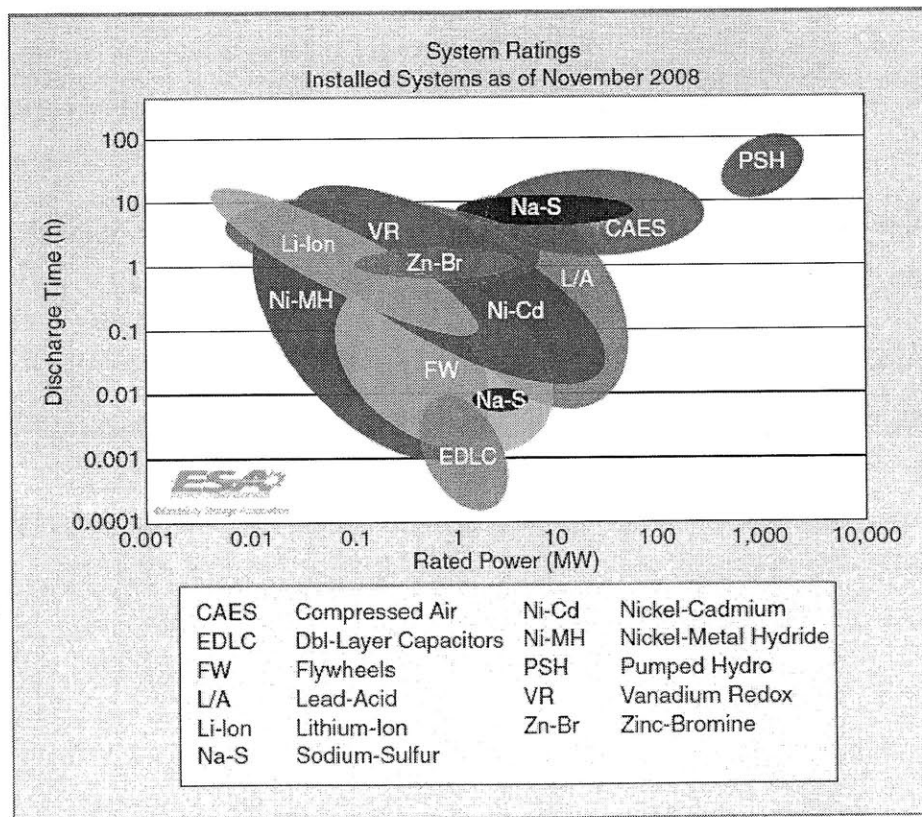


Figure 1: Comparison of Energy Storage Technologies. Source: Roberts, 2009

While pumped storage hydro is alone in its capability to store very large amounts of energy, it is worth describing CAES since it has received recent attention and funding. CAES stores energy by compressing air and storing the compressed air in a vessel until it is needed. The energy is then released by expanding

the air through a turbine. A hybrid system can be created when the compressed air is used to augment the output of a natural gas turbine. These hybrid systems are the only ones to have been constructed of which there are currently 2 in operation; the Huntorf plant in Germany and the McIntosh plant in Alabama. Both use salt domes for their storage vessels. The storage vessel for the air can be a variety of things from steel pressure vessels to underground limestone caverns. Since a larger pressure vessel allows more energy to be stored at a given pressure, large caverns are the pressure vessel of choice and this is the configuration depicted in Figure 2.

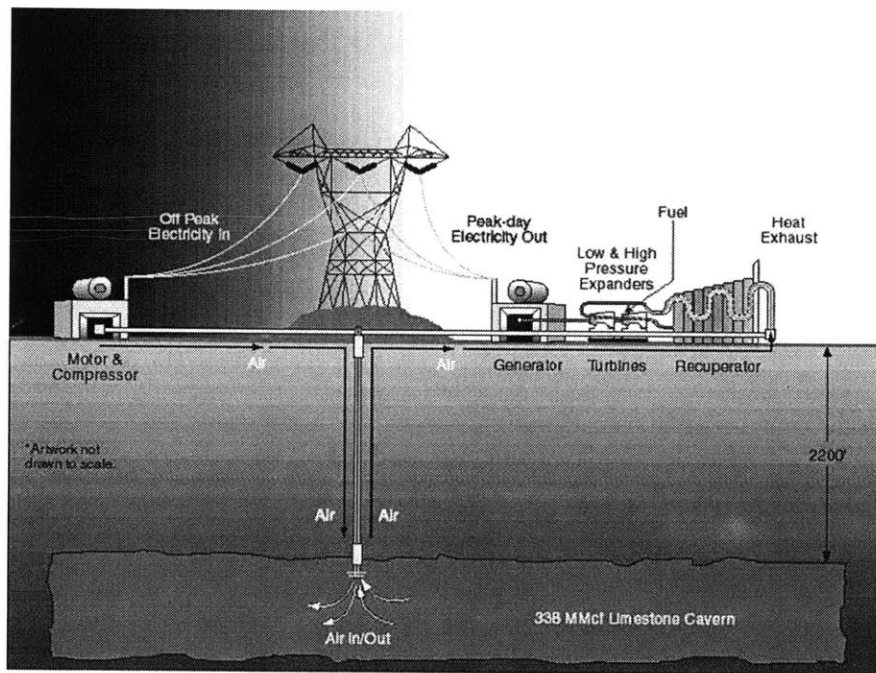


Figure 2: Compressed air energy storage conceptual layout. Source: www.sandia.gov/media/NewsRel/NR2001/images/jpg/minebw.jpg.

Pumped storage hydro, on the other hand, uses water to store the energy. In configurations similar to that depicted in Figure 3, energy is produced in the same way as a conventional hydro power station. Water flows down, from the high reservoir to the lower one, through a turbine spinning it and producing power. Energy is stored by the reverse process, where the turbine is run backwards as a pump and is used to pump water back up the hill. As of 2009, there was 104GW of installed capacity worldwide (USEIA, 2012); the only significant method of grid-scale energy storage in use today.

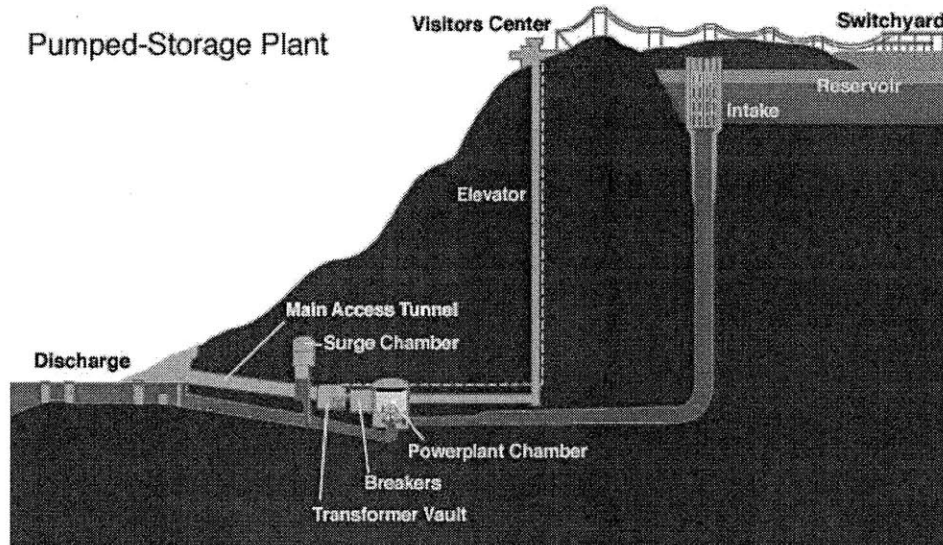


Figure 3: Pumped Storage Hydro conceptual layout. Source: www.tva.gov/power/pumpstorart.htm

Despite PSH being deployed around the globe, it is only available areas with the correct geology to allow a high reservoir and a low one to be adjacent. In regions without the geological features necessary, PSH is simply not possible.

2.2 Ocean energy storage

Because of the high pressures available at depth in the ocean and because so many cities and energy load centers are coastal, several concepts have been put forward in attempts to store large amounts of energy offshore.

2.2.1 Ocean CAES

Hydrostor Inc., Thin Red Line Aerospace and Nimrod Energy Ltd. are all working on almost identical concepts for CAES. The idea centers on using high pressure ocean water to contain the compressed air instead of a rigid pressure vessel. Since water is providing the pressure, stiff materials such as steel and rock formations are not required to contain the compressed air and flexible bags can be used. However, the bags experience buoyancy and must be held in place. The force of buoyancy being substantial, aerospace polymers must be used to form and reinforce the bags which also require a sizable anchor.

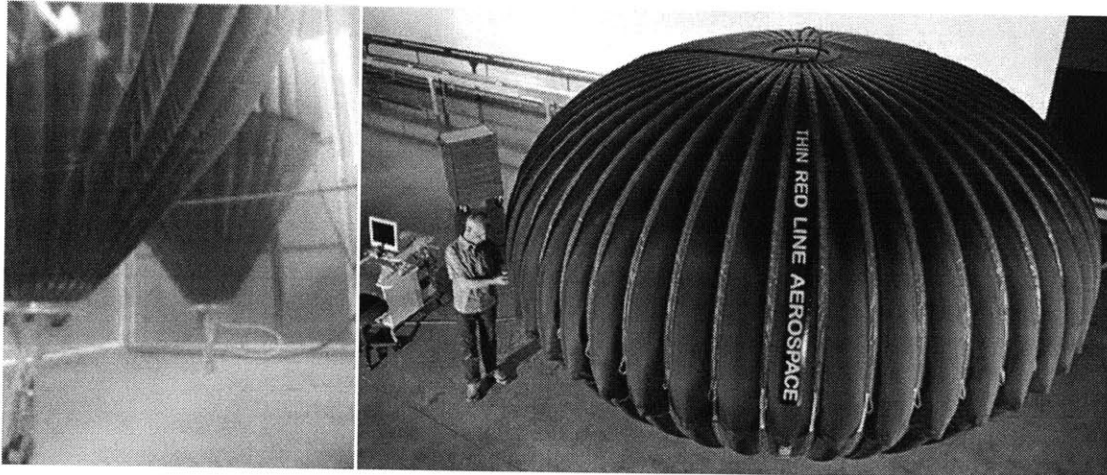


Figure 4: Thin Red Line Inc.'s energy bags. Left: First wet test of the energy bag concept. Right: A larger untested bag. Source: <http://www.thin-red-line.com/>

Bright Energy Inc. was the recipient of an ARPA-E grant for energy storage and has patented a concept whereby CAES is conducted using underwater balloons as the pressure vessel. However these balloons are anchored to the sea floor by virtue of being laden with Sediment. In attempting to use the lowest cost material, and the one most readily available, the material of the sea floor itself was selected. Bright Energy hopes to have a prototype in the coming year but is also working on developing pure CAES onshore in steel vessels.

2.2.2 PSH Ocean Storage

Gottlieb Paludan Architects and Risø-DTU, as well as Kima Inc. are working on the concept of an energy island. The idea is to create an island with either a raised or lowered water level compared to the surrounding waters and to use this height difference as the head for pumped storage hydro. Despite the head being relatively small, the volumes planned are quite large as can be seen in Figure 5. There have not been any prototypes to date nor are any planned at this time.

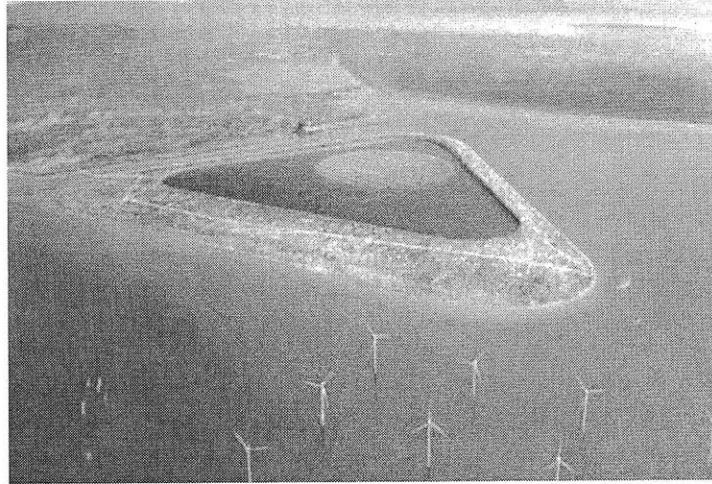


Figure 5: Artist's impression of Gottlieb Paludan Architects and Risø-DTU's Energy Island. Source: http://www.gottliebpaludan.dk/dk/menu_projekter/projekt_gpi/billeder/www/greenpowerisland.pdf

Two physics professors, Horst Schmidt-Böcking and Gerhard Luther have independently conceived of an idea virtually identical to the ORES concept albeit two years later. Their concept consists of a large concrete sphere on the seafloor with a reversible pump-turbine to transfer water in and out of the sphere, shown in Figure 6. The spheres are also connected to wind turbines, although not in any mooring configuration.

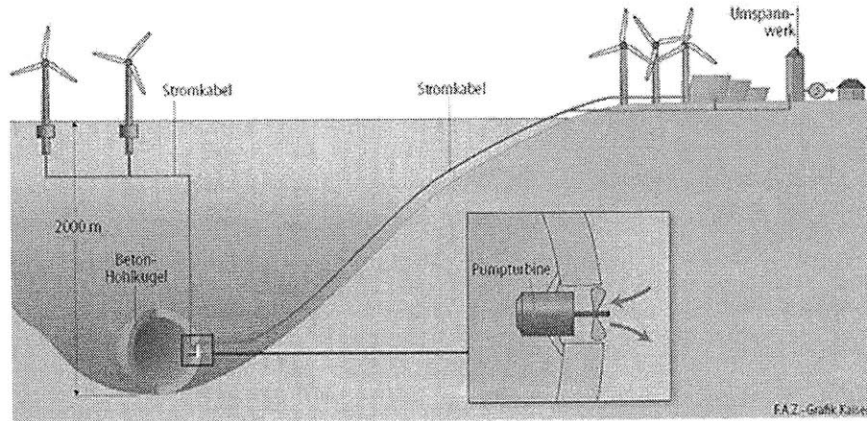


Figure 6: The German professors' depiction of undersea PSH. Source: [faz.net](http://www.faz.net)

3 ORES Concept Overview

The ORES concept is a scheme to store energy in the deep waters offshore. In principle, the idea is very simple: to create large, hollow concrete spheres and drop them down onto the sea floor. By fitting these spheres with a reversible pump-turbine, water can be cycled in and out of the spheres, from high pressure outside to low pressure inside and back. In that way, energy can be stored or discharged, similar to pumped storage hydro. A simple concept image of one of the potential architectures is shown in Figure 7.

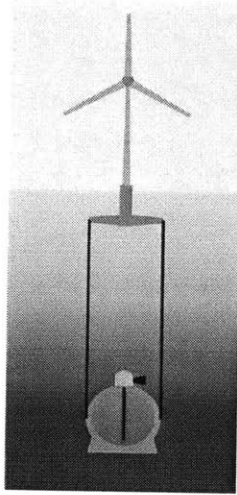


Figure 7: Simple ORES concept image.

The discharging and charging cycles happen as follows:

Discharging: The device is discharging when it allows water to flow into the sphere, passing through a turbine. The turbine spins a generator producing electricity. Eventually, the sphere fills and power production must stop.

Charging: Electricity can be delivered to the generator, running it backwards as a motor. The now motor spins the turbine which acts as a pump, draining the water from the sphere. The energy delivered to the motor caused a volume of water to leave the sphere. That energy can later be recovered by allowing water to flow back in, filling that same volume.

The round-trip efficiency of pumped storage hydro facilities ranges from 75-78% (Eyer & Corey, 2010) so it is expected that similar rotating equipment could be applied to the ORES concept and similar efficiencies would result. A pilot sea-water pumped storage hydro facility was completed in 1999 on the island of Okinawa in Japan. Since then, the facility has demonstrated the successful operation of a pumped storage hydro plant using sea-water.

While conventional pumped storage hydro is well established as a viable and cost effective method of storing large amounts of energy, it is limited by the geology required. In areas without mountains, for example, it would not be possible to create a PSH system. In contrast, the ORES system removes this constraint and brings the proven effectiveness, high power and high energy capacity of pumped storage hydro to the offshore. Given that a large portion of the world's population lives in coastal areas, there are many more sites available for ORES development. A substantial list of potential sites for the ORES concept has been compiled based on several factors but most notably according to water depth, proximity to population centers and the quality of the wind resources available (Fennell, 2011).

Taking a systems approach, as shown in Figure 7, the concrete sphere can be used as a mooring for offshore floating wind turbines. Joining these two technologies provides cost savings in several areas: the moorings themselves are no longer required, only one transmission line to shore is required and that transmission line can be sized for lower power. Since the average output of a wind farm is much less than the rated output, the transmission lines and substations can be sized for less power with peak power from the wind turbines being stored for later use.

3.1 Prototype Concept Overview

This system is the first in a series of test devices that will be created to develop and demonstrate the viability of the ORES concept. The tests devices will be as close to the design of the final concept as possible with each successive build being larger than and improving on the last. With this first device, the goals were as follows:

1. To explore the viability of creating an ORES device by casting concrete spherical sections and joining them together.
2. To successfully demonstrate the ability of an ORES device to store energy in a simulated underwater setting.
3. Evaluate the usefulness of a vent line from the sphere to atmosphere.

For this study, a 1m diameter ORES device was to be designed and built for testing on land. The device would consist of a spherical concrete shell and rotating equipment to transfer energy to and from the water. To test the device, several additional systems would be needed including: An electrical system to power the rotating equipment and accept output power, a reservoir of water at height to simulate the ocean depths including a piping system to deliver the water to the rotating equipment, and a system of sensors and data acquisition modules to collect the test data.

The purpose of the vent line is to maintain the interior of the sphere at constant pressure, allow air to escape from the sphere as water comes in during discharging and the reverse during charging. While a vent line requires additional cost for the line itself, the couplings and its maintenance, the potential lost storage capacity, due to rising internal pressures in the sphere as it fill, has the potential to offset that cost. The sphere would thus be cycled both while open to atmosphere and while sealed.

This prototype was to be built quickly and using a minimum of resources such that potential major issues with the design could be discovered as fast as possible. While there are still major differences in the conditions the prototype was subjected to here and those of the offshore environment, it is hoped that the methods developed and tested in creating the 1m device will be transferable to larger devices.

4 Design

4.1 Overall system design

The design of the prototype will mimic that of the full sized device and consist of the same basic components. To achieve the stated goals of the prototype, it was important to maintain as much fidelity as possible to the design and operation of the full sized ORES concept. However, design choices were made that deviated from the full sized device to simplify and reduce the cost of the prototype. An overview of the choices made follows.

The first and most obvious deviation is the size. With full sized ORES devices potentially having a diameter as large as 33m (Fennel, 2011), the prototype is thus a 1:33 scale model. As the device will be scaled linearly, the volume and energy storage capacity will be reduced by a factor of $33^3=35937$. The deployable depth, however, will remain the same. The prototype will not be deployed underwater but deployable depth may still be useful for design purposes.

Because of its smaller size, handling of the concrete components will be much easier. Thus the concrete sections will be cast with the equatorial plane being horizontal instead of vertical. Vertical casting was desired to reduce the use of heavy lifting equipment however, that is not a concern in this study.

The interior of the vessel will be accessed by 2 ports. The pump suction will be piped to the bottom of the vessel while the turbine draft tube will deliver water through the top. This configuration is necessary due to the type of turbine being used since turgo turbines require a draft tube that discharges to open air. Unfortunately, a loss of 3 feet of head (~10% of the total head) is incurred by having inlets and outlets at different heights. Reaction turbines such as Kaplan and Francis types would not have this issue since their

draft tubes are filled with water and can thus support a pressure change along the draft tube. A turgo turbine, however, has a pressure drop across the nozzle leading into the turbine and nowhere else.

With the prototype not being under water, a piping system to deliver high pressure water directly to the rotating equipment will be needed. While this should not change the behaviour of the rotating equipment, the concrete sphere will not be subject to external compressive forces, unlike the full sized device. Also due to the lack of external pressure, only limited positive gauge pressure will be allowed inside the sphere. The pressure on the exterior of the sphere will only be atmospheric and the tensile strength of the sphere, and its seals in particular, are not able to withstand internal pressure without failing.

Finally, the system must be made air tight, as air leakage is not possible in the production device. To ensure that the behaviour of the prototype does not deviate from that of the production device due to air leakage, those leaks must be managed and reduced to an acceptable level. The sphere must also be sealed since tests will be conducted with internal pressures other than atmospheric.

With these requirements in mind, the following components were designed, built and tested.

1. Concrete sphere
2. Turbine
3. Pump
4. Electrical system
5. Data acquisition system
6. Piping system

The design of these systems is described in detail in the following sections.

4.2 Concrete Sphere

To create the concrete sphere, two hemispheres were to be cast and joined. Previous work explored the possibility of using more than two sections, like barrel staves, to create the sphere but concluded that simply using two halves was best for preventing failure of the section prior to assembly. The individual concrete sections under their own weight are much more susceptible to tensile forces than the assembly itself so failure is more likely to occur prior to assembly being completed. The smaller the number of sections used, the better each section is at resisting gravity as well as stresses exerted during handling so the minimum, two pieces, was chosen.

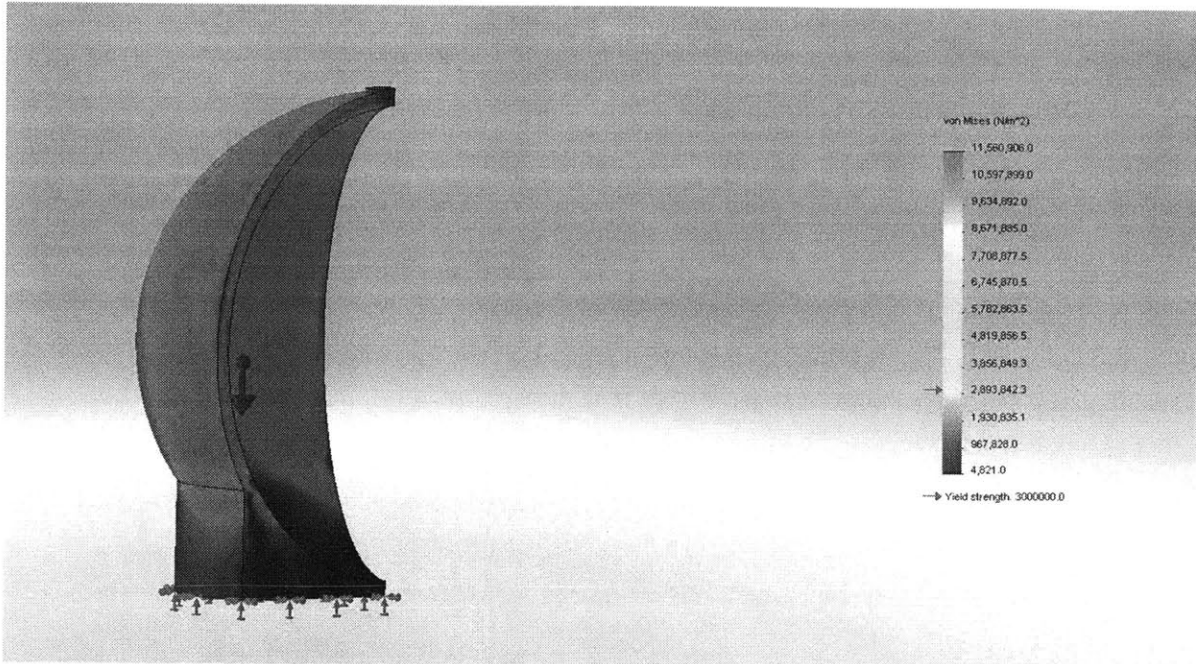


Figure 8 : 120 degree concrete sphere section. The red arrow on the scale at right indicates the yield strength of the concrete. This structure will fail in several locations.

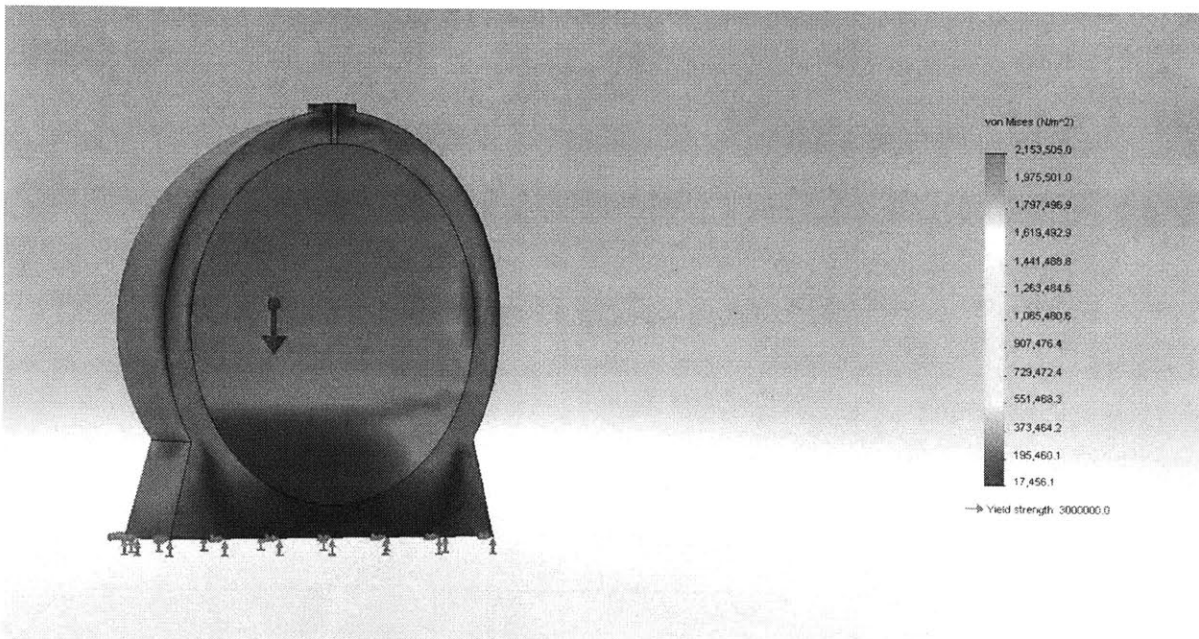


Figure 9: 180 degree concrete sphere sections. While stress concentrations still exist with this geometry, there are no stresses above the yield strength of the concrete.

As seen in Figure 8 and Figure 9, the production model will feature a wider base; the internal cavity will be spherical but the concrete itself will have a conical base added for stability on the ocean floor. For simplicity of fabrication, the prototype’s concrete shell was entirely spherical, thus allowing the use of hemispherical molds for both the inner and outer mold pieces.

The wall thickness of the prototype was selected in accordance with the scale factor applied to the internal diameter. For a 20m sphere, the wall thickness required was approximately 6 feet (Fennell, 2011). The nominal wall thickness for the prototype was thus about 3.5 inches. The exact thickness was subject to the availability of inexpensive mold materials. To facilitate the removal of the inner mold, no part of the inner mold was allowed to contact concrete at an angle parallel to the direction of pull used to release it, i.e. a draft angle was applied to the concrete sphere. To do this, a spacer was placed between the two molds at the pole to keep the inner mold out enough such that a sufficient draft angle exists. Given the mold sections available and the draft angle, the thicknesses at the equator and the pole were approximately 3.75 inches and 4 inches respectively.

While the prototype completed here is not designed to be deployed offshore, the possibility of creating a sphere is this size for deployment was also a factor in the wall thickness selection. For deployment offshore, the sphere must be negatively buoyant so the walls must be thick enough (i.e. weigh enough) to cause the sphere to sink. The turbine and pump in a deployable sphere would likely increase the sphere’s tendency to sink so they were not included in this calculation, shown in Table 2.

Inner Mold Diameter [m]	0.76
Outer Mold Diameter [m]	0.95
Wall thickness [m]	0.10
Concrete Volume [m ³]	0.22
Concrete Density [kg/m ³]	2400
Concrete Mass [kg]	528
Displacement Volume [m ³]	0.45
Seawater density [kg/m ³]	1025
Displaced mass [kg]	463
Net buoyancy [N]	-642

Table 2: Buoyancy Calculations

The maximum depth a sphere can be deployed to also depends on the wall thickness. Stresses in the concrete were calculated modeling it as a thick walled sphere that was linear, isotropic, and continuous, in accordance with Hooke’s Law. Concrete’s strength was 5000psi and a safety factor of 1.5 was applied. The internal pressure of the sphere is also assumed to be 0.

Since only hydrostatic pressure is applied, which is evenly distributed over the entire face it acts on, the shear stresses are zero. The normal stresses are thus equal to the principal stresses. Due to the symmetry of the sphere, two of the three normal stresses are equal. The normal stresses are given as follows:

$$\sigma_1(r) = \sigma_2(r) = \frac{P_i r_i^3}{2r^3} \left(\frac{r_o^3 + 2r^3}{r_o^3 - r_i^3} \right) - \frac{P_o r_o^3}{2r^3} \left(\frac{r_i^3 + 2r^3}{r_o^3 - r_i^3} \right) \quad (1)$$

$$\sigma_3(r) = -\frac{P_i r_i^3}{r^3} \left(\frac{r_o^3 - r^3}{r_o^3 - r_i^3} \right) - \frac{P_o r_o^3}{r^3} \left(\frac{r^3 - r_i^3}{r_o^3 - r_i^3} \right) \quad (2)$$

Where σ_1 , σ_2 and σ_3 are the principal stresses, P_i is the internal pressure of the sphere, P_o is the external pressure (related to the depth), r_i is the inner radius of the sphere, r_o is the outer radius and r is the radius being evaluated. A stress tensor, of the form below, results.

$$\sigma = \begin{bmatrix} \sigma_1 & 0 & 0 \\ 0 & \sigma_1 & 0 \\ 0 & 0 & \sigma_3 \end{bmatrix} \quad (3)$$

And the von Mises stress is calculated from the principal stresses:

$$\sigma_v = \sqrt{\frac{(\sigma_1 - \sigma_2)^2 + (\sigma_2 - \sigma_3)^2 + (\sigma_1 - \sigma_3)^2}{2}} = \sigma_1 - \sigma_3 \quad (4)$$

The maximum von Mises stress will occur when $r = r_i$, as σ_1 is maximized and σ_3 is minimized (and equal to 0), and thus $\sigma_v = \sigma_1$. Taking into account the material properties, the maximum allowable stress, which is the strength of the concrete, S , over the factor of safety, FOS , will be the von Mises stress at the maximum deployable depth.

$$\sigma_v = -\frac{S}{FOS} \quad (5)$$

The external pressure is also related to the depth as follows.

$$P_o = \rho_s g d \quad (6)$$

Simplifying Equations 1 and 2 and substituting for the values stated above, an equation for depth can be found:

$$d = \frac{2}{3} \frac{S}{\rho_s \cdot g \cdot FOS} \left(1 - \frac{r_i^3}{r_o^3} \right) \quad (7)$$

The external pressure, d, is then calculated. The numerical results are shown in Table 3.

σ_v , [psi]	-3333.3
σ_1 , [psi]	-3333.3
Pi, [psi]	0.0
ri, [in.]	15.0
ro, [in.]	18.7
Wall thickness, t [in.]	3.7
t/d	8.1
Po [psi]	1075.2
Depth [ft.]	2443.6

Table 3 Calculation of maximum deployable depth

It should also be noted that the concrete structure is required to be cycled (ie. pressurized and depressurized) potentially several times a day for many years. For the production device, the current thought is to have a 0.05atm internal pressure and 1 atm when the sphere is full, leaving 5% of the volume for air compression. The ratio of von Mises stress in the sphere when “full” to that when “empty” would thus be :

$$R = \frac{22.97 - 0.0051}{22.76 - 0.1013} = 1.013 \quad (8)$$

While the effects of cyclic loading on the planned concrete—self consolidating steel fiber reinforced concrete—have been investigated (Singh, 2004), it is still unclear at this early stage in development which concrete and pressures to use and further work will be necessary to correctly account for cyclic loading and other potential factors relating to sphere thickness.

The stresses throughout the wall thickness are shown in Figure 10 below. Notice the maximum stress occurs at the inner radius (15in.) and is tangential to the shell.

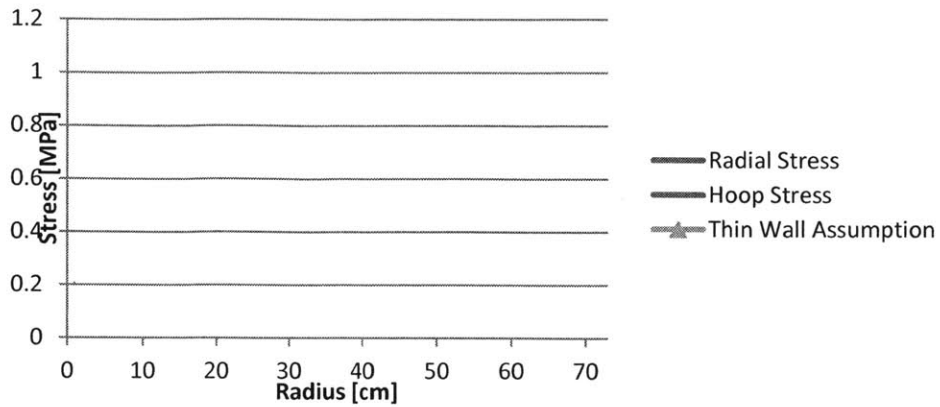


Figure 10: Radial and Hoop stress in the thick-walled spherical shell.

Using the same methods outlined above, the maximum deployable depth for a full size, 25 meter sphere with a safety factor of 1.5 is calculated for various wall thicknesses. The results of these calculations are shown in Figure 11. It can be seen here that the thin wall model has growing error as the wall becomes thicker.

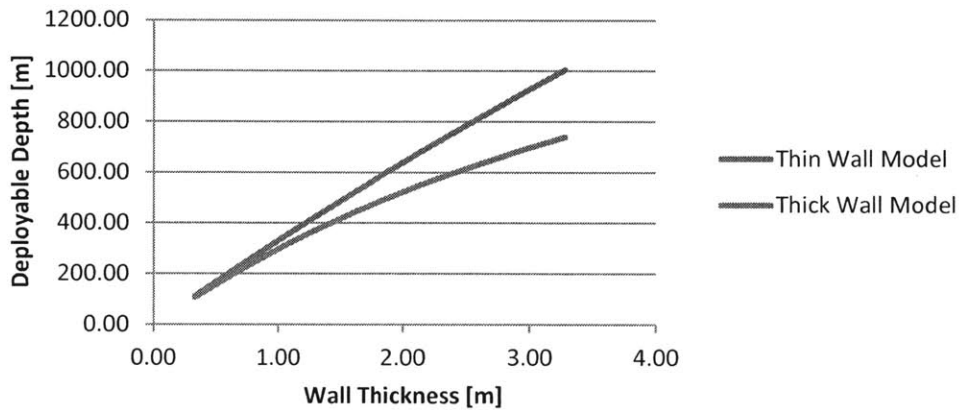


Figure 11: Maximum deployable depth for 25m spheres with varying wall thickness using both the thick-walled spherical shell model and the thin wall approximation

To connect the hemisphere to piping systems and to access the sphere generally, a pipe coupling was used as the spacer between the inner and outer molds and was embedded in the concrete. The seal made between the concrete and the steel coupling was found to be air tight. The embedded pipe coupling also served as a temporary lift point to lift the cured concrete hemisphere out of the lower mold. All lifts using the coupling were successful. However, additional reinforcements to the lift point would be suggested for further use of this practice.



Figure 12 A concrete hemisphere fresh out of the mold. The pipe coupling can be seen embedded in the pole.

Once the sphere is deployed, it will only be subject to the compressive forces of the water above it. Prior to that, however, it is possible that the spheres are subjected to a variety of loads from handling and assembly. While it would be possible to create a cage of conventional re-bar to withstand the tensile forces, it would greatly increase the cost of assembling the sphere (Fennell, 2011). With this cost in mind, the sphere is designed without any re-bar. Instead, either glass, polymer or steel fibre will be used for the full scale device. The type of concrete used here was self-consolidating and Kevlar® fiber-reinforced. The self-consolidating properties allow reduced or even no vibration of the concrete once it has been poured. The specific concrete selection was done by Newstress Inc. of New Hampshire.

At this scale, vibrating the mold as the concrete settles was simple and done by casting the hemispheres while the mold was on a vibration table. Large versions will not be vibrated so effective self consolidating concrete as well as proper mold design will be important to avoid trapped air pockets.

As mentioned above, the sphere is designed without re-bar. There were no indications during the creation of this concrete sphere that would indicate the need for re-bar in the future however, more work will be necessary in modelling and testing to determine the reinforcement method used for the full scale device.

4.3 Hemisphere Joint

To join the two hemispheres together a bonding compound was used. A bonding compound was selected over conventional fasteners because it simultaneously creates a seal between the two hemispheres and also reduces stress concentrations that features in the concrete, through holes or fasteners may apply. Since the bond is only required to handle low loads, a bonding compound capable of handling the load was easily found.

Originally, designs involved creating an annular ring with injection ports in the mating faces into which grout or epoxy could be injected. Since it was envisioned that the full scale device would be joined together via grout injection, the prototype followed suit. The annular channel can be seen in Figure 13.

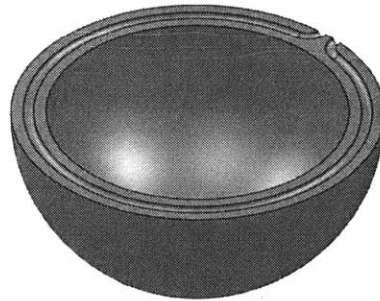


Figure 13: Annular channel with injection ports for epoxy injection.

The gap between the ports was purposefully left small such that enough epoxy would be able to leak across and bridge the gap, sealing the sphere. However, it had to be large enough so that the fluid resistance across it would still be more than the resistance of the channel itself; otherwise the epoxy would simply cross the gap and come out the other side instead of going around the circumference.

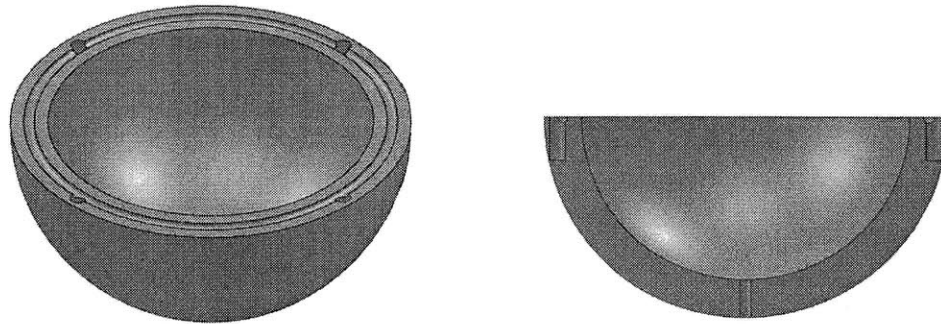


Figure 14: Left: Annular channel with stud ports. Right: Cross section of the same.

Further development brought about the idea of using a continuous ring, which is much easier to manufacture. A hammer drill would then be used to create two diametrically opposed ports; the inlet and outlet for epoxy. Several holes could further be drilled if it was found that the epoxy would not flow fast enough, allowing more to be injected further along the ring. Furthermore, to increase the strength at the interface, studs embedded in epoxy would sit in stud ports formed in the concrete and bridge the gap between the two hemispheres.

The channel for epoxy and the stud ports were all created simultaneously during the casting process using a steel ring with studs welded on, shown in Figure 15. The ring itself was selected to occupy the middle third of the joining faces thus a one inch steel pipe was rolled into a ring of the correct diameter. The stud ports were made by pressing a one inch diameter piece of backer rod onto each of the metal spikes welded onto the ring. The stud port and channel were thus both about one inch in diameter. To prevent the backer rod from sticking to the concrete, it was wrapped in plastic wrap. Unfortunately, the plastic wrap became embedded in the concrete; every fold and wrinkle giving the concrete a gripping point. Furthermore, the stud ports were made too deep such that the concrete at the blind end of the port was very thin on the side closest to the outer wall. This thin concrete failed easily and leaked. Ultimately, the studs were found to be problematic and unnecessary because they caused leaks and only served to provide strength across the joint that was not needed.

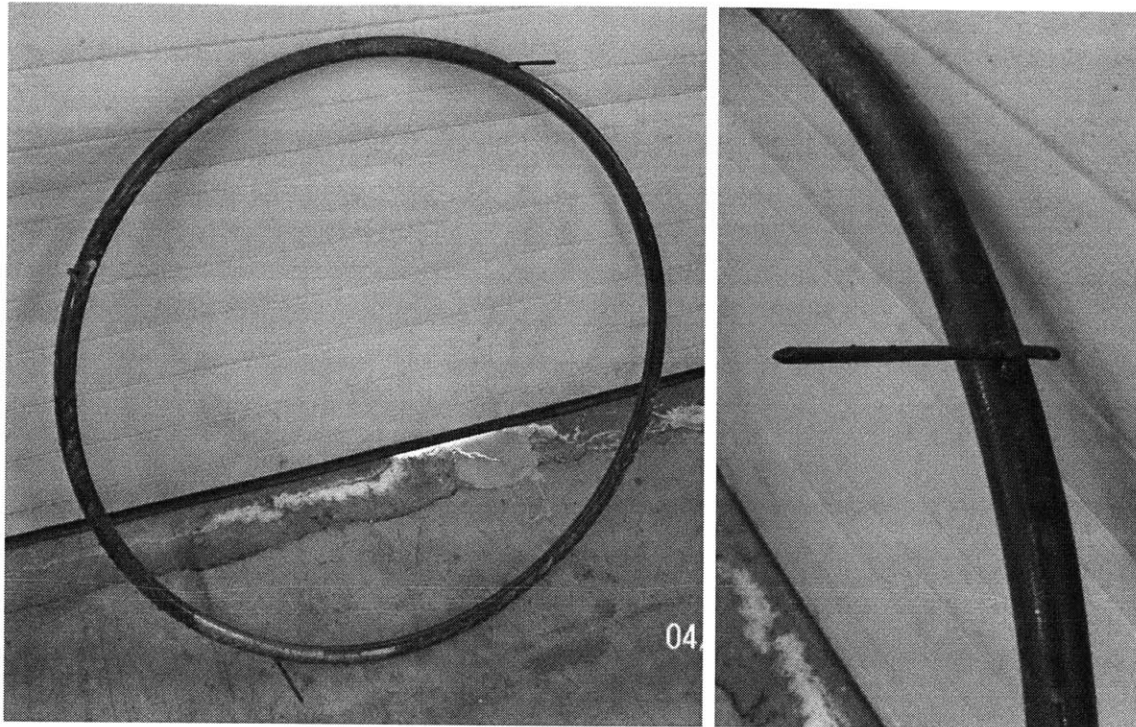


Figure 15: Steel ring with welded studs used to create the epoxy channels.

To inject the epoxy successfully, it must flow fast enough to reach the outlet before it begins to thicken. To accomplish this task, the epoxy must be pumped with sufficient pressure. Sikadur-32 from Sika Corporation was selected for its ability to bond to concrete and its high strength and stiffness. To determine if the required pumping pressure was reasonable and that suitable seals could be made to contain the epoxy, the following calculations, shown in Table 4, were performed using a Moody chart and the Darcy-Weisbach friction factor.

Working time [min.]	22
Target flow time [min.]	1
Dynamic viscosity, μ [Pa·s]	3.00
Channel diameter [cm]	2.54
Channel cross section [cm ²]	5.07
Channel length [m]	2.7
Minimum velocity [m/s]	0.00206
Target velocity [m/s]	0.0452
Flow rate [L/s]	0.0229
Density [kg/m ³]	1400
Reynolds Number	0.536
Flow Regime	Laminar
Darcy–Weisbach factor ($f=64/Re$)	119.4
Pressure Loss [kPa]	18.3

Table 4: Pressure drop of epoxy during injection.

The pressure loss, ΔP , was calculated from the friction factor as shown in Equation 9.

$$\Delta P = f \frac{l \rho v^2}{d \cdot 2} \quad (9)$$

The two mating faces, both being made of concrete, would not be able to form a seal to prevent the epoxy from leaking out so backer rod was to be placed between the two mating hemispheres to seal the epoxy channel. An outer ring and an inner ring of backer rod would be needed to surround the channel in which epoxy would be injected. Backer rod being difficult to lay out and given the low pressures stated above, it was decided that caulking be used instead; it is easy to lay out in any shape and can maintain its shape enough to plug large gaps (observed up to 0.5 inches). Figure 16 shows the hemisphere layed out with sealant and epoxy in the stud holes. The sealant used around the channel was Sonolastic NP-1 Polyurethane Sealant Caulking (white) while the stud ports were filled with Epcon A7 epoxy for its higher strength. The upper hemisphere had the studs epoxied in using the Epcon A7. It was then flipped over, suspended on a chain fall, brought into position above the lower hemisphere and lowered into place.

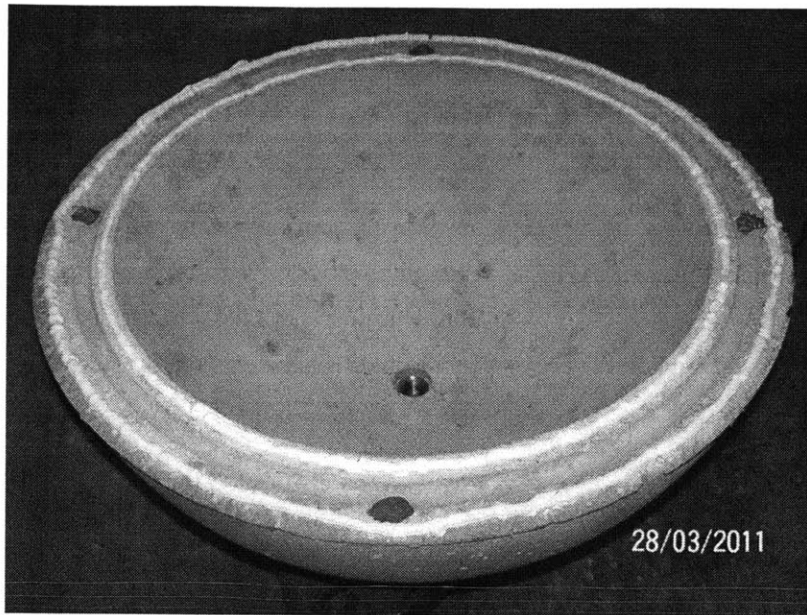


Figure 16: The lower hemisphere with sealant applied and stud ports filled with epoxy.

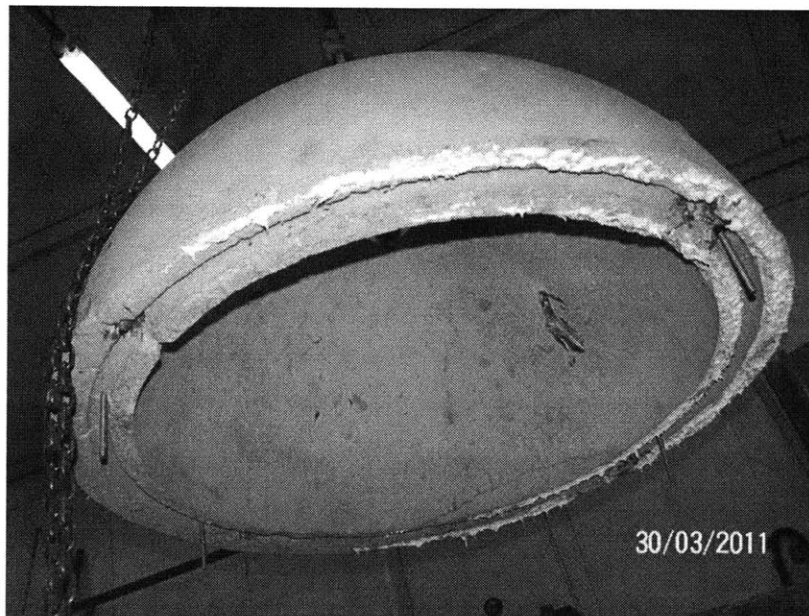


Figure 17: The upper hemisphere prior to being joined with the lower hemisphere. The four studs are visible, protruding downward from the upper stud ports.

Alignment between the upper and lower hemispheres was achieved by eye. This method was sufficient for the mating faces, shown in Figure 16 with the white caulking. However, the studs, whose ports

contain dark gray caulking in Figure 16, were difficult to align by eye and took several attempts. Due to the low pumping pressure and the theoretical simplicity of laying down a continuous bead of sealant, this approach was attempted but was unsuccessful. The end result had leaks from the channel to the interior of the sphere. The reasons for failure of this method are: 1. The surface of the concrete was very rough with large chips having been broken off the edges making the contact area between the mating faces very thin. 2. There was no way to verify that the sealant would bond and seal effectively before the upper concrete hemisphere was lowered into position. 3. It was not possible to test the seal until the sealant had cured and fused the two halves together. 4. The interior ring was no longer accessible once the two halves were joined. The assembled sphere, seen in Figure 18 below appears fully assembled but leaks considerably.

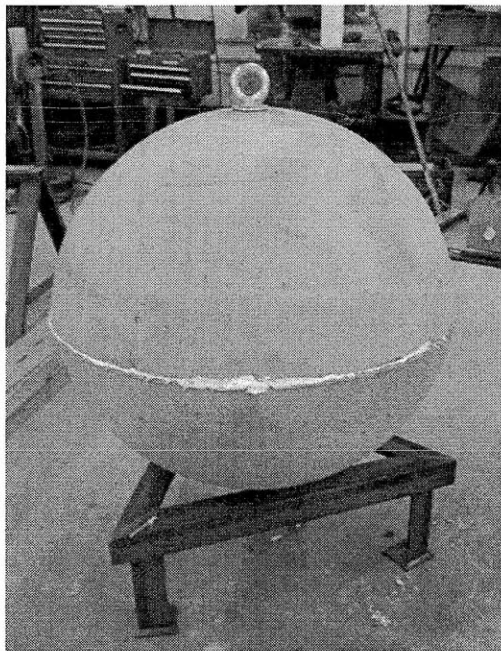


Figure 18: Assembled concrete sphere.

Once the two halves were joined together, it was found that one or more leaks existed on the interior ring seal that were not easily serviceable. However, since this device would only be subjected to external pressures (no internal pressure tests were planned nor undertaken), the channel for epoxy injection was abandoned and the sphere was sealed from the exterior. Instead of using an internal channel to seal the joint, an open channel was created at the interface with the channel depth sufficient to close the gap between the two hemispheres. Figure 19 show the channel cross section and the channel once filled with epoxy, which could easily be poured in from above. The same Sikadur-32 was used here. Once the open channel was filled with epoxy and cured, the equatorial seal was established and the joint was found to be leak free.

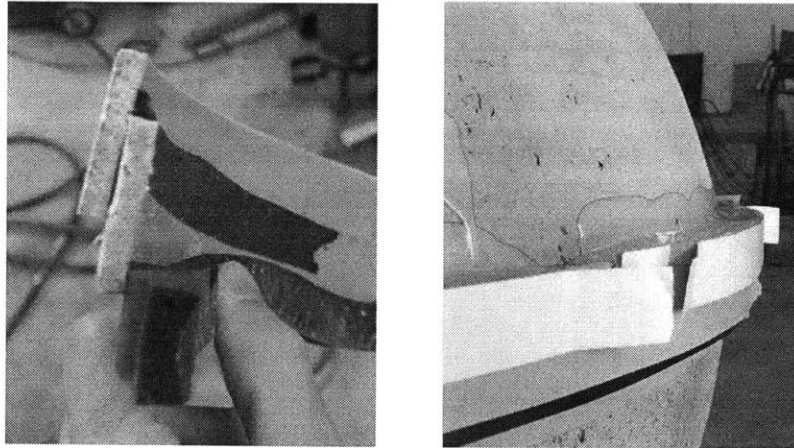


Figure 19: The open channel used to join the two hemispheres. Left: Cross section of the channel. Right: The channel filled with epoxy.

The stud ports were initially filled with Epcon A7 epoxy however, once the sphere was sealed using the open channel technique above, it became clear that the Epcon A7 had not created an adequate seal and air was leaking through the thin concrete at the base of the stud ports. This thin concrete showed cracks and gave way easily to even light taps with a hammer. To fix these leaks, the thin concrete was cleared, revealing the failed epoxy seal inside. Figure 20 shows the clear separation and failed bond between the concrete and the Epcon A7. The failure of these seals was due, in part to the plastic wrap used when making the stud ports. A large amount of the plastic wrap had to be removed in small piece through both the intended opening of the stud ports and the opening created by chipping away the thin concrete. Sikadur-32 was then filled into the ports to create a seal. Weather stripping was again used to retain as much Sikadur-32 as possible within the port. All the ports on the top side were filled, the sphere was then flipped over and the rest of the ports were filled. In the end, all eight ports had to be cleaned and sealed in this way.

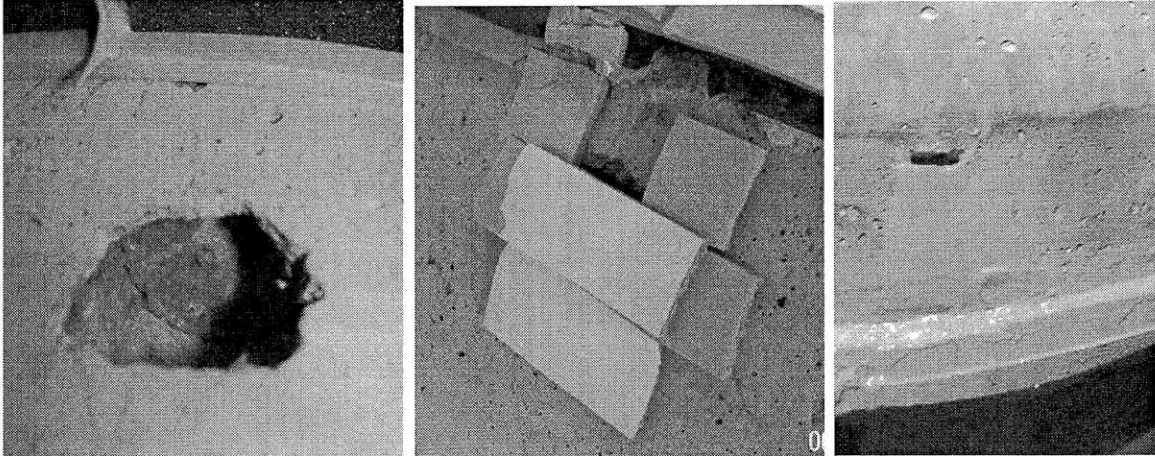


Figure 20: The failed stud ports. Left: Separation between the concrete and the epoxy within the stud port. A gap around the edge is visible. Center: Weather stripping retains the epoxy. Right: The sealed stud port.

On the far right of Figure 20, a large void can be seen on the sealed port. Despite this void, a gas-tight seal was achieved since the epoxy was able to achieve a good bond to the concrete over most of the stud port and the concrete is thick where the void appears. Once the stud ports and the joint between the two hemispheres were sealed, the sphere was successfully pressure tested and an acceptable leak rate was achieved.

4.4 Mold

To create the concrete hemispheres, a custom mold was designed and built. The mold consisted of two steel hemispherical heads of different diameter modified as needed, as well as a device to position the hemisphere relative to each other. These heads were taken from a 250 gallon and a 500 gallon LPG tank (Fennell, 2011). Using prefabricated heads greatly reduced the cost of creating the mold and required only modest concessions in the design. Nominal specifications were for a 1m ID sphere with a wall thickness of 8cm. The steel hemis found sized the sphere created here at 0.76m ID, with a wall thickness of 9cm. For the purpose of this prototype, that was well within the range of acceptable sizes.

While larger versions of the sphere will be cast vertically, resulting in a hemisphere more akin to the model in Figure 9, the current prototype was cast horizontally. Casting horizontally was acceptable because of its small size; handling the hemispheres would be possible using standard chain falls and hoists while a larger sphere would be much more costly to manipulate. By casting the hemispheres

vertically, manipulation is minimized. Another advantage of casting horizontally is that the flat surface is exposed allowing easy insertion of the concrete as well as it being easier to create features on the face.

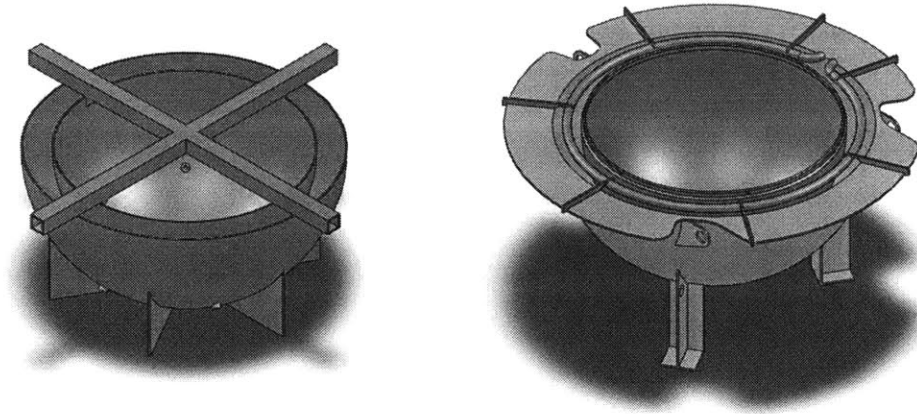


Figure 21: Early models of the mold.

Initial designs resulted in the models shown above in Figure 21. Further refinements to the joint design and consideration of the functional requirements listed below led to the final design shown in Figure 22.

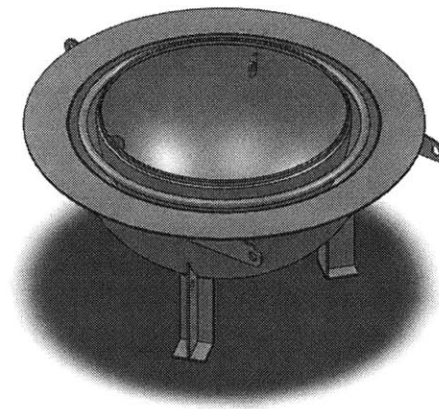


Figure 22: Model of the final mold.

Once the steel hemispheres had been found, they were modified towards satisfying the following functional requirements:

1. The concrete must easily release from the mold.
2. The mold must be easily manipulated when filled with concrete.
3. The inner steel hemisphere must be held in place securely so as not to move while concrete is being poured.
4. The inner hemisphere must be located in the center such that the resulting concrete wall thickness is uniform.
5. The mold must allow for the creation of features for the joint.
6. The mold must accommodate the coupling to be embedded in the pole.
7. The mold must be stable on a flat surface.

The first design feature included to facilitate de-molding is a draft angle on the inner hemisphere. To accomplish this, the inner hemisphere is simply raised up with a spacer, as shown in Figure 26 below. By moving the inner hemisphere up approximately 2.5cm, a draft angle around 4° is achieved. Concrete also shrinks as it cures (Kwon, 2008) which makes it possible for the concrete hemisphere to grab the inner steel one and bind it. Since it is our intent to have the mold be reusable, the inner steel hemisphere was fitted with lift eyes and threaded ports welded to the interior surface to aid in de-molding. Once the concrete had cured, chain falls would be connected to the lift eyes and the inner mold section would be lifted out. Should the concrete bind to the inner head such that the head could not be pulled off with the lift points, pressurized air or water could be injected through the threaded ports to release the mold. The threaded ports were closed off from the concrete with duct tape prior to the concrete being poured to avoid damaging the threads. In addition to these de-molding features, the surfaces of the mold would be covered in mold release prior to the concrete being poured. In this case, engine oil was sufficient as a mold release agent.

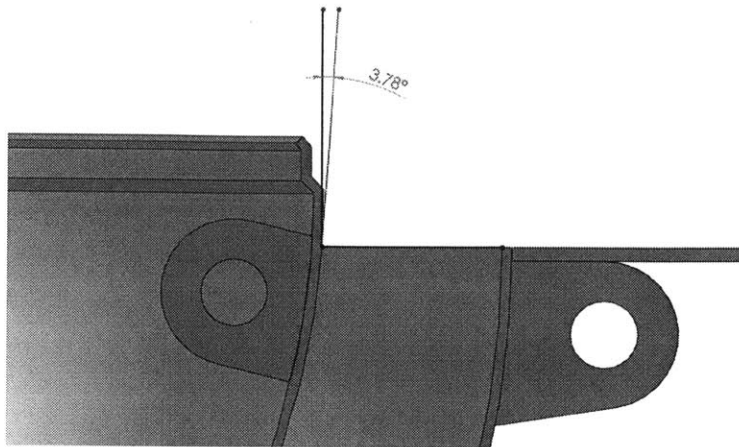


Figure 23: Draft angle on the inner hemispherical mold.

The outer hemisphere was not as much of a concern with respect to de-molding since the concrete's shrinkage would tend to disengage it from the steel. A draft angle was also added to the outer hemisphere by cutting the hemisphere down below the vertical section. As shown above in Figure 23, the inner steel hemisphere is joggled just above the vertical point. The outer hemisphere was joggled in this way as well but the joggle was removed with a plasma cutter because, firstly, the joggle would impinge on the concrete as it began to leave the mold. And secondly, by cutting it off a little further down, the draft angle mentioned above could be created. Once the joggle was removed, the edge of the hemisphere was less stiff so an equatorial flange was added. This flange also aided the pouring process since it made a bigger target for the cement truck and could be used to steady a trowel.

The inner steel hemisphere's lifting lugs were designed for a lift force equal to the weight of the mold when fully loaded with concrete. While they won't be used to lift the mold itself, lift point failure must be avoided even if the inner mold is so bound to the concrete that the mold lifts off the ground. The mold is expected to weigh 131kg when empty so with the concrete a total weight of 659kg is expected. The failure mode analysed is tensile failure on a plane perpendicular to the applied load; thus the two areas on either side of the hole. The applied load is assumed to be directed along the solid blue line shown in Figure 24. The thickness is predetermined since all of the lifting lugs, mold feet and the equatorial flange will be water-jet cut from a single plate of steel. As the hole in the lug must be large enough to accommodate the hooks available, the dimension to be found is the width of the lift eye. The following calculations were performed to determine the minimum size of the lug given a factor of safety of 5 in accordance with ASME B30.20 as reviewed by Williams (Williams, 2006).

Mass to lift [kg]	659
Number of lift points	3
Flift [N]	2155
Angle [degrees]	45
F_{applied} [N]	3047
Strength [Mpa]	200
FOS	5
$\sigma_{\text{allowable}}$ [Mpa]	40
Area [mm ²]	76.17
Thickness [mm]	6.35
Length [mm]	6.00

Table 5: Lifting eye calculations.

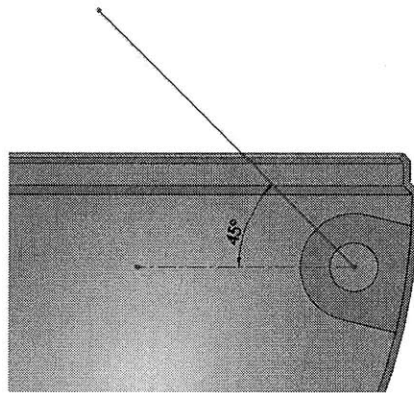


Figure 24: Lifting on the inner steel hemisphere and the direction of loading.

The outer hemi was modified in three ways: 1. It fitted with legs to prevent it from rolling, 2. The equatorial flange was added and 3. lifting eyes were added under the equatorial flange. The legs were T sections, each one being water-jet cut from steel plate and welded together so that a shape conformal to the sphere was made. Welding the foot to the sphere was stronger and easier to accomplish as a result. Three legs were used (instead of 4 or more) to prevent wobble on uneven surfaces. The equatorial flange was cut out of the same sheet of steel and welded on. This flange provides stiffness to the edge of the outer hemisphere and helps maintain circularity. The flange also provides support to the outer hemisphere's lifting eyes and facilitates the concrete pouring process. The flange's outer diameter was specified to be 1.2m (4ft.) so it could be cut out of a single 4'x4' sheet of steel. However, as cutting began the large piece began to warp out of plane. Internal stresses are suspected however the reason is unclear.

This deformation would have been problematic should the flange have required higher precision but simply clamping and welding the flange onto the hemisphere flattened it sufficiently. Should large parts need to be cut from thin plate, de-stressed material or a process of relieving internal stresses must be employed. The lifting eyes were included to allow the concrete hemisphere to be flipped over prior to de-molding to reduce the chances of handling damage. The lifting eyes also served as connection points for the vibration table. Despite self consolidating concrete being used, if too many voids were found, subsequent hemisphere could be vibrated.

Calculations for the outer lift eyes were conducted in the same manner as for those on the inner steel hemisphere. An FEA study was also conducted, in addition to the hand calculations, to verify the design. Several loading cases were evaluated to ensure that the lifting eyes would not fail at any point while the mold is flipped over under load. Figure 25 shows one of the cases.

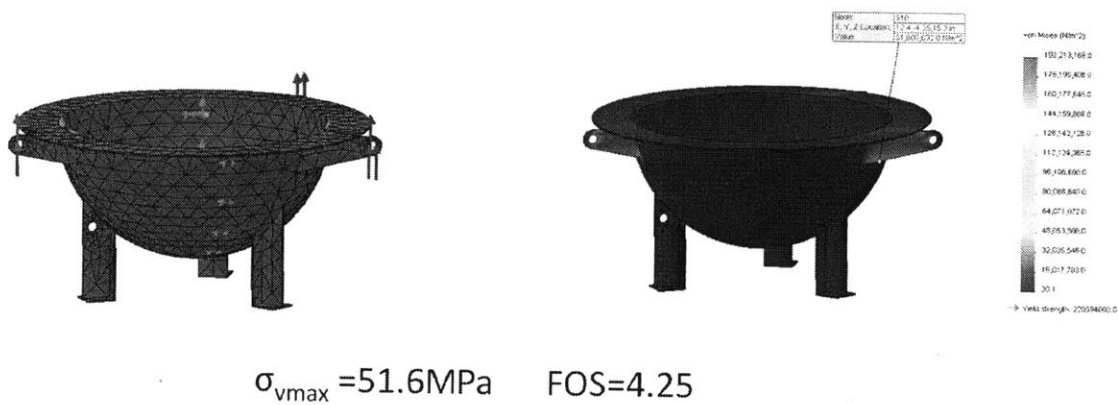


Figure 25: FEA of the outer mold. Loading case based on lifting the sphere.

To position the inner hemisphere, a threaded rod and spacers were used. The threaded rod was sized to be used as a lift point, in conjunction with a large washer, allowing the mold and concrete to be lifted from the pole. The spacer consisted of a pipe coupling in the middle and plastic spacers at the outside to give additional height and help seal the coupling against the steel hemisphere. A model of the configuration used is shown in Figure 26.

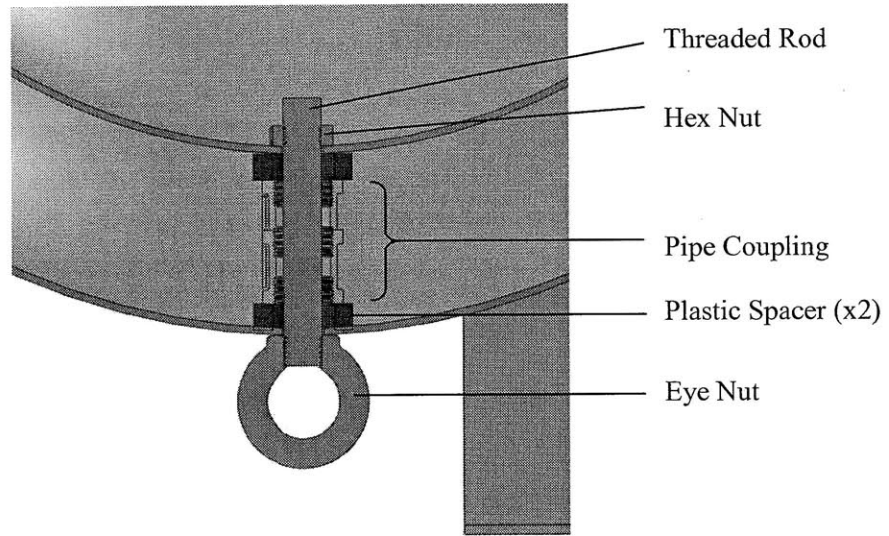


Figure 26: Model of the pole assembly.

It should be noted that because leakage of concrete onto the threaded rod was minimized, it was easily removed from the assembly allowing the concrete to be removed from the mold and at no point was bound to the internal threads of the coupling or otherwise.

4.5 Turbine

To store energy using the concrete sphere, rotating equipment was needed. In one direction, efficient energy collection was needed and in the other, efficiently created pressure and flow were required. The functional requirements of this equipment were:

1. The device must be capable of operating in both directions at the head available from the tower.
2. The flow rates must enable the sphere to be filled and emptied several times in one day.
3. Reasonable efficiencies must be achieved in both directions.
4. It must be small enough to be mounted on or within the sphere.
5. It must be inexpensive.
6. It must use DC power

DC power was used to simplify the measurements of electrical power in and out of the device. Had AC been used, it would have been very difficult to accurately record power and energy usage.

With these criteria in mind, devices were evaluated and, initially, the use of a combined pump/turbine device was explored. Available small turbines, such as Pelton, Turgo, Francis, Kaplan and propeller type are either very expensive, very poor pumps or not reversible at all so pumps were instead evaluated for use as turbines. Diaphragm and piston pumps are not typically reversible. Flexible vane pumps are also not reversible due to the friction of the flexible vane against the housing. However, centrifugal pumps have been successfully deployed and are commercially available as turbines (Andritz, 2010) and it was hoped that this design could be inspired by those past successes. Unfortunately, centrifugal pump could not be used. While there is literature describing methods of predicting pump performance when used as a turbine (Singh, 2011) and a large variety of centrifugal pumps commercially available, a pump could not be found that satisfied all of the requirements listed above nor was it practical to model and predict the performance of these devices. A custom built pump/turbine was also considered but outside the scope of this study. Without any way of viably using a single device, a two device system was conceived where a separate pump and turbine would be used that could independently be optimized for efficiency.

For larger ORES prototypes and possible production models, the rotating equipment would be similar to what is used in existing pumped hydro energy storage facilities. These facilities make use of a specially designed runner as shown in Figure 27. These types of runners are designed for high efficiency in specific applications (usually grid scale) and are available in the sizes needed here. A runner of this type was not a viable option for this prototype. These runners are capable of delivering high performance within the depth range that a future ORES system would be deployed to, however further work must be undertaken to specify the rotating equipment for future systems.

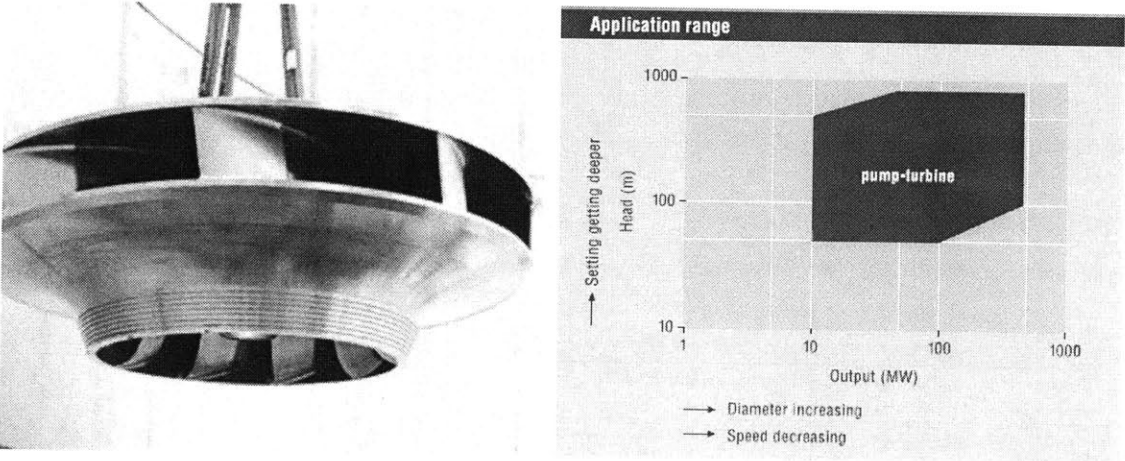


Figure 27: A reversible pump/turbine. source: www.voithydro.com

The functional requirements of the turbine as a stand-alone piece of equipment are the same as those of the pump/turbine, (requiring the device to work at the head and flow ranges needed, etc.) except for the pump specific requirements. To facilitate the selection of a turbine, the functional requirements were developed into design parameters. The target specifications are listed in Table 6.

Sphere I.D. [m]	0.762
Sphere volume [m ³]	0.232
Minimum time to fill [minutes]	5
Flow rate [L/s]	0.77
Head [m]	15.0
Head Pressure [kPa]	144
Vacuum Pressure [kPa]	101
Effective head pressure [kPa]	245
Efficiency	75%
Power [W]	142

Table 6: Minimum specifications for the turbine unit (shown in red). Values used to estimate the specifications are shown in black.

Turbines of this size exist for micro hydro power applications but the market for this size of turbine is very small and as such, there are very few options available to the designer looking to avoid customization. Despite 15m being a very low head for conventional hydro, this height is falls under high head micro hydro by many vendors classification. Only two types of turbines are made in this size range for high head sites: Pelton and Turgo types. These are the simplest to construct and are the least expensive by far, with the Turgo being less expensive still. Due to the small number of vendors and limited demand for micro-hydro devices, the performance of the devices available is not well documented. Figure 28 shows the turbines available that meet or potentially meet the specifications. After contacting the vendors directly, additional information was gathered regarding the capabilities of the vendor and lead times for acquiring the turbine assemblies.

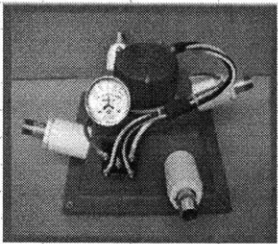
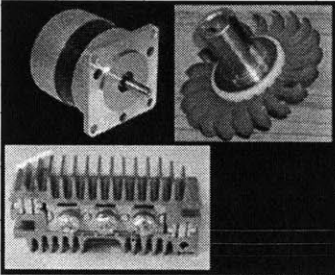
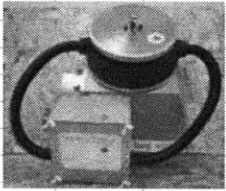
	Model	Maker	Price	Notes
	LV750	Hydro Induction Power	\$1,450.00	1 Nozzle model. Turgo turbine. Nozzle size adjustable to control flow
		Nominal	Operating point	
	Head [ft]	46-208	69	
	Flow [gpm]	3.2-107	9.9	
	Power [W]	750	49	
	Efficiency	40-65	40	
<hr/>				
	Model	Maker	Price	Notes
	MHG-500HH	Rocky Hydro	\$ 838.95	Custom casings are built on order (longer lead time)
		Nominal	Operating point	
	Head [ft]	65	65	
	Flow [gpm]	9	9	
	Power [W]	?	?	
	Efficiency	?	?	
<hr/>				
	Model	Maker	Price	Notes
	Stream Engine	ES&D Ltd	\$2,345.00	1 Nozzle model. Turgo turbine. Customizable Nozzle
		Nominal	Our Operating point	
	Head [ft]	9-450	65	
	Flow [gpm]	10-150	10	
	Power [W]	1000	60	
	Efficiency		49%	

Figure 28 Available turbines capable of meeting the project requirements.

The LV750 from Hydro Induction Power Inc. was selected based on the versatility of the turbine unit, dependability of the supplier and robustness of the casing which would have to be altered to be mounted on the sphere. The unit allows easy changes of the nozzle which, as the tightest constriction, can be used to regulate the flow rate.

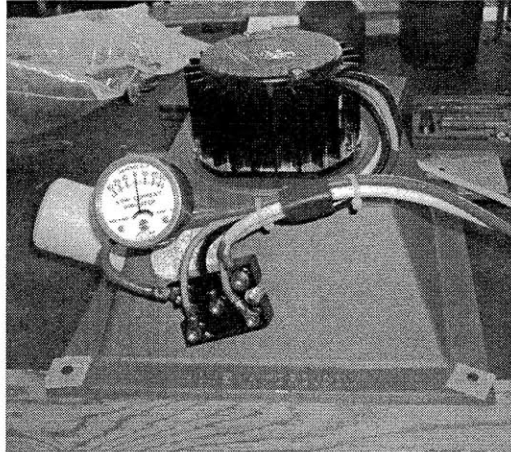


Figure 29: The LV750 fresh out of the box. The nozzle port is seen protruding from the left of the turbine casing. The generator is shown connected to the rectifier that was included with the turbine.

The LV750 has a turgo turbine coupled directly to a Transmagnetics Inc. 4'' brushless DC motor which is supplied for use as a generator. The housing is cast aluminum and is open at the bottom allowing water to disperse after striking the turbine. The turgo runner itself is 10cm in diameter and is supplied by a single nozzle. The nozzle is housed in a port that can accommodate nozzles up to 16mm in diameter. The manufacturer-measured flow rates associated with various nozzle sizes are shown in Table 7. Notice that the speed of the turbine depends solely on the pressure at the inlet. While other factors not shown in this table affect the speed, the flow rate does not. The efficiency of the turbine is also stated by the manufacturer and is summarized in Figure 30.

FLOW THROUGH NOZZLES IN GPM AT VARIOUS HEADS													
Feet	Psi	1/8"	3/16"	1/4"	5/16"	3/8"	7/16"	1/2"	5/8"	3/4"	7/8"	1.0"	RPM for 4" Turbine
5	2.2	-	-	-	-	6.18	8.4	11	17.1	24.7	33.6	43.9	460
10	4.3	-	-	3.88	6.05	8.75	11.6	15.6	24.2	35	47.6	62.1	650
15	6.5	-	2.68	4.76	7.4	10.7	14.6	19	29.7	42.8	58.2	76	800
20	8.7	1.37	3.09	5.49	8.56	12.4	16.8	22	34.3	49.4	67.3	87.8	925
30	13	1.68	3.78	6.72	10.5	15.1	20.6	26.9	42	60.5	82.4	107	1140
40	17	1.94	4.37	7.76	12.1	17.5	23.8	31.1	48.5	69.9	95.1	124	1310
50	22	2.17	4.88	8.86	13.6	19.5	26.6	34.7	54.3	78.1	106	139	1470
60	26	2.38	5.35	9.51	14.8	21.4	29.1	38	59.4	85.6	117	152	1600
80	35	2.75	6.18	11	17.1	24.7	33.6	43.9	68.6	98.8	135	176	1850
100	43	3.07	6.91	12.3	19.2	27.6	36.6	49.1	76.7	111	150	196	2070
120	52	3.36	7.56	13.4	21	30.3	41.2	53.8	84.1	121	165	215	2270
150	65	3.76	8.95	15	23.5	33.8	46	60.1	93.9	135	184	241	2540
200	87	4.34	9.77	17.4	27.1	39.1	53.2	69.4	109	156	213	278	2930
250	108	4.86	10.9	19.9	30.3	43.6	59.4	77.6	121	175	238	311	3270
300	130	5.32	12	21.3	33.2	47.8	65.1	85.1	133	191	261	340	3590
400	173	6.14	13.8	24.5	38.3	55.2	75.2	98.2	154	221	301	393	4140
3/4" NOZZLE HOLDER									TURGO ONLY				

Table 7: Flow rates for various nozzle sizes in the LV750 micro-hydro turbine. Source: Hydro Induction Power

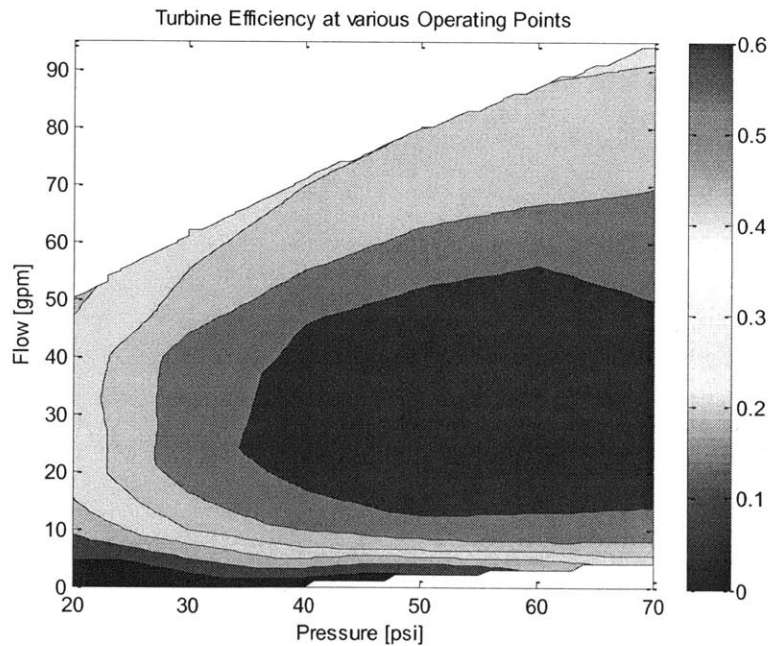


Figure 30: Turbine efficiency as stated by the manufacturer.

The efficiency was calculated by the manufacturer in the following way:

$$\eta = \frac{VI}{\rho gHQ}$$

Where H and Q are set specifically while I was measured. These tests were conducted with the turbine connected to a 24V battery bank being charged at 28V, thus V in the equation above was 28.

The method of power measurement and efficiency calculation used by the manufacturer makes sense in the context of charging batteries with the turbine—its typical commercial use—but for the purpose of maximizing energy storage, it is not ideal. To maximize efficiency, the manufacturer’s chart was used as a guideline however it was not the only input into tuning the system. For a given head and flow rate, different efficiencies were achieved by changing the electrical load applied. Thus, the efficiency is a function of the load, the flow rate and the head. The characteristics of the turbine such as bearing friction also play a role but were not observed to change in any way over time.

Due to the nature of a turgo turbine, behaviour of the rotor does not communicate back upstream. In other words, a slowing of the rotor does not change the backpressure on the penstock. Water will flow into the turbine at the same rate and fill the sphere in the same amount of time regardless of turbine activity. As such, for a given flow rate, the maximum efficiency is achieved when the power output is maximized; this behaviour making it much easier to bring the system to its best efficiency point (BEP) as variables affecting efficiency can be changed independently. Since the height of the tower is fixed, the head cannot be adjusted. The flow rate can thus be controlled directly via nozzle selection. So the flow is set by selecting a nozzle and the electrical load is varied until maximum output is achieved. The turgo runner and nozzle placement are shown in Figure 31.

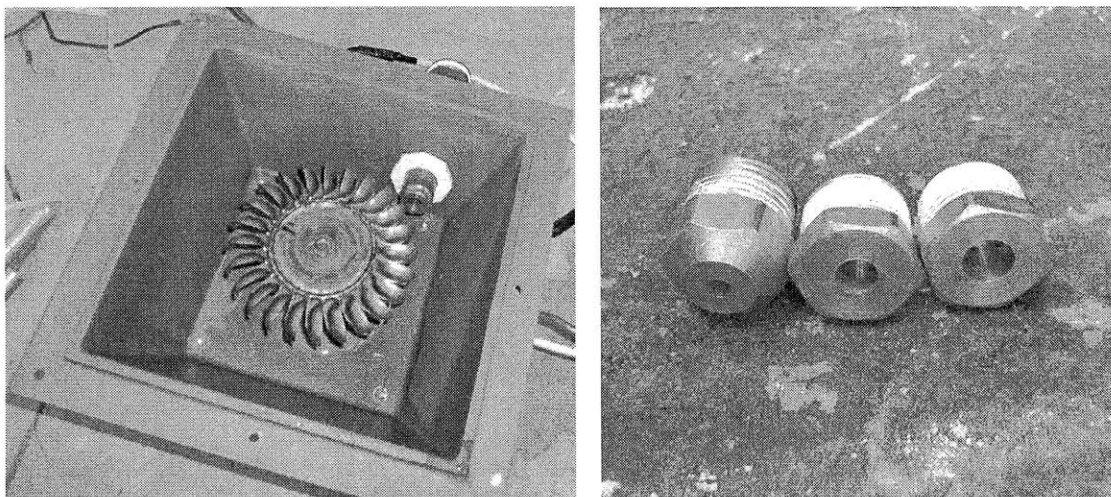


Figure 31: Left: The turgo turbine runner and nozzle. Right: Several of the different nozzles used.

The outlet of the turbine was required to be connected in an airtight manner to the upper pole of the sphere so that the sphere could collect the discharged water. The base of the turbine housing is entirely open so a plate or pan was needed to collect the water. While pans would provide more volume for exiting water to pool below the turbine, a steel plate was used for simplicity of construction. The steel plate was made to be bolted to the bottom of the turbine housing. A pipe coupling or stub could then be welded to the plate, once an appropriate hole had been cut, and piped to the sphere. A number of sensors and ports were also required to allow water and air into and out of the sphere and sense pressure. Initial designs had a 1-1/4" pipe coupling welded to the plate and piping of the same size running to the sphere. A number of pipe fittings were included between the sphere and the turbine for the ports and sensors. This assembly is depicted in Figure 32.

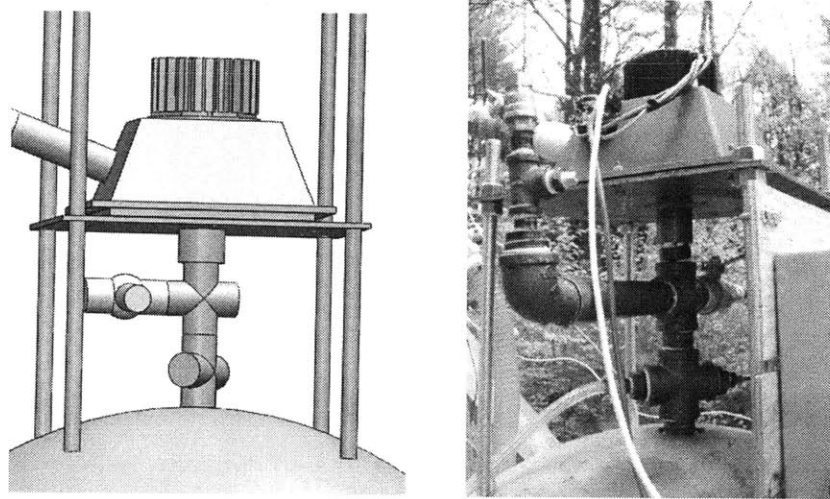


Figure 32: First iteration of the turbine draft tube.

To seal the turbine to the plate, initially, a rubber gasket was used. However, to achieve a seal using a gasket and bolts requires a substantial number of bolts, given the geometry of the joint and the stiffness of both the plate and casing. The gasket was eventually abandoned for the use of silicone liquid gasket, whose adhesive abilities and flexibility allow much less compression to be used in order to achieve an airtight seal.

This design was initially successful, while low flow rates were being tested. Upon higher flow rates being introduced into the turbine, the turbine housing quickly flooded. Due to the geometry of the water collection plate and the diameter of the outlet, water was not leaving at a sufficient rate. It was then undertaken to widen the turbine outlet and eliminate constriction between the turbine and the sphere. A 6 inch diameter connection from the turbine to the sphere was devised. A modified pipe stub was thus

welded onto the turbine bottom plate after a larger hole was flame cut into the plate, thus removing the pipe coupling used previously. To connect the 6'' pipe to the sphere without any constrictions, a large bore hole was cut into the sphere at the pole using a core drill. The pipe could then be glued into the bore hole.

Since no fitting were to be used between the turbine and the sphere, the ports previously on fittings had to be reintegrated into the system. This was accomplished by welding pipe coupling directly to the 6'' diameter pipe stub, and again cutting the appropriate holes. To facilitate welding, counter bored radial holes were drilled in the pipe stub at mid length such that the pipe coupling could rest on the counter bore during welding and, once welding was completed, no flame cutting would be required.

The model and implementation of the 6 inch pipe stub addition can be seen in Figure 33.

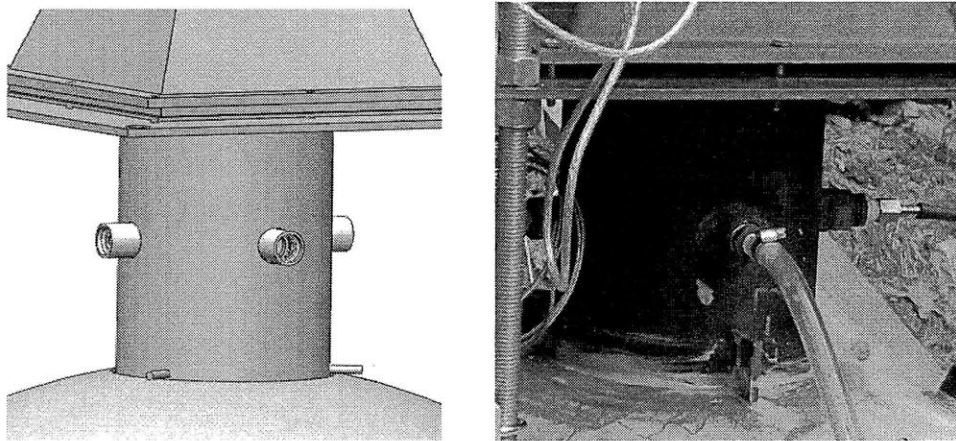


Figure 33: 6 inch turbine draft tube. Model and completed installation.

With the 6'' pipe in place, pooling was eliminated in the turbine casing and much higher flow rates could be achieved as the available head became the limiting factor for increased flow, instead of the outflow from the turbine casing.

While the connection between the turbine casing and the sphere was air-tight, the turbine casing itself was not. The interface between the generator and the casing was not sealed in the factory, nor was it designed to be. Since the turbine was coupled directly to the generator, any changes in the position of the generator relative to the casing would cause the water jet exiting the nozzle to strike the turbine at the wrong angle. While modification to the casing and the generator could have allowed a seal between the two, it was thought easier to create a cap which would go over the generator and seal to the casing. The cap would also need to allow power to be passed out from the generator. Since the pressure to be contained was

relatively low, caps of plastic as well as steel were designed. The design selected consists of a flanged steel pipe stub with a steel plate welded on to close off the un-flanged end. The turbine casing was drilled and tapped in 4 places and the flange was drilled with clearance holes to mate. Silicone liquid gasket was then used to create a seal. A ½ inch size pipe stub was also welded to the plate such that a bulkhead fitting could be used to pass electricity out. The model and finished assembly is shown in Figure 34 and the bulkhead fitting is shown in Figure 35.

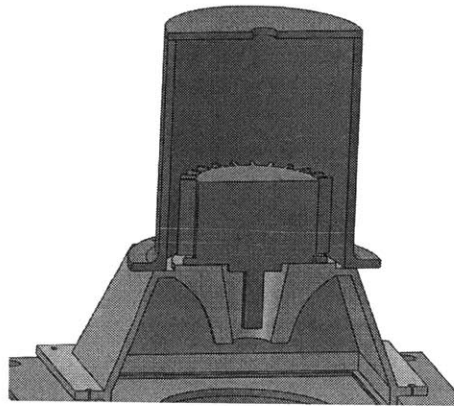


Figure 34: Model section view of the generator cap, showing the turbine casing, generator and cap. Coloured to distinguish the separate components.

The bulkhead fitting was made by taking a plastic pipe adapter—one side with ½ in NPT—and running 3 wires through it. The wires were stripped where the seal was to be made and the interior of the fitting was sanded lightly to improve adhesion. The end of the fitting was then closed off with hot glue and filled from the other side with epoxy in two batches. It was done in two batches to avoid melting the hot glue or the pipe fitting since the epoxy heats up as it cures.

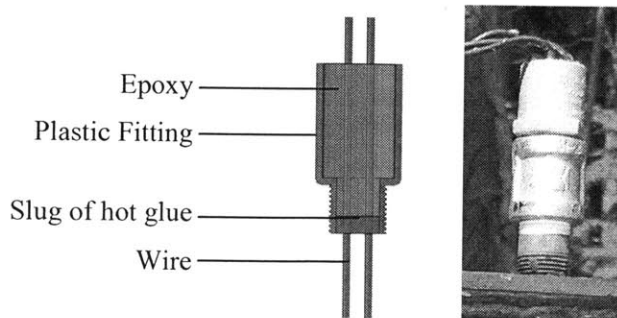


Figure 35: Right: Model section view of the bulkhead fitting. Note that the fitting has three wires; one is not visible due to the sectioned view. Left: The completed bulkhead fitting (grey fitting at top) is shown fastened to the generator cap via a pipe coupling.

4.6 Pump

Selection of the pump was much less constrained than the selection of the turbine as many more pumps in this size range are available. The pump was to be connected to the sphere via the pipe coupling embedded at the lower pole of the sphere and was required to empty the sphere, returning the water to the high reservoir, for all test cases. As such, functional requirements for the pump are as follows:

1. The pump must develop sufficient head to push water back up to the tower at maximum vacuum in the sphere.
2. There is no limit on the flow rate of the pump but it must not take so long as to disallow several test runs in a given day. The flow rate must also not be so high that significant piping losses are incurred. These flow rates must be developed at the head desired.
3. Since some tests involve low initial pressure in the sphere, the pump should have a low requirement for net positive suction head (NPSH_r). Pumps that rotate at higher speeds accelerate the pumped fluid to a higher speed internally and are more likely to have a higher NPSH_r as a result. A lower speed pump is thus desired.
4. Does not need to be self priming as it will be located below the sphere, allowing water to flow spontaneously to it. However, it should be able to run dry for a short period of time and be robust in the face of short periods of cavitation as testing may involve taking into those regimes temporarily.
5. Maintenance and pump life are not a concern as testing will involve very few hours compared to the operational lifetime of any commercial pump. However, the pump will be left outdoors for an extended period and it should not be rendered inoperable due to corrosion, or any other, during that time.
6. The pump should be as inexpensive to purchase as possible. Lifetime costs for the pump in this application are equal to its purchase price so the purchase price should be minimized to minimize overall cost.

An estimate of the head, flow and power specifications for the pump are shown in Table 8.

Parameter	min.	max.
Minimum time to fill [minutes]	5	30
Flow rate [L/s]	0.77	0.13
Head (tower height) [m]	15.0	
Vacuum Head [m]	10.3	
Total head [m]	25.3	
Efficiency	0.5	
Power [W]	383.8	64.0

Table 8: Pump performance requirements.

Centrifugal pumps are often the least expensive and so were evaluated first. The centrifugal pumps evaluated were all incapable of developing sufficient head. High head centrifugal pumps were found to satisfy the head, flow and power requirements but operated at 3600rpm; the high speeds making them more susceptible to cavitation. In the end, a centrifugal pump was not found that would be acceptable for this application. Given that a relatively low NPSH is required, lower speed pumps were more desirable. With positive displacement pumps being generally lower speed, several were evaluated. Piston pumps can be operated very slowly and would be able to accommodate very low NPSH requirements, however, at those slow speeds and the flow rate would be too slow and larger piston pumps would not be financially viable. A rotary vane pump was selected, satisfying all of the above mentioned requirements. The unit selected was the PO4060 from Clark Solutions Inc. which operates at 1725rpm to deliver .55L/s. The pump's flow is shown over a range of pressures in Figure 36.

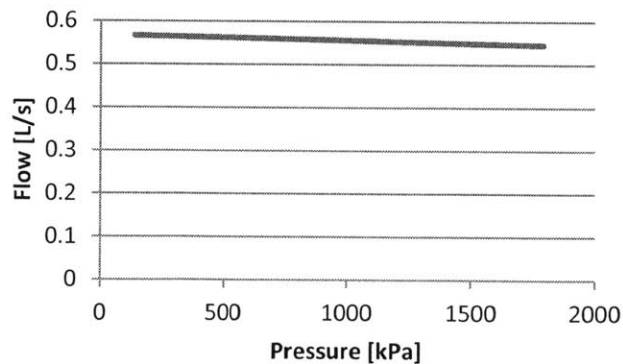


Figure 36: Pump performance curve as given by the manufacturer.

Once the pump was selected, the pump's power requirements could be known in greater detail and were estimated using the empirical formula provided by the pump manufacturer, shown in Equation 10.

$$Power = (3.265 \cdot 10^{-5} \cdot \rho_f g H + 8.8) \cdot \frac{n}{84.52} \quad (10)$$

In Equation 10 above, H is the head in meters, n is the rotational speed of the pump in rpm and power is given in Watts. With a 25.3m head and a rotational speed of 1725rpm, the required power is 345W. A ½ horsepower (373W) DC induction motor with a rotational speed of 1800rpm was then selected. The 3/8” diameter shaft and NEMA 56C flange mount required by the pump were also matched in the motor selection. The pump and motor were then coupled with the appropriate hardware which was supplied with the pump. The assembled pump was then mounted on a skid via the motor’s base plate. The skid supported the pump and allowed it to be easily joined with the sphere and remaining system components. The maximum size of particle tolerable to the pump was 20µm so a filter was added to the system just upstream of the pump.

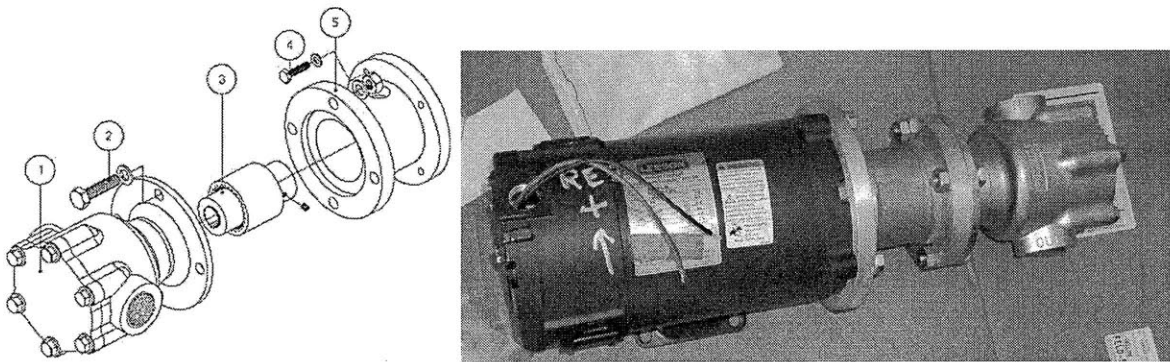


Figure 37: Left: A schematic drawing of the pump(1), motor coupling(3) and flange adapter(5). Right: The pump coupled to its motor.

4.7 Electrical

The purpose of the electrical system was to provide power to the pump and to provide a load to the turbine in such a way that the flow of electricity to any component could be easily and cheaply measured. To that end, the electrical system was entirely DC as it is much more complicated to measure power in an AC circuit. Two simple circuits were created; one each for the turbine and the pump. Both circuits contained elements which facilitated power measurement and fuses to prevent equipment damage in the case of a surge. The majority of circuit elements along with the data acquisition module were housed in a weather-proof box to protect them from rain and the general outdoors, as shown in Figure 38. Information concerning the data acquisition system can be found in section 4.8.

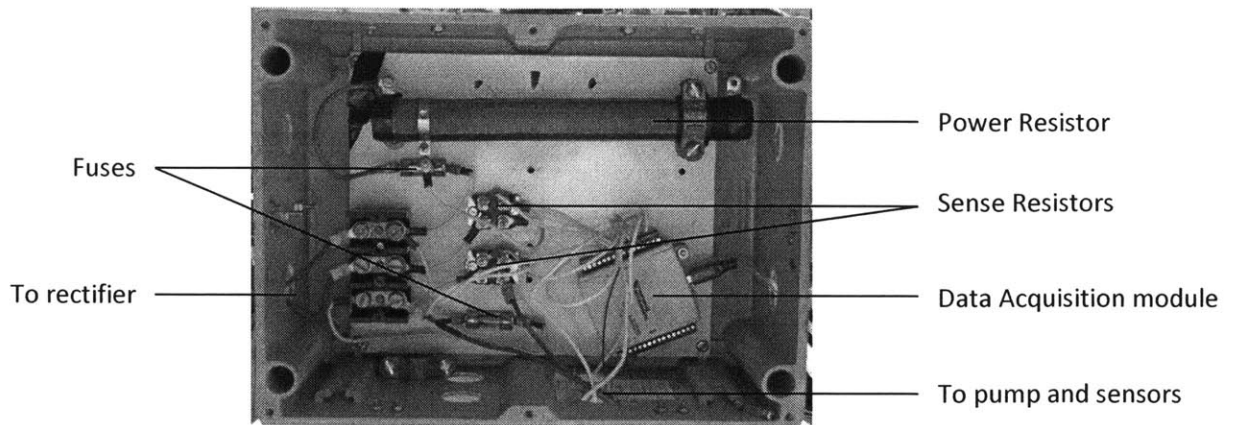


Figure 38: Electrical system box.

4.7.1 Turbine Circuit.

The turbine circuit's main components were the turbine generator, a rectifier and an adjustable power resistor. The turbine generator was a 12 pole brushless DC motor and is shown with the top cover and bearing removed in Figure 39. Of the four wires that can be seen exiting the bottom of the casing, one of them carries unused control wires for running the generator as a motor and the other three carry the 3 phase AC current that the generator produces when it is turned.

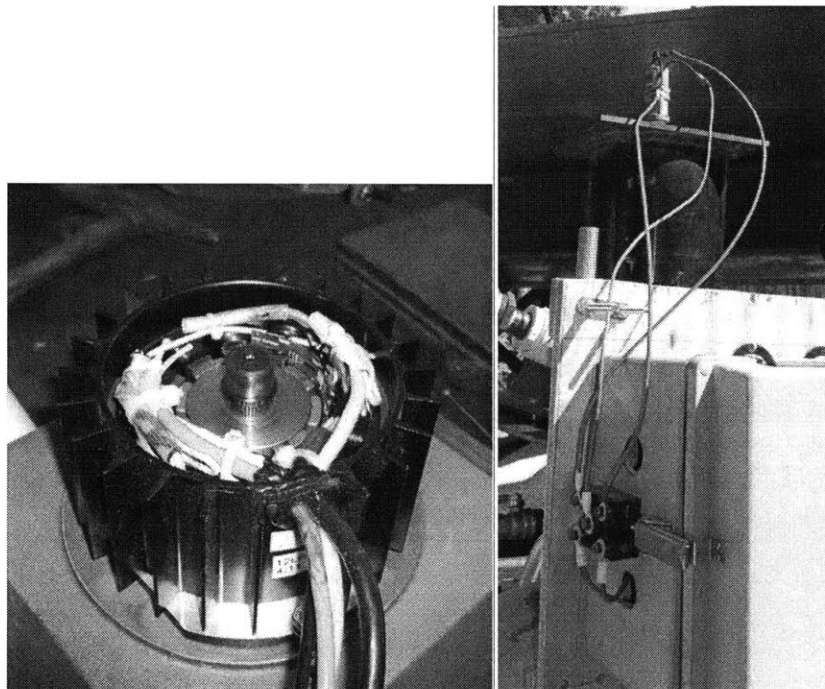


Figure 39: Left: The generator with its top cover and bearing removed. Right: The connection between the bulkhead fitting and the rectifier.

The generator is wired directly to the rectifier which transforms the 3 phase AC into DC current. The DC current then runs through a fuse and to the adjustable power resistor. The power resistor is rated to 1000W and can be adjusted to resistances between 1 and 25 Ω . The power resistor was sized to handle the maximum output of the turbine. To determine the resistance range, the turbine's output was assumed to have a minimum voltage of 12V. The unit was designed to charge batteries at up to 28V so a 12V minimum was a conservative estimate. With the turbine producing 142W (estimated in figure [###]) at 12V, the output current would be 11.8A. The load resistance at that operating point would be 1.02 Ω thus a minimum resistance of 1 Ω is acceptable. At the other end of the scale, if 28V is output, the current will be 5.1A and the resistance required will be 5.5 Ω .

Given the currents estimated above, a fast-acting fuse was selected to break at 15A. 12AWG wire was used for long runs and 16AWG was used for short runs between adjacent circuit elements.

After the power resistor, a sense resistor was connected to measure the current. The higher the sense resistor's resistance, the more accurate the reading since the voltage across it is measured. Given $V=IR$, the resistance is the gain between the current being measured and the reading. However, the higher the resistance, the higher the amount energy the sense resistor will have to dissipate. With a target for dissipated energy of about 10W, a 0.1 Ω resistor was chosen. Despite the resistor being rated to 100W, higher temperatures change the characteristics of the resistor so heating was kept to a minimum.

4.7.2 Pump circuit

The pump circuit served to power the pump and to allow easy measurement of the power being delivered. To provide power, a ZeroUp 800W programmable DC power supply from TDK-Lambda Inc. was used which could deliver up to 24A at 36V. The operating voltage of the pump was 24V so the power supply was set to provide a constant voltage at 24V and the current was then measured to determine the power. The LRA of the pump motor was below 20A so a current limit of 22A was also set. The pump was then started and stopped by pressing the OUT key on the power supply, which initiates its output. The external control connector on the rear panel of the power supply was configured for a single load and single connection, as depicted in Figure 40.

A fast acting fuse set to break at 30A and a sense resistor were also included in the circuit. The same considerations were taken when selecting this sense as with that of the turbine circuit and a 0.01 Ω resistor was chosen, again with a rating of 100W.

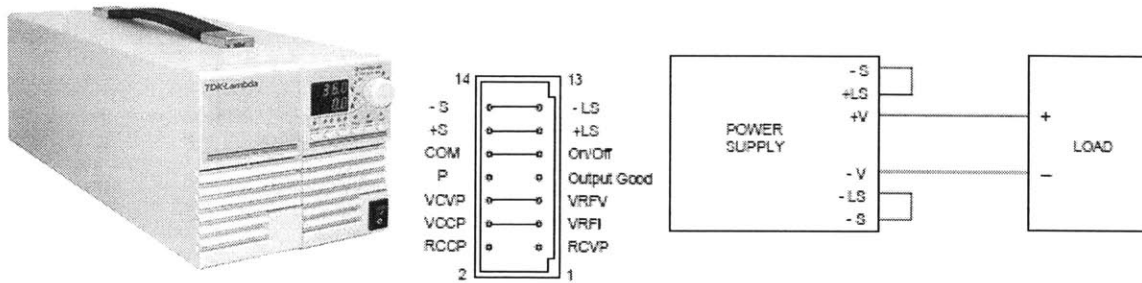


Figure 40: *Left: The TDK-Lambda Zup36V-24A. Source: datatec.de. Center: The external control connector on the rear panel of the power supply; the horizontal lines indicate jumpers between connecting ports. Source: User manual. Right: Connections on the rear panel of the power supply. Source: User manual.*

4.8 Data Acquisition and sensors

Data was acquired and recorded through the use of a USB-6009 data acquisition module and LabView both from National Instruments. The USB-6009 has a maximum sampling rate of 10kS/s and a resolution of 13 bits. The maximum input voltage on a single channel is 10V but two channels can be used for a total of 20V differential on one reading. The unit has 8 analogue input channels, a 32-bit counter, a 5V supply port, several grounds and several other ports that were unused. The input impedance on the analogue channels is 144kΩ. The unit is shown in Figure 41.

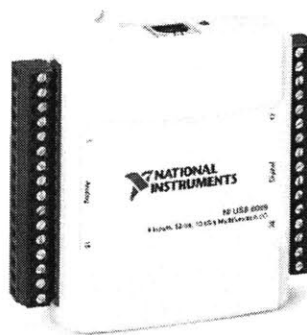


Figure 41: *USB-6009 Source: ni.com.*

Connections to the unit were as shown in Table 9.

Terminal	Connected to:
A0	Unused
A1	Pressure transducer
A2	Pump sense resistor (for current)
A3	Turbine voltage + (used with A7)
A4	Pressure transducer
A5	Pressure transducer
A6	Turbine sense resistor (for current)
A7	Turbine voltage - (used with A3)
PFIO	Flow meter

Table 9: Connections to the data acquisition module.

The 9kΩ resistors connected between the pressure transducer inputs and ground were used to decrease the signal offset. This was necessary due to the design of the USB-6009 as shown in Figure 42. The signal inputs on the USB-6009 are connected to a voltage divider so when the output impedance of the sensor connected to it is very high, or the terminal is open, the voltage delivered to the multiplexer is 1.4V as shown by Equation 11. To reduce this offset, the resistors were added. This was only necessary for the pressure transducers since they have a relatively high output impedance of 2000Ω and was not necessary for the voltage or current sensing elements as their output impedances were around 3Ω and .1Ω respectively.

$$2.5V \left(\frac{39.2k\Omega}{39.2k\Omega + 30.9k\Omega} \right) = 1.4V \quad (11)$$

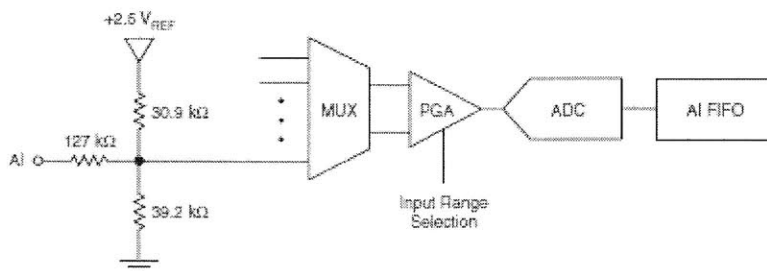


Figure 42: Internal layout of the USB-6009. Source: ni.com

The USB-6009 was also connected to the appropriate reference (i.e. ground) for each sensor. The turbine voltage was grounded from the same location as the turbine current sensors to prevent unwanted ground currents. The pump current reference was taken from negative side of the sense resistor. Particularly when high voltages are used, care should always be taken to ensure that circuits are properly grounded for safety purposes.

Series 628 pressure transducers from Dwyer Instruments Inc. were used as shown in Figure 43. These pressure transducers had a range of 0 to 3.4 bar absolute pressure (0-50psia) and output a voltage between 0 and 10V. These sensors are compatible with liquids and gases and have ¼ inch NPT threading so they could be screwed directly into the system wherever needed. The excitation voltage of the pressure transducers was 13-30V so a separate power supply was needed to power them. This separate supply was a Tenma 72-6626 DC regulated power supply able to provide up to 15V and 12A, ample power for the pressure transducers. The Tenma 72-6626 was then grounded to the data acquisition module to ensure a proper reference voltage.

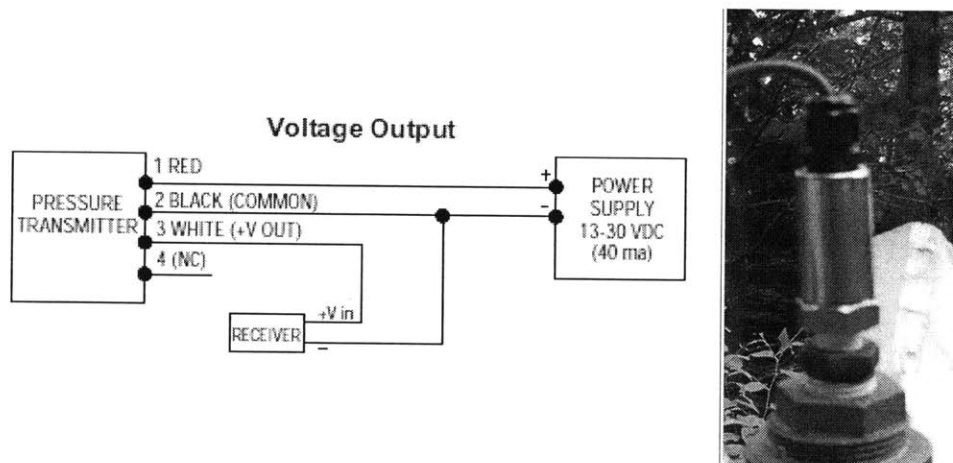


Figure 43: Pressure transducers.

To measure flow rates, the FP-5603 flow meter from Omega Engineering Inc. was used. This unit uses a paddle wheel that is inserted into the pipe via a special T joint. The paddle wheel is held in the pipe such that the lower paddle is exposed to the flow and the upper ones are higher within the fitting. As the wheel spins, the passage of each paddle causes a pulse in the signal output. The pulses are then counted by the data acquisition module. The wheel is calibrated such that the number of pulses per second is multiplied by a correction factor and the flow rate is determined. Due to the nature of the paddle wheel, the pipe delivering water to the sensor must always be full and even small bubbles in the line can disrupt the sensor and stop the paddle wheel from turning. To mitigate these effects, the sensor was mounted at a 45°

angle to vertical causing the majority of small bubbles to pass by the paddle wheel without stopping it. The flow meter may not, however, be mounted at a greater angle than that from vertical, as per its specifications. Unfortunately, larger bubbles were still able to disrupt the sensor so care was taken to make sure a minimum amount of air was passed to the sensor and that it was cleared of bubbles as fast as possible. The flow meter required an excitation voltage between 3.3 and 24V and draws less than 1.5mA so it was powered from the data acquisition module at 5V.

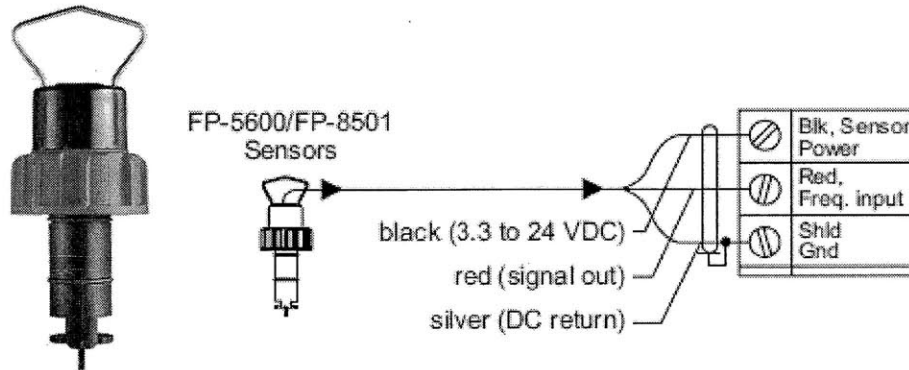


Figure 44: Left: The FP-5603 shown without its pipe housing. The paddle wheel paddles can be seen at the bottom of the unit. Right: Wiring for the FP-5600 series of which the FP-5603 is a part.

Figure 45 shows the locations of the pressure transducers and the flow meter. The pressure transducers were positioned to measure the change in pressure across both the turbine and the pump, as well as to measure the internal pressure of the sphere and the hydrostatic head upstream of the nozzle. The flow meter was positioned to allow its use during both the charging and discharging of the sphere.

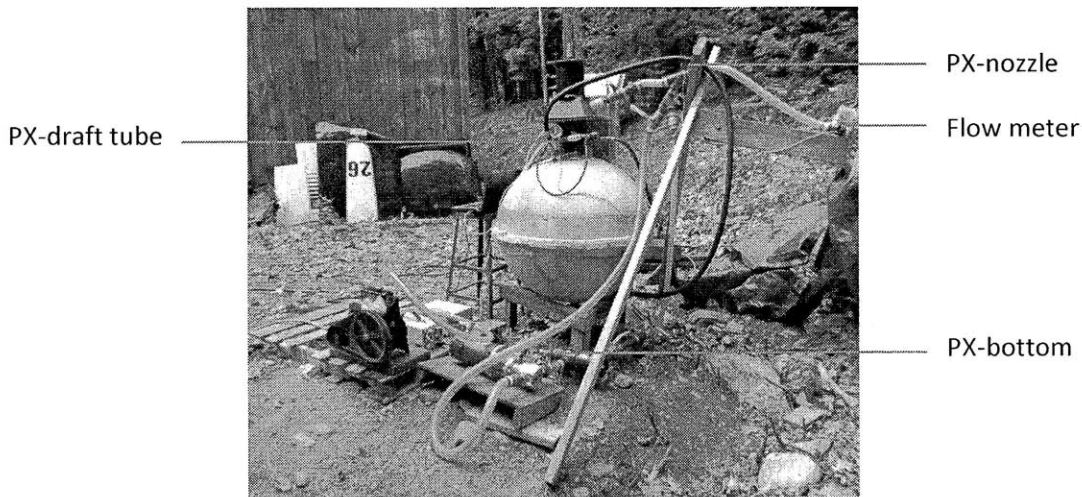


Figure 45: Locations of the sensors. PX indicates a pressure transducer.

The USB-6009 unit was then connected to a computer via USB cable and interfaced with data acquisition software. The software package used was LabVIEW, by National Instruments. LabVIEW accommodates current measurement through sense resistors in such a way that the resistance is entered and the current is displayed directly. This was done for both sense resistors. Once all of the signals were detected by LabVIEW, they were entered into a virtual instrument (VI), LabVIEW's signal processing module. The VI processed and recorded the information as well as displayed a user interface that allowed easy monitoring of the system while tests were underway. The data was then recorded to a .csv file that could be opened and analysed in Microsoft Excel. Data was sampled at a rate of 4Hz, which was far below the capacity of the equipment but more than fast enough for the testing conducted but having the advantage of more manageable data files.

4.9 Piping

Piping was needed to connect the sphere to the high reservoir both through the turbine and the pump as well as to allow the system to be filled from an outside source and emptied again. Several factors were considered during the design of the piping system:

1. Pressure loss due to pipe friction
2. The pressure rating and vacuum rating of the pipe
3. The ease of assembly
4. The ease with which the system can be modified
5. The ability of the system to hold a vacuum
6. The cost.

Given the experimental nature of the system and the high likelihood of changes being required, NPT black iron pipe and fittings were selected as the type of piping to use. These fittings can be easily assembled and disassembled unlike soldered or glued fittings. They are robust against a large range of pressure including vacuum and can be made to hold very high vacuum. Their disadvantage is cost vis-à-vis plastic fittings. However, when it is considered that plastic is more likely to be broken and much harder to modify, the increased initial cost was justified.

Other constraints on the system included the piping needs for the flow meter. To ensure straight flow into the meter and to get reliable results, the flow meter must have a sufficient length of straight pipe leading up to it. The precise amount required is shown in Figure 46.

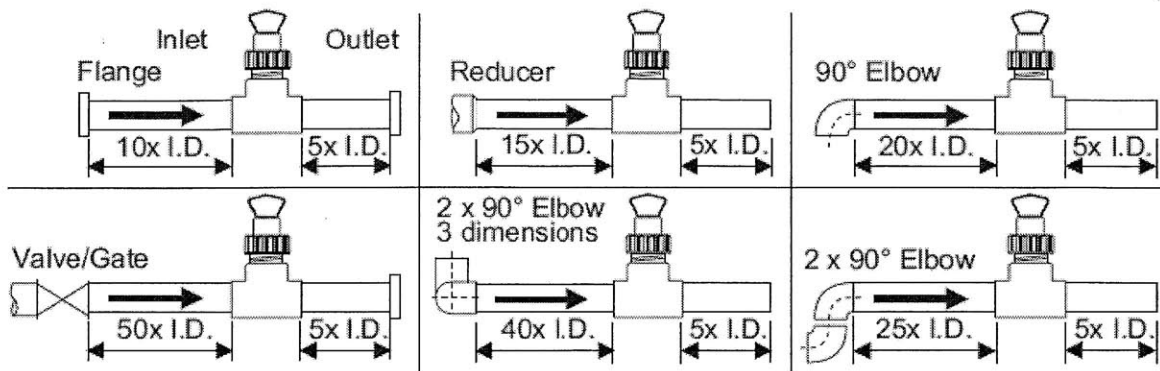


Figure 46: Manufacturer's recommended length of straight pipe prior into and following the FP-5603 flow meter.

A single line drawing was created for the system, laying out the major components and their connectivity as shown in Figure 47. The major components were selected ahead of time such that the fittings required to connect to them were known. The single line drawing was changed several times until no more improvements could be found. The single line drawing was then used to estimate pressure loss in the system and, using this information, the piping and fittings were sized. While the exact fittings required were not known at that time, a rough estimate of the required fittings enabled a standard pipe size, with fittings to match, to be selected.

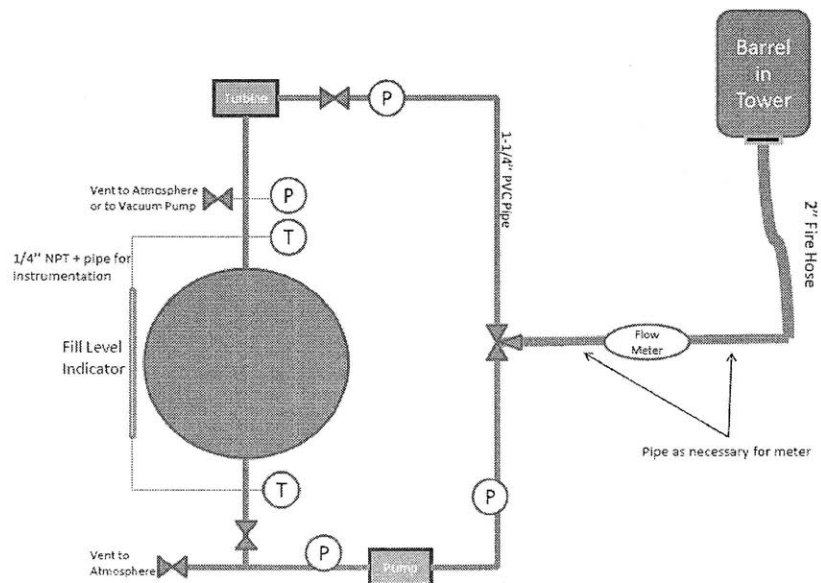


Figure 47: The first version of the single line drawing.

At this stage, other characteristics of the system could be specified. For sections not subject to vacuum pressures, flexible tubing could be used. Flexible tubing also facilitated the installation of the sections between the pump and the turbine which otherwise might have been complicated by alignment issues.

The single line drawing was then used to create a 3D model of the system (Figure 48) so that the length of each pipe run and the exact fittings required could be determined. Given the geometric constraints of certain parts of the system, the 3D model was also used to ensure that the pipes would not intersect other components and that they could be installed easily. From the 3D model, a detailed piping diagram showing all of the correct fittings as well as a parts list was generated. Once the parts list was verified, the parts were sourced. Despite this effort, the selection of some components changed at later stages of the piping system design and modifications to the design were made accordingly. A certain amount of standardization was used while creating the parts lists to facilitate changes in the system at a later time. For example, all of the ball valves ordered were the same size regardless of whether a smaller one would have sufficed in a given instance. When design changes were needed, the components could be easily switched and the system modified often without ordering additional parts. For an experimental apparatus such as this, standardization was beneficial. In a production run, the costs of this type of standardization would be very high and its benefits would vanish.

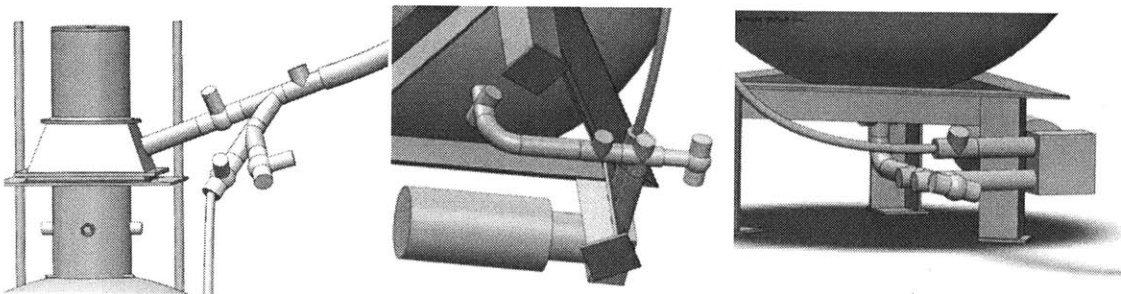


Figure 48: Left: Close-up of the turbine piping. Center and right: Close-up of the pump piping.

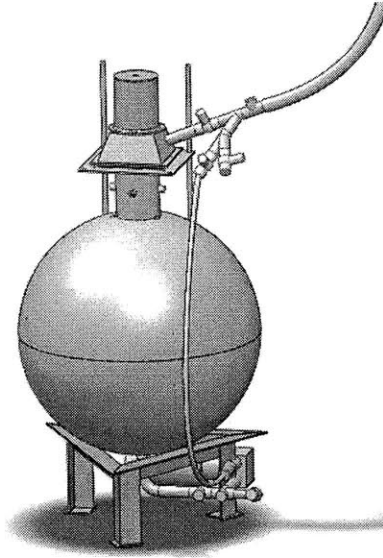


Figure 49: 3D model of the piping system close to the sphere.

As mentioned above, with the single line drawing completed, piping losses were estimated as follows. Piping losses were calculated for straight runs by solving the Colebrooke-White equation for the Darcy-Weisbach friction factor using the bisection method. The pressure losses from fittings were estimated using standard minor loss coefficients (Cengal, 2005). These pressure losses were then weighed against the higher cost of larger fittings which then resulted in a piping size being selected. The piping system to the turbine was designed to be as direct as possible since flow rates to the turbine could have varied and higher flow rates were possible. As a result, most of the piping and fitting would be between the pump and the high reservoir. Calculations for the piping system were completed for various sizes of pipe; an example calculation is shown in Table 10 and the results for all the sizes calculated are shown in Table 11. When calculating the losses from other pipe sizes, only the inner diameter (ID) was changed from the calculations shown here.

Major Losses

Q [L/s]	0.770
μ [Pa.s]	0.001519
ρ_s [kg/m ³]	1025
D _h [in.]	0.824
D _h [cm]	2.09
L [m]	5
ϵ [mm]	0.0025
A [cm ²]	3.44
V [m/s]	2.24
Re	31619
ϵ/D_h	0.000119
ΔP [kPa]	14.44

Minor Losses

Fitting	K	ΔP [kPa]
Sharp Entrance	0.5	1.25
90° Elbow	1.5	3.76
T, Inline flow	0.9	2.26
T, Branch flow	2	5.01
T, Inline flow	0.9	2.26
T, Inline flow	0.9	2.26
T, Inline flow	0.9	2.26
T, Inline flow	0.9	2.26
T, Branch flow	2	5.01
Total minor ΔP		26.31

Total Losses

Major [kPa]	14.44
Minor [kPa]	26.31
Total [kPa]	40.75
Total [psi]	5.91

Table 10: Example calculations of the piping losses in the pump system near the sphere using ¼ inch size threaded pipe fittings. Black numbers are inputs and red numbers are calculated.

Size [in.]	ID [in]	ID [cm]	ΔP [kPa]	Price [\$]
0.75	0.824	2.09	40.75	12.47
1	1.049	2.66	14.57	20.04
1.25	1.38	3.51	4.57	29.98
1.5	1.61	4.09	2.40	37.54
2	2.067	5.25	0.84	56.13

Table 11: The total pressure loss estimated for the pump piping system near the sphere. The price, in the right-most column, is the price of a typical brass ball valve in that size from McMaster Carr Supply Company.

The price column in Table 11 is the price of a typical brass ball valve in the size shown. This price was used as a proxy for system price. However, the total system price for the piping near the sphere would be approximately 10 times the price shown. In the end, 1 ¼ inch pipe size was chosen for the system as a compromise between cost and piping losses, keeping in mind that the results shown in Table 11 above only apply to the pump. Piping losses for the turbine side are shown in Table 12 and are noticeably less significant than those of the pump system.

Size	ID [in]	ID [cm]	ΔP [kPa]
0.75	0.824	2.09296	10.28
1	1.049	2.66446	3.53
1.25	1.38	3.5052	1.065
1.5	1.61	4.0894	0.545
2	2.067	5.25018	0.185

Table 12: Turbine piping system pressure loss for various pipe sizes.

All of the piping near the sphere was to be a single size to facilitate changes to the system, as mentioned above. However, in addition to that piping system, a hose was required to connect the near-sphere piping to the high reservoir. This hose was sized separately from the other system but the same method of calculation and the same flow parameters were used except for the length, which was 15.25m for the hose. Table 13 summarizes those results.

ID [cm]	ΔP [kPa]
1.91	69.09
2.54	17.43
3.18	6.01
3.80	2.52
5.08	0.64
6.35	0.22
7.62	0.09
8.89	0.05
10.16	0.02

Table 13: Summary of piping losses for the hose connecting the near-sphere piping system to the high reservoir.

Unlike the most of the near sphere system, the hose will contain flow during the operation of both the pump and the turbine. In the end, the hose size was selected to be 5.08cm inner diameter however, the availability of suitable hoses resulted in a higher diameter being used and the 6.35 (2.5in.) ID hose was selected.

5 Build (Procedure)

5.1 Concrete Hemispheres

The concrete was poured by Newstress Inc. of New Hampshire at their facility. The pour was scheduled to coincide with their regular production schedule. Fitting this smaller experimental job in between

production was important as it reduced the cost of pouring and made it logistically feasible for all those involved. Just prior to pouring the concrete, the mold was coated in engine oil and bolted to a pneumatic vibration table. Wooden spacers were inserted between the two hemisphere to center the inner mold and provide an even wall thickness. Ply wood was also used to prevent concrete from spilling into the inner hemisphere; the thin gap between the two hemispheres being a difficult target for the cement truck driver. As concrete began to flow, the mold was tilted through the use of chain falls to reduce the chances of air being trapped in the bottom. As the mold filled, it was levelled out and the wooden spacers were removed.

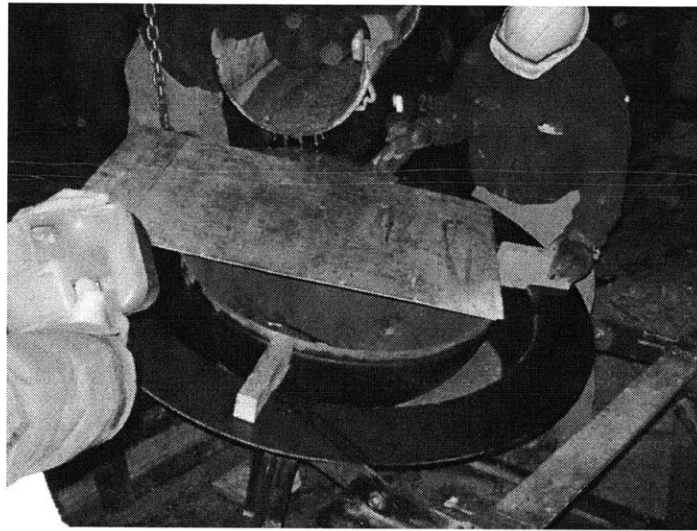


Figure 50: The mold being filled with concrete. Mold release (engine oil) can be seen to darken the surfaces of the mold where contact with the concrete will occur. Bolts holding the mold to the vibration table can be seen bottom right.

The mold was vibrated in short bursts in attempts to eliminate voids. The studded steel ring was then pressed into the exposed concrete face to create the required channels and stud pockets, as seen in Figure 51: The studded steel ring being pressed into the concrete. The plastic wrap used in attempts to seal the backer rod can be seen on the stud in the foreground. This plastic wrap caused several problems during assembly.. As mentioned in sections above, this ring proved problematic.



Figure 51: The studded steel ring being pressed into the concrete. The plastic wrap used in attempts to seal the backer rod can be seen on the stud in the foreground. This plastic wrap caused several problems during assembly.

Once each hemisphere was cured, they were de-molded and brought to Iron Dragon Corporation facilities, where they were assembled. The assembly procedure is described in section 4.3.

5.2 Handling

The hole in the pole of each concrete hemisphere was the lift point in all cases prior to assembly. For removal from the mold, a pipe with a lift point welded to it was used. This custom pipe section was threaded into the pipe coupling embedded in the concrete at the pole. However, all subsequent lifts were done with a threaded rod that was passed through the coupling with a large washer and nut on one side and an eye nut on the other. The threaded rod is used to lift a concrete hemisphere in Figure 52.

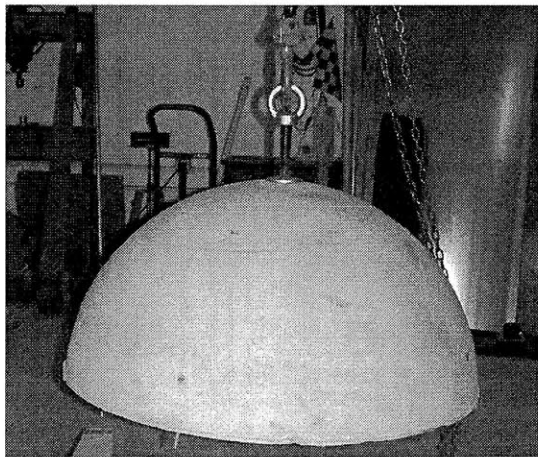


Figure 52: Lifting a concrete hemisphere.

Because of the relatively small size of the hemispheres, tires could be used to flip a hemisphere over while the concrete is steadied by hand. The hemisphere was lowered onto stacks of tires so that it would almost be at the bearing point, i.e. its center of mass was almost over its contact point with the ground but it was still stable on its current side. The lift point could then be changed to the other side of the threaded rod and the hemisphere could be eased onto other tires and eventually lifted onto its other side.

Once the sphere was assembled, it was lifted from the bottom with slings. The slings were passed through one another in such a way that a triangle was formed for the sphere to sit in. Chain falls or a tractor was then used to lift the sphere and reposition it. The assembled sphere could also be rotated by picking it up and lowering it again so that contact on one side of the sphere was achieved first causing it to roll a small amount before contacting the other supports. Repeating this process allowed the sphere to be oriented in any way desired.

It was particularly useful to flip the sphere over when filling the malfunctioning stud holes with epoxy. Since half of the stud holes were on the lower side of the sphere, the top four stud holes were filled, the sphere was flipped and the remaining four stud holes were filled.

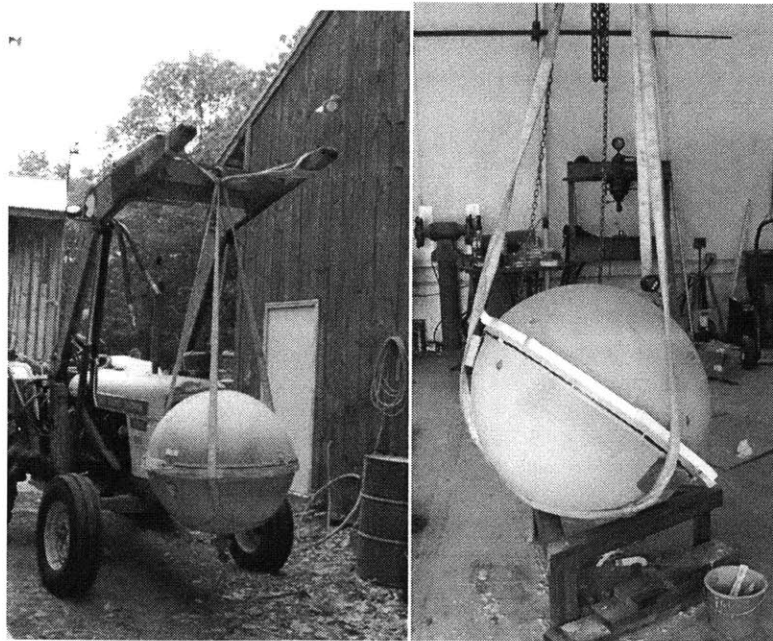


Figure 53: The assembled concrete sphere being manipulated through the use of nylon slings. Left: A tractor lifts the sphere. Right: The sphere is rotated through successive lifts with a chain fall.

5.3 Core drill

Once it was realized that the 1 ¼ inch coupling would be insufficient to drain the turbine housing, it was undertaken to enlarge the connection between the turbine and the sphere. To do this, a larger hole had to be cut in the sphere and it was done using a core drill. A 7 inch diamond studded bit was mounted on a M1-C Diamond Products core drill rig with a Core Bore (CB) 748 drill rented for this purpose. The CB 748 is a two speed drill and was run at 350rpm for this application.

To prepare for drilling, the sphere was lifted and brought into position. A steel cage was then fabricated around it and welded to the shop floor. Cross beams were welded on to hold the drill and the sphere's stand was also welded to the cage. The drill was lifted with the chain fall, brought into position above the sphere and clamped in place. A ratchet strap was then passed around the sphere to hold it to its stand. Water and power were connected and drilling proceeded. The bit was advanced slowly but cut smoothly through the 4 inches of concrete. Figure 54 depicts the process and Figure 55 depicts the results.

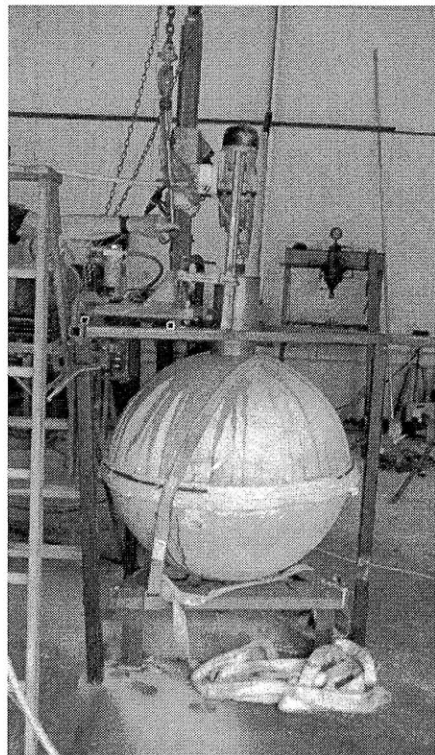


Figure 54: The core drill in action.

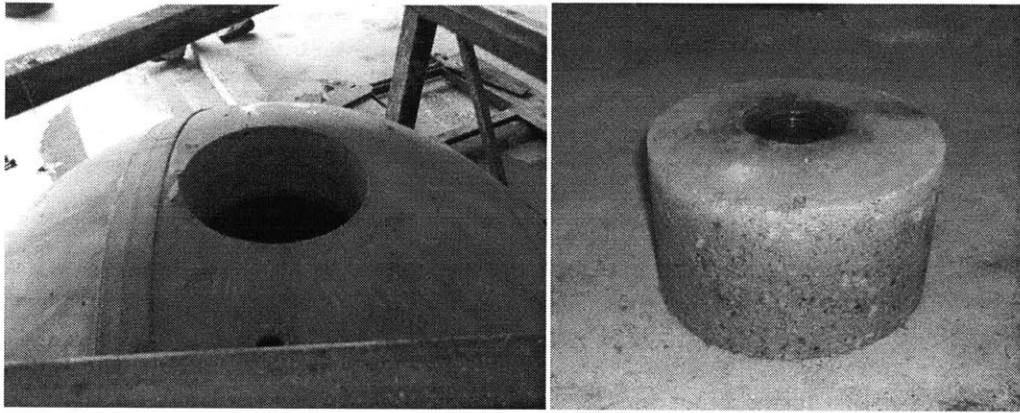


Figure 55: Core drill results. Left: The enlarged hole in the sphere. Right: The core resulting from the drilling process. The pipe coupling used previously can be seen embedded in the centre.

5.4 Turbine Installation

Once the 6 inch diameter pipe stub was welded to the turbine water collection plate and all the necessary modifications to it had been made, it was ready for installation on the sphere. The primary concern during installation was creating an airtight seal. Once the pipe was glue in place, it would be very difficult to remove and any repair would be of much lower strength than a proper initial seal.

To prepare the 6'' diameter pipe stud for gluing into the sphere, two additional features were added: 1. Positioning bosses and, 2. Weather stripping. To ensure an airtight seal and sufficient strength to support the turbine, a maximum contact area between the pipe and the sphere was desired. However, if the pipe was lowered too far into the sphere, the reduced area available to fasten the surrounding fittings would cause difficulty and possible delay when installing fittings. Bosses were thus welded onto the 6'' sphere so that when it was placed in the bore hole it would rest at the correct height. Finally, to prevent epoxy from leaking into the sphere, the bottom 2 cm of the 6'' diameter pipe stub was wrapped in weather stripping such that the outer diameter of the weather stripping and pipe was slightly more than that of the hole. Care was taken to ensure the butt ends of the weather stripping met end to end, leaving very little space for epoxy to leak through. As the pipe was inserted into the bore hole, the weather stripping was compressed, eliminating any remaining leaks.

Inserting the pipe into the bore hole consisted then of preparing the pipe, with its ports and bosses, welding it onto the base plate of the turbine, wrapping weather stripping around the bottom and slowly pressing and rotating it into place. Once the pipe was in place, Sikadur-32 was poured into the gap between the pipe and the bore hole sides. No leaks were observed and a strong, airtight seal was achieved.

The turbine was then installed on the water collection plate. Silicon liquid gasket was again used to create a seal. The liquid gasket was applied and the turbine was put in place with the bolts holding it down only finger tight. Once the liquid gasket was cured, the bolts were fully tightened. The generator cap was then put in place using the same method and liquid gasket. Finally, to complete the seal, the bulkhead fitting was installed using Teflon tape to seal the threads.

Once the turbine was in place, the electrical box was mounted to it. Threaded rods were passed through the turbine water collection plate using holes created for the initial turbine outlet design. The threaded rods were bolted in place and U-bolts were used to secure a sheet of plywood to them. The electrical box was then screwed directly to the plywood.

With the electrical box in place, the turbine was wired to the rectifier.

The completed turbine assembly, sealed, wired and joined to the sphere is shown in Figure 56.



Figure 56: The completed turbine assembly.

5.5 Piping installation and manifold support

The piping system was installed in sections separated by pipe unions. Unions were of particular importance because if one section leaked, the unions allowed easy removal of that section without requiring a larger scale disassembly. A pipe union was also used just upstream of the turbine so that it could be easily disconnected to have its nozzle changed.

All NPT connections, both black iron and plastic, were sealed with Teflon tape. Flexible tubing took barbed fittings and hose clamps.

Flexible tubing was used upstream of both the pump and the turbine to relieve stress in the piping due to misalignment. In the case of the pump, the flexible section was on the vacuum side however, the flexible section was so short that it was impossible for it to be crushed when containing a vacuum. On the turbine side, the flexible section was longer however only positive gauge pressure would ever be contained there. This tubing was necessary because the valve assembly near the turbine was too heavy to be held up by only the nozzle connection. To support this valve assembly, a wooden structure was constructed. This structure not only supported the weight of the valve assembly but also the approaching tubing which was able to take a more direct route as a result.



Figure 57: A wooden structure provides support for the valve assembly.

A piece of flexible tubing was also added to the discharge port for the tower. This tube made it possible to direct the large volumes of water being discharged, avoiding the wide area soaking and possible damage to electronic equipment that may otherwise occur.

Longer connections between pieces of equipment were also done with flexible tubing to simplify installation and avoid alignment issues, such as the connection between the pump and the valve assembly.

Flexible tubing was used for handling air as well as to indicate the water level in the sphere. The connection between the sphere and the vacuum pump was flexible tubing. Since vacuum was to be contained, wire-reinforced tubing was selected. The wire maintains the cross section of the tubing, stopping it from being crushed flat by atmospheric pressure. The water level indicator was also flexible tubing subject to vacuum pressures; however, wire reinforcement would have obstructed a view of the water level. Instead, thick walled PVC tubing with a small lumen was selected and was effective at both displaying the water level of the sphere and resisting the crushing force of atmospheric pressure. It should be noted that after repeated cycling, water residue began to build up inside the tubing making water level readings more difficult.

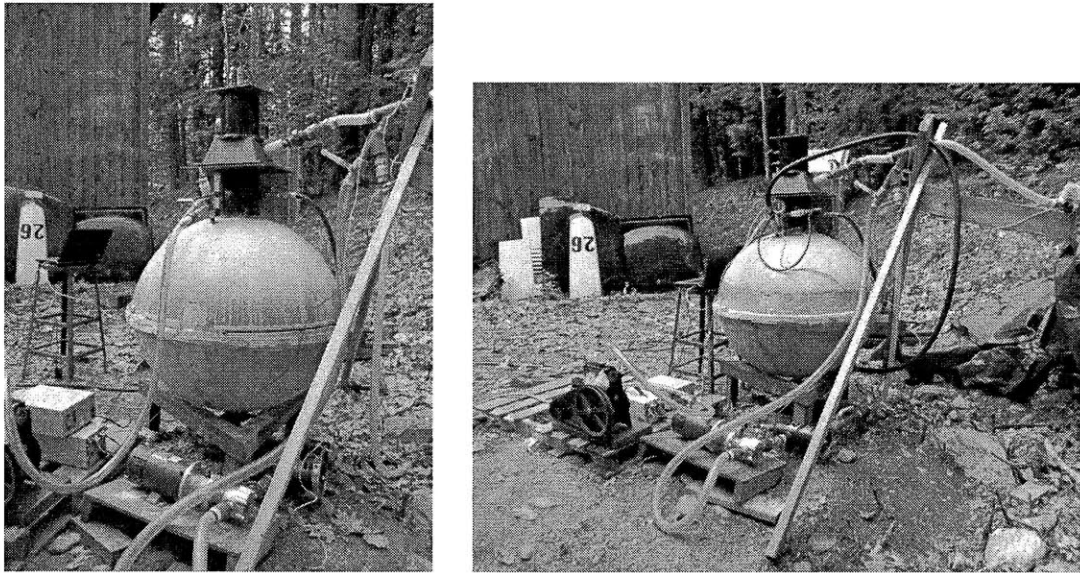


Figure 58: The completed piping assembly. Left: “No Vent line” case testing. Right: “Vent line” testing. Notice that the vacuum pump is not connected to the system for this test.

5.6 High Reservoir

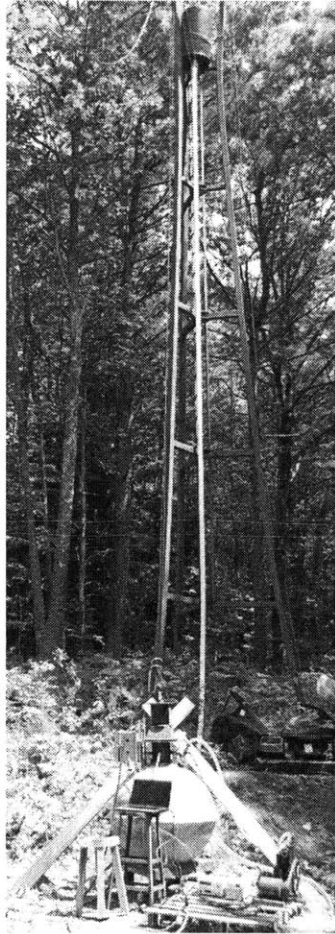


Figure 59: The high reservoir shown behind the completed system.

A high reservoir was needed to provide the hydraulic head used to store energy. To maintain a head that is roughly constant, a reservoir with a capacity at least as big as the sphere was needed. With the sphere containing 232L, a 238L (63 gallon) rain barrel was acquired for this purpose. The rain barrel was fitted with a pipe stub and coupling allowing it to be connected to the piping system and holes were cut in the bottom to allow air to enter and leave. The barrel was then mounted in an antenna tower at Iron Dragon Corporation's facility. The tower was approximately 14.5m tall however the barrel could not be mounted at the very top. The lowest point on the barrel was 11.6m above the turbine inlet and with a height of 0.9m, the average head height provided by the tower was 12.05m. The barrel was secured in place with rope and was never left full for an extended period of time to minimize the potential hazard of a full barrel falling from height.

5.7 Vacuum Sealing

Sub-atmospheric pressures were created in the sphere using a vacuum pump. The pump used is shown in Figure 60. Connections to the vacuum pump were made using a wire-reinforced vacuum resistant hose and a hose clamp. Care was taken to ensure water was not introduced into the vacuum pump as damage to the pump could occur as a result. To that end, the tubing leading to the pump had a U bend made in it such that any droplets moving toward the pump would be caught in the trough. Water caught could then be returned to the sphere by lifting the tubing and tilting the hose toward the sphere.

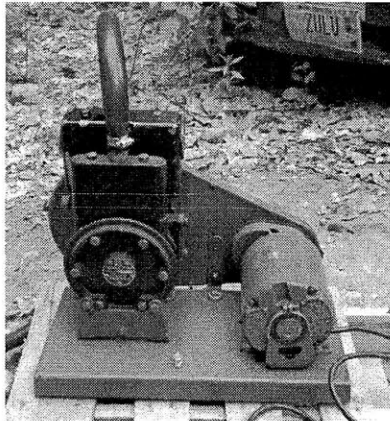


Figure 60: The vacuum pump.

As with all vacuum systems, there is a finite leak rate which must be managed to reduce the error that the leaks may introduce. To this end, vacuum pressures were measured at first using a compound gauge and later using a pressure transducer and the achieved vacuum was characterized in two ways: first by the lowest pressure achievable while running the pump and second by the leak rate as measured at the lowest pressure achievable. Two methods were used because each is more valuable at different leak rates. For large leak rates, measuring the leak rate directly is more time consuming than simply watching the gauge while running the vacuum pump. If the vacuum pump reaches equilibrium at a relatively high pressure, it is clear that there are large leaks. However, once the leak rate has been reduced, it may take a long time for the vacuum pump to reach equilibrium so measuring the leak rate directly becomes easier.

When large leaks are present, a small amount of pressurized air is delivered to the sphere, raising the internal pressure to approximately 10kPa gauge. The leaks could then be found simply by listening for them. The method used for fixing the large leaks depended on the location of the leak. In the case of the equatorial seal leaking, an epoxy dam was created, as outlined in section 4.3. For the leaking stud holes, each hole was filled with Sikadur-32. Small leaks were found through the use of bubble tests. A mixture of soap and water was sprayed on the fitting or location in question and the sphere was again pressurized

to 10kPa gauge. If a leak was present, bubbles would begin to grow from the hole. This method was used repeatedly as many leaks were present. To seal a leak of this size, the area with the leak was cleaned and dried with compressed air. A vacuum was then pulled inside the sphere and quick-setting epoxy was applied over the location of the hole in hopes that some of the epoxy would be drawn into the leak.

Other measures taken to improve the vacuum seal of the system were taken as well. In addition to the epoxy dam created at the sphere's equator, 15cm above and certain regions below it were painted with several coats of epoxy. Thin cracks in the concrete were observed in this region that appeared moist; alluding to the possibility of very slow leaks. All compression fittings and o-rings were greased liberally and tightened as appropriate. No components of the system was assumed leak free. A three way ball valve was found to leak. After the valve packing was tightened without success, it was replaced by two regular brass ball valves. Several welds were also found to have leaks and fixed with epoxy.

These methods of leak detection and correction were effective but also have their limitations. Bubble testing is only able to detect leaks that are large enough to form visible bubbles with the overpressure applied. Also, it is thought possible for leaks to self-seal under positive pressure and open again under vacuum, rendering the bubble test useless for those leaks; however no large leaks have been observed to behave this way. Smaller leaks, which may be significant if lower vacuum pressures are desired, are thus not detectible using this method.

5.8 Vents/ports and gas handling

To allow access to the interior of the sphere a number of ports were created, including the 6 inch pipe stub which was fitted with four pipe couplings. One coupling was used for the fill level indicator, one for water addition, one for pressure measurement and air bleed and one for temperature measurement. The air bleed port was used to deliver small amounts of pressurized air into the system and initially during "vent line" case testing. However, this port was found to be insufficient for those tests. As water entered the turbine and then the sphere, air needed to escape. With water falling down through the 6 inch diameter pipe, air would escape through the port located there and entrain a significant amount of water.

To eliminate the issue of water entrainment, a new port was created. A hole was drilled in the sphere near the upper pole using a hammer drill. A ½ inch diameter pipe stub was then glued in place using a similar process to the 6 in diameter pipe. Since this port was away from the turbine and associated water inflow, air exiting through this port did not entrain any water. However, due to the port being located lower on the sphere than any of the others, the maximum volume of water allowed in the sphere had to be reduced as higher water levels would result in water flowing out through the port. This new maximum water level

was marked on the sphere and designated the “high fill mark”. It was reached when the sphere contained 193 litres (51 gallons).

This additional port was also used for the “no vent line” tests as the vacuum pump was connected there. In those cases, it was useful to have a second bleed valve as the pressure within the sphere could easily be returned to atmospheric without having to disconnect the vacuum pump.

6 Test

6.1 Overview

The primary goal of testing was to demonstrate the ability of the system to store energy, i.e. to verify that the system had been designed and constructed effectively. So long as the device was able to store energy and discharge it, this goal would be satisfied. However, there were three secondary goals:

1. To measure the efficiency.
2. To gain insight into system improvement towards achieving the highest efficiency possible.
3. To compare the performance of the device with a vent line and without.

Improving the efficiency of the system was an iterative process which consisted of running tests, measuring the efficiency, making adjustments or modifications to the system and repeating. This approach led to higher efficiencies both through calibration (adjusting the load resistance and turbine nozzle for maximum efficiency) and through major modifications (e.g. expanding the turbine outlet to allow larger nozzles to be used).

6.2 Test procedure

Tests were conducted for two cases: “vent line” and “no vent line.” The procedure common to both is given below. After the procedures begin to differ, the steps taken are listed in their respective sections.

6.2.1 Start-up

1. Remove the protective covering from overtop of the system.
2. Bring the DC power supplies out to the prototype and wire them as appropriate using the quick connections.
3. Connect the system to grid power and water.

4. Set the DC power supplies to their appropriate voltages: 24V for the pump. 15V for the pressure transducers.
5. Open a vent from the sphere to atmosphere. IMPORTANT. The sphere will suffer damage if this step is forgotten.
6. Connect a computer to the data acquisition module.
7. Open LabVIEW and open the ORES VI.
8. Run the VI without saving.
9. Check to make sure the pressure transducers' signals are being acquired. The pressure transducers should all read approximately 14.7psi.
10. Begin filling the sphere with water; open the makeup water valve. Water should now be flowing into the sphere.
11. Once the sphere is half full, as read from the sight glass, open the valves connecting the sphere to the pump and those from the pump to the high reservoir. Ensure the turbine nozzle and the reservoir discharge valves are closed.
12. Engage the pump. Water should flow from the sphere to the high reservoir. If the sphere empties and the pump begins sucking in air, stop the pump and wait until the sphere has filled enough again before resuming pumping.
13. Check that the flow meter's signal and the pump current are being acquired.
14. Open the turbine nozzle valve (momentarily) and check that the turbine's voltage and current are being acquired. Close the turbine nozzle valve.
15. Once the high reservoir is filled, made obvious by water flowing through the air vents and falling from the tower, stop the pump and close all valves except the vent from the sphere to atmosphere.
16. Open the lower discharge valve, allowing the sphere to empty any remaining water.
17. Close the lower discharge valve once the sphere is empty.

The upper reservoir should now be full. The sphere should now be empty. All electronic systems should be checked and powered, and the data acquisition system should be ready. All valves are closed except the vent from sphere to atmosphere.

6.2.2 Vent line

1. Free the concrete mounted vent. If the vacuum pump line is connected, remove it.
2. Open the concrete mounted vent.
3. Run the VI with saving. Ensure that the VI is in fact saving the data.
4. Start the flow of compressed air onto the load resistor.

5. Open the turbine nozzle valve. From this point on, pay careful attention to the water level in the sphere.
6. Water should be flowing into the turbine. Check the VI front panel to ensure all the sensors are functioning.
7. Once the water level reaches the high fill mark, quickly close the turbine nozzle valve. The high fill mark is a line denoting the water level in the sphere when it contains ### litres (51 gallons).
8. Stop the flow of compressed air onto the load resistor.
9. Open two valves: from the sphere to the pump and from the pump to the high reservoir.
10. Engage the pump.
11. Continue pumping until the sphere is empty once again.
12. Stop the pump. Close all valves except the vent mounted in concrete.
13. Stop the VI.

6.2.3 No Vent Line

A leak test was done at the beginning of each round of testing, if the device sat unused for more than a few days or if an even occurred which might have caused additional leaks. If any abnormalities related to possible leaks were observed, a leak test was also conducted. Once the system has been tested to have a leak rate of 1kPa/min or less, the following procedure was followed.

1. Close all vents on the sphere. The sphere should be sealed.
2. Attach the vacuum pump to the concrete mounted vent.
3. Open the vent to the vacuum pump.
4. Engage the vacuum pump.
5. Check that the pressure is dropping. If the pressure is dropping too slowly or stops dropping , do a leak test.
6. Once the internal pressure in the sphere has reached the desired initial pressure for the test, close the vent to the vacuum pump and turn the pump off.
7. Run the VI with saving.
8. Start the flow of compressed air over the load resistor.
9. Open the turbine nozzle valve. From this point on, pay very close attention to the pressure inside the sphere.
10. Water should be flowing into the turbine. Check the VI front panel to ensure all the sensors are functioning.
11. Once the sphere's internal pressure has reached 14.7psia, quickly close the turbine nozzle valve. If this pressure is exceeded, damage to the device is possible.

12. Stop the flow of compressed air.
13. Open the valves between the sphere and the pump, and the pump and the high reservoir.
14. Engage the pump.
15. Check the VI's front panel to ensure proper operation of the device.
16. Continue pumping until the sphere is empty.
17. Stop the pump, close all the valves and stop the VI.

6.2.4 Shut down

Once testing for the day has been completed, the following steps should be taken to ensure a safe work environment and the continued functioning of the device.

1. Stop all running equipment and close all valves.
2. Open the sphere's vent to atmosphere.
3. Shutdown LabVIEW, disconnect the computer and remove it from the area.
4. Turn the power supplies off.
5. Wait a few seconds for their voltages to fall to 0. Disconnect them and remove them from the area along with the power cable.
6. With a firm grip on the reservoir discharge hose, open the reservoir discharge valve and aim the ensuing spray of water in a safe direction. Once the reservoir is empty, close the valve again.
7. Open the lower discharge valve to empty the sphere of any remaining water. Once the sphere is empty, close the valve.
8. Turn off the makeup water supply. Disconnect its line and put it back into its storage area.
9. Replace the protective covering over the system, making sure to cover both the flow meter and the vacuum pump, and tie the cover in place.

6.3 Leak test

To ensure the reliability of results and to maintain the similarity between the onshore tests and those conducted at depth, the rate at which air was able to leak into the sphere under vacuum had to be controlled. The leak rate was measured and if it was found to be above 1kPa/min, leaks were sought and plugged as outlined in section 5.7. With experiments lasting approximately 10 minutes, this corresponds to a maximum accepted pressure variation of 10kPa. When compared to the available pressure at the turbine nozzle, which is approximately 220kPa, this leak rate represents a maximum head loss of 5%.

Typical results showed less than half of that loss. To measure the leak rate, the following procedure was followed.

1. Prepare the sphere as outline above in section 6.2.1. However, it is not necessary to fill the sphere or reservoir with water.
2. Open the lower discharge valve and drain any water from the sphere.
3. Connect the vacuum pump to the sphere.
4. Close all of the valves and vents. The sphere should be sealed.
5. Run the VI without saving.
6. Open the vent to the vacuum pump and engage the vacuum pump.
7. Check that the pressure inside the sphere is dropping.
8. The pressure should be allowed to drop until one of the following conditions is met. Note that it can sometimes take more than 30 minutes for this to occur.
 - a. The pressure is dropping at a rate less than 700Pa every minute.
 - b. The lowest pressure expected to occur during a test is reached.
9. Once one of the above conditions is reached, simultaneously close the valve from the sphere to the vacuum pump and start the VI with saving.
10. Turn off the vacuum pump.
11. Allow the data to be collected for the expected duration of future tests. Typical times were between 10 and 15 minutes.
12. Stop the VI.
13. Open the vent from the sphere to atmosphere.

The results of a leak test conducted using the procedure above are shown in Figure 61. Once the data is collected, the pressure is plotted and linear regression is used to fit a straight line to it. The slope of that line is the stated leak rate. Using the bubble test and sealing methods as described in section 5.7, a leak rate of 253Pa/minute was achieved at an initial pressure of 7kPa.

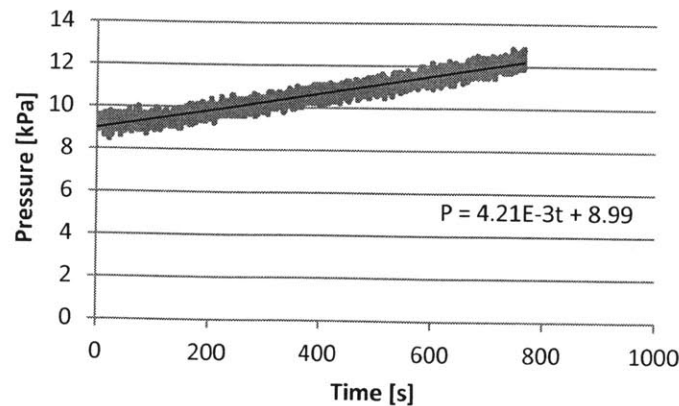


Figure 61: Results of a leak rate test. The pressure in the draft tube was measured for over 10 minutes after the system had been brought to 9 kPa internal pressure. Linear regression yielded the equation shown. The leak rate was 4.21 Pa/s or 0.253kPa/min.

6.4 Turbine Tuning

To maximize the system's efficiency, the turbine BEP had to be found. Since the height of the high reservoir was fixed, so was the head. However, the flow rate and the applied load could be varied so the turbine was tuned by changing these two parameters.

The average flow rate was changed by changing the size of the hole in the nozzles used. Some of the nozzles used are shown in Figure 31. The flow rate itself was not controlled directly and because of the small loss of head that occurs as the high reservoir drains, the flow rate slowly decreases over the course of a test run. Also, since a fixed amount of water can be brought into the sphere, the lower flow rates, despite generating lower power, ran for longer. To account for the longer run times, the total energy was measured and compared. The total energy discharged from the turbine was measure for a "vent line" type test as outline in section 6.2.2 using different nozzles. The load resistance was optimized only roughly for these tests with more accurate load tuning to come later, however a clear trend appeared. The results of these tests are shown in Figure 62. As it became clear that larger flows would yield higher outputs, the largest nozzle possible for this turbine (12.7mm or 0.5in.) was created, installed and used for all subsequent tests. The outlier to the far right is the result of a test conducted without a nozzle. While the nozzle holder was 19mm and resulted in the highest flow rate, without the accelerating effect of a nozzle, the energy recovered by the turbine suffered.

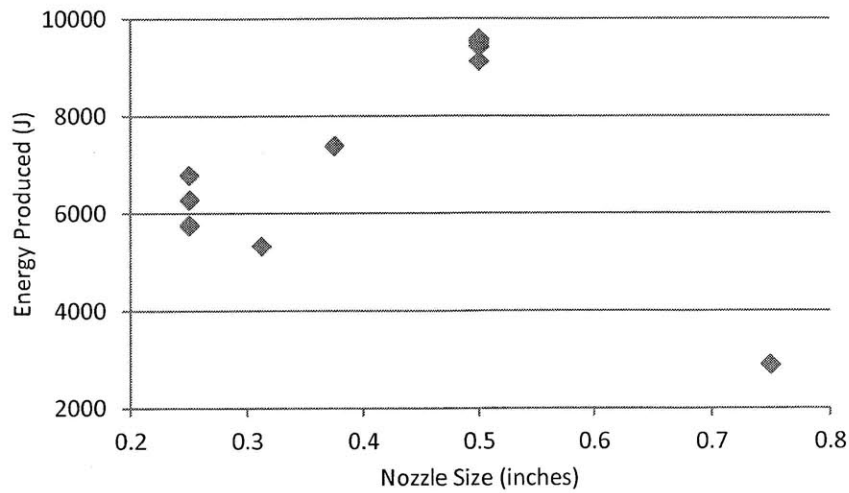


Figure 62: Energy recovered by the turbine using various nozzle sizes.

Once the optimal nozzle was found, the load resistance was tuned. Since the flow rate does not depend on the electrical load on the turbine, the maximum energy would be recovered when the turbine was producing at maximum power. As a result, it was not necessary to measure the total energy over the course of an entire test. The steady state power could simply be measured and maximized. The procedure for a “vent line” test was followed with one exception using a different load resistance for each run. The exception was that the test was stopped after the turbine had run at steady state for a few minutes instead of waiting for the high fill line to be reached. Even though a large amount of water remained in the high reservoir, the reservoir was always completely refilled before every test as differences in head affect the power output of the turbine. The results of these tests are summarized in Figure 63. As a trend became apparent, more tests were conducted around the point of maximum power. A final load resistance of 2.5Ω was determined to yield the best results and was used for all subsequent tests.

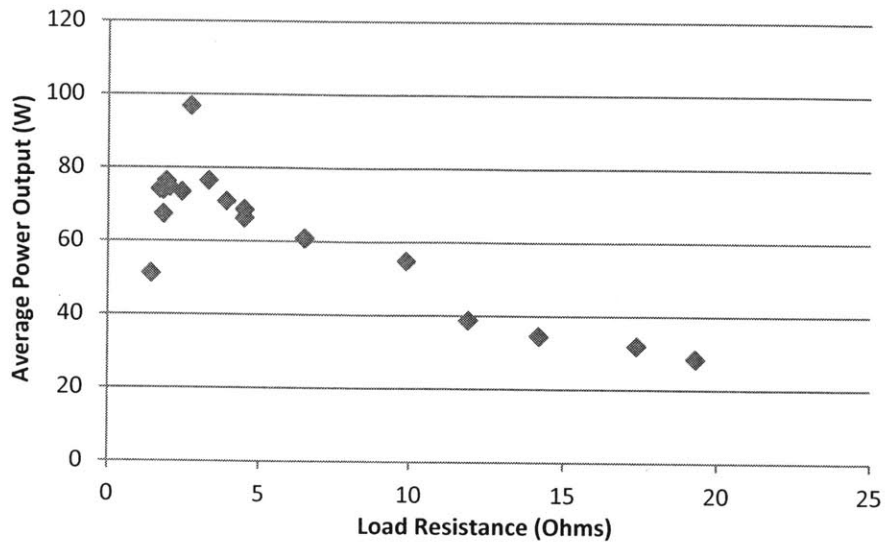


Figure 63: Turbine power output using a 12.7mm nozzle with various load resistances applied.

6.5 Results

6.5.1 Calculations

A minimum of 5 runs were done for each test case in accordance with the procedures outlined in section 6.2, which includes one complete discharge and one complete charge. Seven signals were measured:

1. Turbine voltage, V_t
2. Turbine current, I_t
3. Pump current, I_p
4. Voltage from PX-nozzle, $V_{px-nozzle}$
5. Voltage from PX-draft tube, $V_{px-draft\ tube}$
6. Voltage from PX-bottom, $V_{px-bottom}$
7. Flow meter total pulse count, C

Time was recorded in addition to the signals above. $t=0$ occurs when the VI is run. However data from the run is only evaluated for each piece of equipment while $t_{start} \leq t \leq t_{end}$. The times t_{start} and t_{end} are the time at which the power (regardless of input or output) reaches approximately $\pm 20\%$ of its steady state value, thus removing the power spikes involved in starting and stopping the rotating equipment. n_{start} and n_{end} are the sample indices for the samples taken at times t_{start} and t_{end} . A backward difference was used between adjacent samples to determine Δt , which is equal to the sampling period but also accounts for

small deviations recorded at each step. However, when calculating the flow rate, a centered difference is used since a larger time interval was desired. Energy is calculated from power by summations using the rectangle rule. The flow rate and other values of interest were then calculated as shown in Table 14.

Instantaneous Turbine Power, P_t [W]	$I_t \cdot V_t$
Total Turbine Energy, E_t [J]	$\sum_{i=n_{start}}^{n_{end}} P_{t_i} \cdot \Delta t$
Instantaneous Pump Power, P_p [W]	$I_p \cdot 24$
Total Pump Energy, E_p [J]	$\sum_{i=n_{start}}^{n_{end}} P_{p_i} \cdot \Delta t$
Pressure p from PX, [Pa]	$V_{px} \cdot 5$
Instantaneous Flow rate Q, [L/s]	$Q_i = \frac{C_{i+1} - C_{i-1}}{2\Delta t} \cdot \frac{1}{32.07}$
Roundtrip efficiency, η	$\frac{E_t}{E_p}$
Turbine efficiency, η_{turb}	$\frac{1}{n_{end} - n_{start}} \cdot \frac{E_t}{\sum_{i=n_{start}}^{n_{end}} Q_i \cdot (p_{nozzle} - p_{draft})}$
Pump efficiency, η_{pump}	$\frac{1}{n_{end} - n_{start}} \cdot \frac{\sum_{i=n_{start}}^{n_{end}} Q_i \cdot (p_{nozzle} - p_{draft})}{E_p}$

Table 14: Equations used to determine energy flows for a given test.

6.5.2 Result

The energy stored and recovered for each test is plotted in Figure 64 showing the repeatability of the tests.

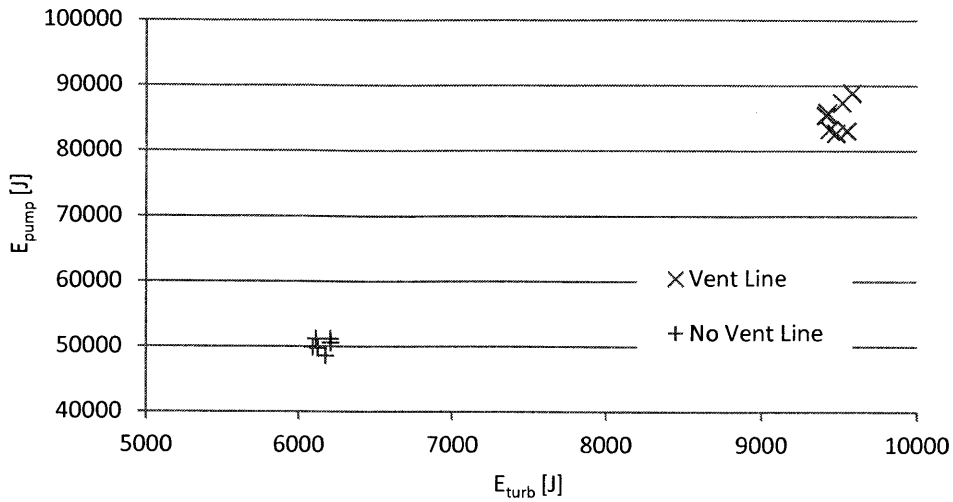


Figure 64: Energy stored and discharged for all tests.

Typical power usage results for a vent line and no vent line case are shown in Figure 65 and Figure 66 respectively. The available pressure, which is the pressure difference across the turbine nozzle, is also shown in both graphs. The effects of the vent line can be seen clearly in the differences between the figures; the vent line case has more constant power levels and available pressure. Each run begins with the device fully charged. Power is then discharged from the device via the turbine's output (shown in blue). Once full discharge has been achieved, the device is recharged using the pump (shown in red). Upon starting or stopping the charge and discharge modes, a spike is seen in the available pressure due to the abrupt opening and closing of valves. Also seen during starting and stopping are step changes in the pressure likely due to piping pressure losses. As the turbine operates at a higher flow rate than the pump, the pressure losses (and step change in pressure) associated with it are higher. Furthermore, the pump's power spikes due to the higher current draw of the motor when starting.

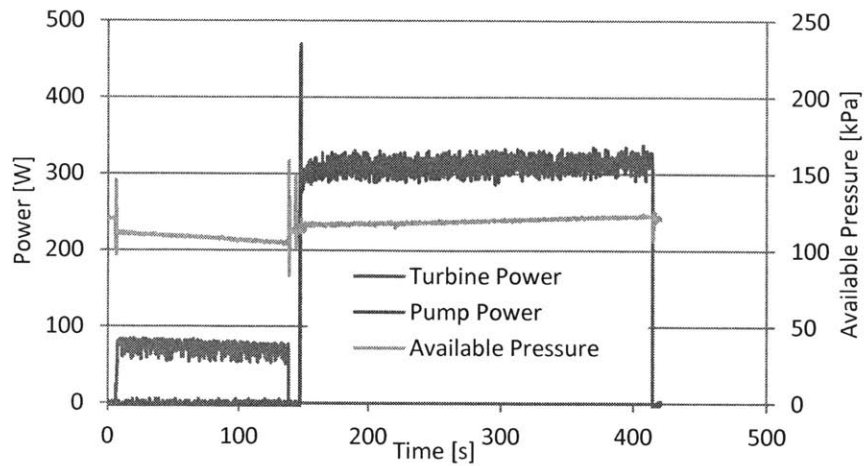


Figure 65: Typical charge and discharge power curves during a “vent line” test cycle.

The slight changes in the available pressure shown in the vent line case are due to the changing height of the water column. Due to the size of the high reservoir, (which is only marginally larger than the sphere itself) the water level in the reservoir changes throughout a given test, resulting in changing pressures at the nozzle. The height lost in the reservoir for the volume of water used in this test corresponds to a pressure of 8.5kPa. The pressure drop observed here was 6.4kPa. The power levels of both the pump and the turbine follow the changes in pressure.

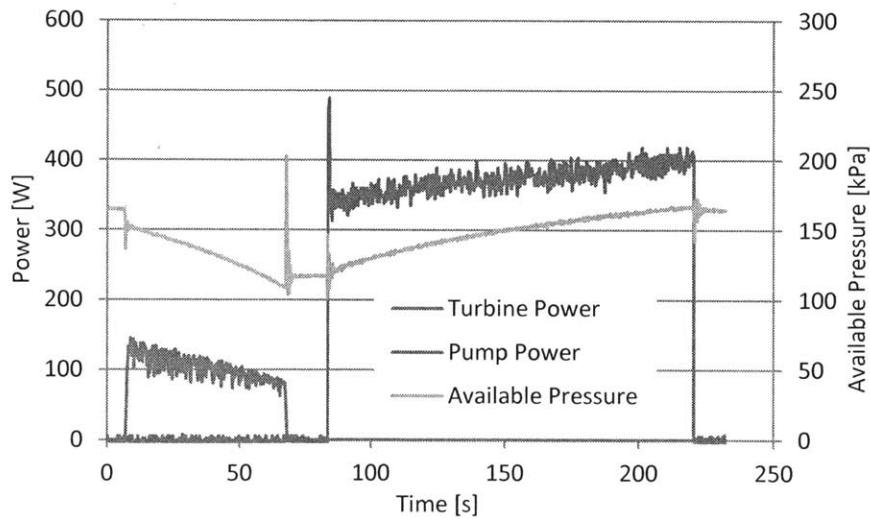


Figure 66: Typical charge and discharge power curves during a “no vent line” test cycle.

The “no vent line” case shows the same characteristics as the “vent line case” except here, the pressure inside the sphere changes. As water flow through the nozzle into the sphere, the air inside is compressed.

With a rising internal pressure and a relatively constant water column height, the available pressure decreases. As the turbine is shut off, the sphere has reached its fullest state resulting in the lowest available pressure.

The results from the tests graphed above are summarized in Table 15.

	Vent line	No vent
Head, average water column [m]	12.0	12.0
Head, vacuum [m]	0.0	4.8
Head, total [m]	12.0	16.9
Cycle water volume [L]	189.0	75.6
Sphere volume [L]	208.3	208.3
Volume utilization	91%	36%
Turbine		
Total energy produced [J]	9434	6203
Average power [W]	73	103
Average flow rate [L/s]	1.10	1.16
Run time [s]	130	60
Average efficiency	61%	67%
Pump		
Total energy consumed [J]	83294	51196
Average power [W]	312	374
Average flow rate (Gallons/min)	0.48	0.56
Run time (s)	267	137
Average efficiency	21%	24%
Overall System		
Total recovered energy (J)	9434	6203
Energy recovered per gallon H2O (J/L)	50	82
Total recovered energy (Wh)	2.6	1.7
Rountrip storage efficiency	11%	12%

Table 15: Detailed results comparing the “vent line” and “no vent line” cases.

Comparing the two test cases, the “no vent line” case is able to store more energy per litre and is also more efficient overall. However, the “vent line” case is able to store more energy overall.

The limitations of the analogy to devices deployed offshore become apparent. The “no vent line” case has a working volume of only 75 litres due to the fact that using more water would cause damaging overpressures inside the sphere. Underwater, where the stress throughout the concrete will be compressive only, this limitation would not exist.

The difference in head between the cases will decrease as the depth increases since the vacuum's maximum benefit is atmospheric pressure.

Efficiency increase only exists because of the equipment used and would not be present in larger devices who's rotating equipment purpose built.

7 Conclusion

7.1 Lessons Learned:

7.1.1 Joint

The most significant technical challenge encountered during the creation of this prototype was forming the sealed joint between the two concrete halves. Creating a seal at the interior surface of the concrete sphere was difficult because there was very limited access to the seal once the two hemispheres came together. Studs that crossed the plane of the joint also caused alignment and filling issues. Should larger sphere be constructed in two halves, they will require large equipment that has relatively fine resolution of movement to facilitate alignment. This sphere could be adjusted by hand. Larger versions will not have that luxury. It is likely that creating a successful joint between two large hemispheres will be labour intensive. Finally, any features to be added to the concrete by hand, such as the stud ports, must have a mechanism to limit the depth to which any device can be inserted into the concrete.

7.1.2 Mold

The steel hemispherical mold was robust, durable and produced concrete hemispheres with a sufficient degree of repeatability and without any noticeable warping or deformation. It is likely that many hemispheres could have been made using that mold. However, this type of mold has one major drawback in that it would be expensive to scale up. Due to the difficulties associated with handling and joining the hemispheres, it is not likely that a similar mold will be used in the future.

7.1.3 Pump/Turbine

The efficiency of small rotating equipment can be quite low resulting in even lower round-trip efficiencies as demonstrated here. It would be possible to achieve higher efficiencies with specially built equipment, however the cost of that equipment would be very high. For larger spheres, a large centrifugal pump (on the order of 10kW or more) might serve as a reversible pump-turbine for a reasonable cost

however, demonstrating a system with high efficiency would be beneficial to the perceived value of the concept.

7.2 Future Work

Funding has been secured for the development of a 3m ORES system to be constructed and deployed off the shores of Castine, Maine. Massachusetts Institute of Technology and Maine Maritime Academy are collaborating in the construction and deployment of the device and hope to couple its storage capabilities with the generating capacity of a floating wind turbine. The concrete sphere will be fabricated, loaded onto a deployment ship and lowered to the bottom of the ocean to act as moorings for the floating wind turbine. The storage vessel will be fitted with a reversible pump-turbine and controlled from the surface.

The long-term plans for concept development of increasingly larger prototype construction is as follows:

- Phase 1: Construct and deploy a 3m storage vessel to the undersea test site at MMA.
- Phase 2: Construct and deploy 2 additional storage vessels in triangle formation with the storage vessel from Phase 1. Install a floating energy harvester using a catenary mooring anchored by the three storage vessels.
- Phase 3: Construct 3 storage vessels each 9m in diameter and deploy them in an appropriate testing area in the gulf of Maine. Install a 100kW floating wind turbine anchored using the storage vessels.
- Phase 4: Construct a full-scale prototype 27m in diameter and deploy to the design depth of 700m.

The overall dimensions of the sphere were calculated and are shown in Table 16. A simple model of the sphere is shown for scale in Figure 67.

OD	3.6 m	11.8 ft
ID	3 m	9.8 ft
Wall thickness	0.3 m	1.0 ft
Volume	10.3 m ³	13.5 yards
Density	2400 kg/m ³	4050 lbs/yd
Weight	24700 kg	54518 lbs
	25 m tons	27 tons

Table 16: Overall specifications of the 3m concrete sphere.

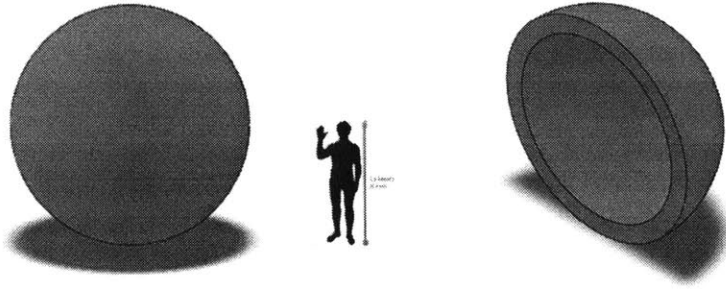


Figure 67: Storage Vessel. Left: Size comparison. Right: Cut-away showing wall cross section.

7.3 Closing Remarks

An energy storage device based on the ORES concept was successfully designed, built and cycled, demonstrating the concept's ability to store energy. From the lessons learned here, larger versions of the device will be built mitigating the now-known issues. Future devices will be much larger as the device is scaled up from 1m to 3m and onward to the production sized of 27m. In addition to larger sizes, the system will have to be designed for operation on the sea floor. There is still a long road ahead and much work needed for the concept to reach commercialization however, with hardware now being built and more knowledge of the system being created, the path to commercialization is becoming increasingly clear.

8 Bibliography

- Anagnostopoulos, J. S., & Papantonis, D. E. (2007) Flow Modeling and Runner Design Optimization in Turgo Water Turbines. *World Academy of Science, Engineering and Technology*. Athens, Greece: National Technical University of Athens
- Andritz AG (2010) Pumps used as Turbines: ACT/FPT Series. Retrieved 07/10/11 from: http://atl.g.andritz.com/c/www/00/06/02/-253484924/60200/1/1/0/centrifugal_pump_mini-turbine.pdf
- Cengel, Y., & Cimbala, J. (2005) *Fluid Mechanics: Fundamentals and Applications*. McGraw Hill
- Cao, J., Chung, D.D.L. (2001) Degradation of the bond between concrete and steel under cyclic shear loading, monitored by contact electrical resistance measurement. Buffalo, NY: *Cement and Concrete Research* 31 (2001) 669-671
- Corbus, D., Milligan, M., Ela, E., Scheurger, M., & Zavadil, B. (2009). *Eastern Wind Integration and Transmission Study - Preliminary Findings*. National Renewable Energy Laboratory. Golden, CO.
- Eyer, J., & Corey, G. (2010). *Energy Storage for the Electricity Grid: Benefits and Market Potential Assessment Guide*. Sandia National Laboratories. Albuquerque, NM: Sandia National Laboratories
- Eyer, J., Iannucci, J., & Corey, G. (2004). *Energy Storage Benefits and Market Analysis Handbook: A Study for the DOE Energy Storage Systems Program*. Sandia National Laboratories. Albuquerque, NM: Sandia National Laboratories
- Eyer, J. (2009). *17 Benefits from Electricity Storage for Electric Utility-related Applications*. Proceedings of the ASME 3rd International Conference on Energy Sustainability. San Francisco, CA
- Fennell, G. (June 2011). System Design and Manufacturability of Concrete Spheres for Undersea Pumped Hydro Energy or Hydrocarbon Storage. Massachusetts Institute of Technology, Mechanical Engineering. Cambridge, MA: MIT Libraries
- Greenlee, A. (June 2009). Design of Subsea Energy Storage Chamber. Massachusetts Institute of Technology, Mechanical Engineering. Cambridge, MA: MIT Libraries
- Jaliu, C., Visa, I., Diaconescu, D., Saulescu, R., Neagoe, M., Climescu, O., (2010) Dynamic Model of a Small Hydropower Plant. *12th Int. Conf. on Optimization of Electrical and Electronic Equipment*. Brasov, Romania.
- Kovler, K., Roussel, N., (2011) Properties of fresh and hardened concrete. *Cement and Concrete Research*, 41 (7), pp. 775-792.
- Kwon, S. H., Ferron, R.P., & Shah, S.P. (2008) Restrained shrinkage cracking of fiber-reinforced self-consolidating Concrete. In Loizos, A., Scarpas T., & Al-Qadi, I., *Pavement Cracking: Mechanisms, Modeling, Detection, Testing and Case Histories*, pp. 179-188.
- Morros, C. S., Oro, J. M. F., Diaz, K. M. A. (2011) Numerical modelling and flow analysis of a centrifugal pump running as a turbine: Unsteady flow structures and its effects on the global performance. *Int. J. Numer. Meth. Fluids* 2011; 65:542-562
- Oberlender, G. D. (2010) Formwork for Concrete Structures 4th Ed. New York, NY, USA: McGraw-Hill Professional Publishing. pp. 414-430 Retrieved on: 12/9/11 from: <http://site.ebrary.com/lib/mitlibraries/Doc?id=10430570&ppg=440>

Roberts, B. (2009) Capturing Grid Power: Performance, Purpose and Promise of Different Storage Technologies. *IEEE Power & Energy Magazine*. 1540-7977/09

Singh, S. P., Goel, S., Lal, R., Kaushik, S. K. (2004) Prediction of Mean and Design Fatigue Lives of Steel Fibrous Concrete using S-N Relationships. *Asian Journal of Civil Engineering (Building And Housing)* 5 (3-4), pp. 175-190

Singh, P. & Nestmann, F. (2011) A Consolidated Model for the Turbine Operation of Centrifugal Pumps *Journal of Engineering for Gas Turbines and Power* Vol. 133 / 063002-1

Stelzer, R. S., Walters, R. N. (1977) Estimating Reversible Pump-Turbine Characteristics. Denver, CO: The United States Department of the Interior, Bureau of Reclamation. Eng. Monograph No. 39

United States Energy Information Administration (USEIA) (2012) International Energy Statistics. Retrieved: 01/15/2012 from:
<http://www.eia.gov/cfapps/ipdbproject/iedindex3.cfm?tid=2&pid=82&aid=7&cid=regions&syid=2004&eyid=2008&unit=MK>

Vinatoru, M., Iancu, E. (2006) The Design of Control Systems for Hydraulic Turbines. *IEEE International Conference on Automation, Quality and Testing, Robotics*. pp. 32-36

Voith Hydro Holding GmbH & Co. KG (2009) Pumped Storage Machines. Retrieved 08/13/11 from:
http://www.voithhydro.de/media/VSHPO90009_Pumped_Storage_72dpi.pdf

Williams, D. K. (2007) Proposed Design Criterion for Vessel Lifting Lugs in Lieu of ASME B30.20. *Journal of Pressure Vessel Technology*, 129 (2), pp. 326–333

9 Appendices

9.1 Turbine Efficiency Chart

OUTPUT/EFFICIENCY CHART LV750 - LOW PRESSURE MODEL

Psi	Feet	1/8		3/16		1/4		5/16		3/8		7/16		1/2		9/16		5/8	
		GPM	Watts																
20	46					8.1		12.6		18.2		24.9		32.3		40.9		50.6	
		Efficiency				18%	12	27%	28	33%	50	33%	68	35%	93	33%	111	28%	119
30	69					9.9		15.5		22.3		30.4		39.6		50.2		62.0	
						40%	49	49%	94	57%	157	56%	211	55%	269	43%	266	36%	280
40	92			6.4		11.4		17.9		25.8		35.1		45.8		57.9		71.6	
				35%	42	55%	103	61%	181	64%	274	63%	365	60%	452	47%	447	39%	466
43	100			6.7		11.9		18.5		26.8		36.5		47.6		60.2		74.4	
				39%	47	56%	119	64%	213	63%	303	65%	429	60%	512	47%	514	40%	539
50	115	3.2		7.2		12.7		19.9		28.8		39.2		51.1		64.7		80.0	
		12%	8	47%	70	61%	160	64%	264	66%	393	66%	534	61%	650	48%	638	40%	668
52	120	3.26		7.3		13.0		20.3		29.3		39.9		52.1		65.9		81.5	
		14%	10	47%	74	60%	169	65%	285	65%	414	63%	540	61%	687	48%	677	41%	713
60	139	3.51		7.9		14.0		21.9		31.6		43.0		56.0		70.9		87.7	
		21%	18	51%	100	62%	216	65%	357	64%	506	62%	662	60%	835	46%	812	40%	869
65	150	3.64		8.2		14.5		22.7		32.8		44.7		58.2		73.7		91.1	
		28%	28	51%	113	63%	245	66%	404	64%	569	62%	750	58%	910	46%	914	39%	962
70	162	3.79		8.5		15.1		23.6		34.1		46.4		60.5		76.6		94.7	
		33%	36	52%	130	62%	271	66%	455	65%	646	61%	829	57%	1005	44%	987	39%	1072
80	185	4.05		9.1		16.1		25.2		36.4		49.6		64.7		81.9		101.2	
		36%	49	54%	165	60%	323	66%	558	63%	770	61%	1004	54%	1170	44%	1213	38%	1292
90	208	4.3		9.7		17.1		26.8		38.7		52.7		68.7		86.9		107.4	
		39%	62	55%	200	60%	382	65%	654	63%	914	60%	1179	53%	1357	44%	1420	36%	1454

9.2 Additional Design Calculations

9.2.1 Pressure Drop Calculator

The pressure drop calculator was created in Microsoft Excel using a spreadsheet and a simple VBA macro. It was used to estimate pressure losses in piping systems by solving the Colebrooke-White equation using the bisection method. The calculator and the equation can be seen in Figure 68. The macro used to solve the Colebrooke-White equation is executed when the "Solve" button shown in the lower middle of the figure is pressed.

	A	B	C	D	E	F	G	H	I	J	K
1											
2	Flow properties			Fluid Properties							
3	Flow rate	12.21 gpm		μ		0.001519 Pa.s					
4		0.000770248 m ³ /s		ρ		1025 kg/m ³			Minor Losses		
5									Sharp Ent		Pa
6	Pipe Properties								90deg Elbow		Pa
7	Dh	2.067 in		*Must be circular pipe					T line	56.963438	Pa
8		5.25018 cm							T branch		Pa
9	L	2 m							T line	56.963438	Pa
10	ϵ	0.0025 mm							T line		Pa
11	Calculated								T line		Pa
12	A	21.65 cm ²							T line		Pa
13	V	0.36 m/s							T branch		Pa
14	Re	12605		*Check. Above 2300 for turbulent					Total Losses		
15	ϵ/Dh	4.762E-05									
16	Colebrooke-White Solver			*Don't forget to push Solve!!!!						185.97227	Pa
17	Tolerance	1.00E-06		<div style="border: 1px solid black; padding: 5px; display: inline-block;"> <input type="button" value="Solve"/> $\frac{1}{\sqrt{f}} = -2 \log_{10} \left(\frac{\epsilon/D_h}{3.7} + \frac{2.51}{Re\sqrt{f}} \right)$ </div>						0.0269804	psi
18	fhigh	0.029152									
19	flow	0.029151									
20	f	0.029152	Turbulent								
21	Cweqn	7.40144E-06		<div style="border: 1px solid black; padding: 5px; display: inline-block;"> $\Delta P = f \frac{\rho V^2 l}{2 d}$ </div>							
22	Iterations	21									
23											
24	$\Delta P/m$	36.02 Pa/m									
25	ΔP	0.0720 kPa									
26		0.01 psi									

Figure 68: The pressure drop calculator spreadsheet.

The Excel macro used to implement the bisection method and solve the Colebrook-White equation is as follows:

```

Sub Macro1()
'
' Macro1 Macro
'
fh = 2
fl = 0.0001
er = fh - fl
tol = Range("B17")

If Range("B14").Value > 2300 Then
Range("C20") = "Turbulent"

ii = 1
Do While (er > tol) And (ii < 100)

Range("B20").Value = (fh + fl) / 2
If Range("B21").Value = 0 Then Exit Do
If Range("B21").Value > 0 Then fh = (fh + fl) / 2
If Range("B21").Value < 0 Then fl = (fh + fl) / 2

er = fh - fl

```

```
Range("B22").Value = ii
ii = ii + 1
Loop
Range("B18").Value = fh
Range("B19").Value = fl

Else
Range("B20").Value = Range("B14").Value / 64
Range("C20") = "Laminar"

Range("B18").Value = "N/A"
Range("B19").Value = "N/A"

End If

End Sub
```

9.2.2 Piping Losses in the turbine piping system

Major Losses

Q [L/s]	0.00077
μ [Pa.s]	0.001519
ρ_s [kg/m ³]	1025
Dh [in.]	2.067
Dh [cm]	5.25018
L [m]	2
ϵ [mm]	0.0025
A [cm ²]	21.64902
V [m/s]	0.355789
Re	12604.69
ϵ/D_h	4.76E-05
ΔP [kPa]	0.072

Minor Losses

Fitting	K	ΔP [kPa]
T, Inline flow	0.9	56.96349
T, Inline flow	0.9	56.96349

Total Losses

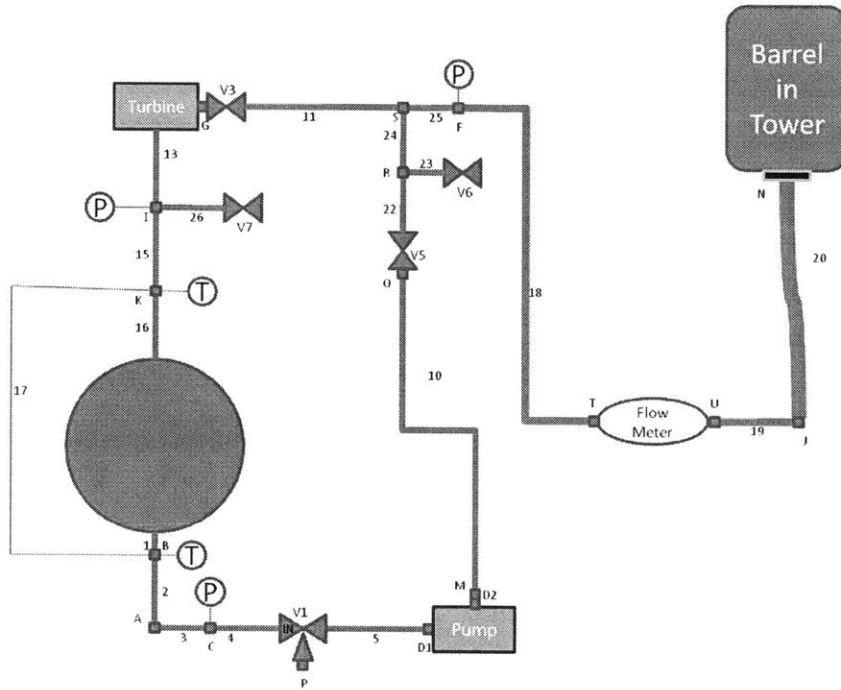
Major [kPa]	0.072
Minor [kPa]	0.114
Total [kPa]	0.186

Table 17: Estimated turbine piping system losses. This is an example calculation. For each pipe size, the internal diameter is entered as the hydraulic diameter, D_h , and the calculations are completed.

Size	ID [in]	ID [cm]	ΔP [kPa]
0.75	0.824	2.09296	10.28
1	1.049	2.66446	3.53
1.25	1.38	3.5052	1.065
1.5	1.61	4.0894	0.545
2	2.067	5.25018	0.185

Table 18: The summary of turbine piping loss estimates.

9.3 Piping Diagram



Fittings		22-Apr-11											
Fitting #	Description	Pipe Size	Fitting #	Description	Pipe Size	Totals							
A	Street 90	1 1/4	K	Cross	1 1/4	Type	Size #	p/n					
B	Cross	1 1/4	K1	Bushing	1 1/4x1 1/4	Street 90	1 1/4	1 44605K137					
B1	Bushing	1 1/4x1 1/4	K2	Bushing	1 1/4x1 1/4	Street 90	1	2 44605K136					
B1a	Barb	1/4x1 1/4	K2a	Barb	1/4x1 1/4	Barb	1/4x1 1/4	2 5047K16					
B2	Bushing	1 1/4x1 1/4	L	Filter	1 1/4	Barb	1 1/4x1 1/4	6 5372K142					
C	T	1 1/4	L1	Nipple	1 1/4	Bushing	1 1/4x1 1/2	8 44605K283					
C1	Bushing	1 1/4x1 1/4	L2	Union	1 1/4	Bushing	1/2x1 1/4	8 4513K344					
D1a	Union	1 1/4	L3	Barb	1 1/4x1 1/4	Bushing	1 1/4x1	2 44605K281					
D1b	Bushing	1 1/4 x 1	M	Barb	1 1/4x1 1/4	Bushing	1 1/4x???	1					
D1c	Nipple	1 x close	N	Nipple	2	Bushing	2 1/2x2	1 44605K398					
D1d	Street 90	1	N1	NPTxNH/NST	2x2 1/2	Cross	1 1/4	3 44605K164					
D2a	Union	1 1/4	N1	Bushing	2x2 1/2	Filter	1 1/4	0 98775K48					
D2b	Bushing	1 1/4 x 1	O	Bushing	1 1/4x1 1/4	Nipple	1 x close	2 44615K436					
D2c	Nipple	1 x close	P	Bushing	1 1/4x1 1/4	Nipple	1 1/4	0 44615K437					
D2d	Street 90	1	Q	Barb	1 1/4x1 1/4	Nipple	2	1 -					
E	T	1 1/4	R	Wye	1 1/4	NH/NSTxNTP	2 1/2x1 1/2	0 6523T35					
E1	Bushing	1 1/4x1 1/4	S	Wye	1 1/4	NPTxNH/NST	2x2 1/2	0 6494T72					
F	Cross	1 1/4	T	Barb	1 1/4x1 1/4	Reduc Coupl	1 1/4x1 1/2	0 44605K324					
F1	T	1 1/4	U	Barb	1 1/4x1 1/4	Reduc Coupl	2 1/2x1 1/4	1 44605K542					
F1	Barb	1 1/4x1 1/4				T	1 1/4	2 44605K157					
F2	Barb	1 1/4x1 1/4				Union	1 1/4	2 44605K197					
F3	Bushing	1 1/4x1 1/4				Wye	1 1/4	2 44605K356					
G	Bushing	1 1/4x???				Note: Location of fitting is specified by the first letter in Fitting#.							
I	Cross	1 1/4											
I1	Bushing	1 1/4x1 1/4											
J	Reduc Coupl	1 1/4x1 1/2											
J	Reduc Coupl	2 1/2x1 1/4											
J1	NH/NSTxNTP	2 1/2x1 1/2											
J2	Barb	1 1/4x1 1/4											

Piping/Hose				22-Apr-11					
All black pipe threaded				Totals					
Pipe #	Type	Pipe Size	Length (in)	Type	Pipe Size	Length (in)	#	Supplier	P/N
1	Black	1-1/4	close	Black	1-1/4	close	12	McMaster	44615K437
2	Black	1-1/4	close	Black	1-1/4	8	2	McMaster	44615K527
3	Black	1-1/4	12	Black	1-1/4	12	1	McMaster	44615K547
4	Black	1-1/4	close	PVC	1/4	10'	1	McMaster	55525K12
5	Black	1-1/4	8	PVC	1-1/4x3/16	10'	1	McMaster	5393K47
6	Black	1-1/4	8	PVC braid	1 1/4	14'	1	McMaster	52375K18
7	Black	1-1/4	close	Fire hose	2 1/2	35'	1	McMaster	5310K13
10	PVC	1-1/4x3/16	10'						
11	Black	1-1/4	close						
12	PVC	1-1/4x3/16	4'						
13	Black	1-1/4	close						
14	Black	1-1/4	close						
15	Black	1-1/4	close						
16	Black	1-1/4	close						
17	PVC	1/4	10'						
18	PVC braid	1 1/4	7'						
19	PVC braid	1 1/4	7'						
20	Fire hose	2 1/2	35'						
21	Black	1-1/4	close						
22	Black	1-1/4	close						
23	Black	1-1/4	close						
24	Black	1-1/4	close						
25	Black	1-1/4	close						
26	Black	1-1/4	close						

Valves					22-Apr-11	
All black pipe threaded						
Valve #	Type	Pipe Size	Material	Supplier	P/N	
V1	Ball 3way	1-1/4	Polyprop	McMaster	97745K28	
V2	Ball 3way	1-1/5	Polyprop	McMaster	97745K29	
V3	Ball	1-1/4	Brass	McMaster	47865K26	
V4	Ball 3way	1-1/6	Polyprop	McMaster	97745K30	
V5	Ball	1-1/4	Brass	McMaster	47865K26	
V6	Ball	1-1/4	Brass	McMaster	47865K26	
V7	Ball	1-1/4	Brass	McMaster	47865K26	

9.4 Wiring Diagram

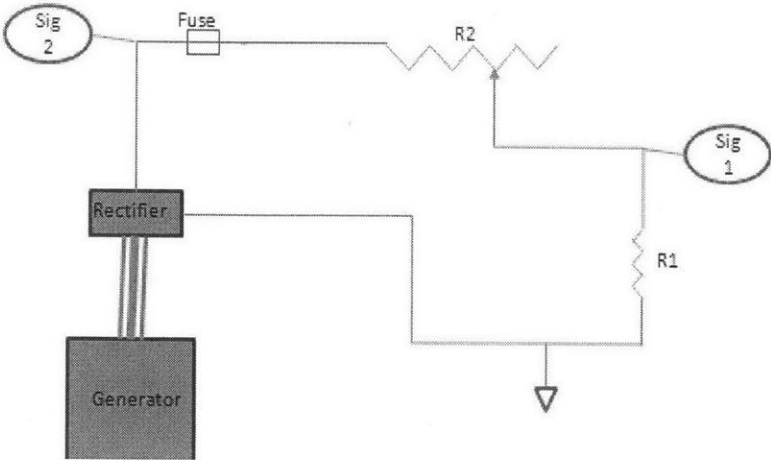


Figure 69: Turbine Circuit

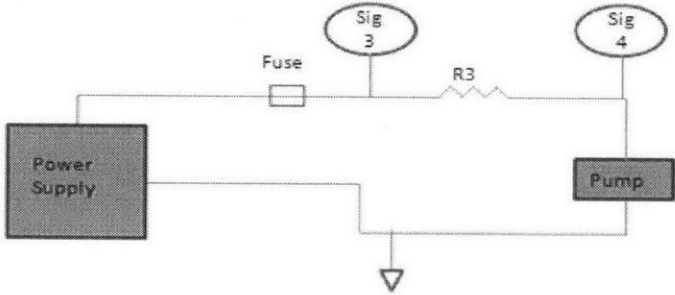


Figure 70: Pump Circuit